Cotranslational Folding and Assembly at the Single-Molecule Level

Cotranslational Folding and Assembly at the Single-Molecule Level

Dissertation

for the purpose of obtaining the degree of doctor
at Delft University of Technology
by the authority of the Rector Magnificus,
prof. dr. ir. T.H.J.J. van der Hagen,
Chair of the Board for Doctorates
to be defended publicly
on Thursday 18 September 2025 at 17:30 o'clock

by

Katharina TILL

Master of Science in Physics, Bielefeld University, Germany
born in Düsseldorf, Germany.

This dissertation has been approved by the promotors.

Composition of the doctoral committee:

Rector Magnificus,	chairperson
Prof. dr. ir. S.J Tans,	Delft University of Technology / AMOLF, promotor
Dr. ME. Aubin-Tam,	Delft University of Technology, promotor
Independent members:	
Prof. dr. ir. S.J.J. Brouns,	Delft University of Technology
Dr. C. Cecconi,	University of Modena and Reggio Emilia, Italy
Prof. dr. C.M. Kaiser,	Utrecht University
Prof. dr. T.S. Shimizu,	VU Amsterdam
Dr. A.S. Wentink,	Leiden University
Prof. dr. B.D. Rowland,	Delft University of Technology, reserve member

The work described in this dissertation was performed at AMOLF, Science Park 104, 1098 XG, Amsterdam, The Netherlands. This work was financially supported by the Netherlands Organisation for Scientific Research (NWO).

Printed by: Ridderprint

Cover by: Katharina Till

ISBN 978-94-6522-640-8

An electronic version of this dissertation is available at http://repository.tudelft.nl/ and http://www.amolf.nl/. Printed copies can be obtained by request via e-mail to library@amolf.nl.

Contents

Summary i

Samenvatting v

1 Introduction 1

1.1 The protein-folding problem, an enigma solved? 2
1.1.1 Forces governing protein folding 3
1.1.2 Folding speed and mechanism 3
1.1.3 Computational protein structure prediction from amino acid sequences 5
1.2 What's next? The new era of the protein-folding problem 5
1.2.1 The Ribosome: Significant beyond protein synthesis 6
1.2.2 Chaperones: Major regulator of proteostasis. 9
1.3 Optical tweezers: A tool to unveil detailed folding dynamics . . . 11

2 Unveiling functions of Trigger Factor with single-molecule studies 15

2.1 Trigger Factor: A more versatile chaperone than previously thought 16
2.1.1 Trigger Factor Structure 16
2.1.2 Ribosome-independent functions of Trigger Factor 16
2.1.3 Functions of Trigger Factor at the ribosome. 19

3 Trigger factor accelerates nascent chain compaction and folding 23

3.1 Introduction 24
3.2 Results. 25
3.2.1 DHFR interacts with trigger factor late in translation . . . 25
3.2.2 TF promotes partially folded states during translation . . . 26
3.2.3 TF enhances nascent chain collapse and accelerates partial folding 28
3.2.4 TF accelerates folding by stabilizing collapsed states . . . 30
3.2.5 TF binds longer to compacted nascent chains 31
3.3 Discussion 32
3.4 Methods 35
3.5 Author Contributions 39
3.6 Supplementary Figures 40

4 Co-translational ribosome pairing enables native assembly of misfolding-prone subunits 49

4.1 Introduction . . . 50
4.2 Results . . . 51
4.2.1 *In vivo* detection of lamin nascent chain interactions . . . 51
4.2.2 *In vitro* formation of lamin RNC pairs . . . 51
4.2.3 Nascent lamin complex formation observed by fluorescence . . . 53
4.2.4 Delayed RNC interaction promotes non-native lamin dimer conformations . . . 54
4.2.5 Co-co assembly suppresses intra-chain lamin misfolding . . . 56
4.2.6 Ribosome pair asymmetry and proximity . . . 57
4.2.7 Proteome-wide considerations . . . 58
4.3 Discussion . . . 59
4.4 Methods . . . 60
4.5 Author Contributions . . . 66
4.6 Supplementary Figures . . . 67

5 Translation-driven temporal control for intertwined protein assembly 83

5.1 Introduction . . . 84
5.2 Results . . . 85
5.2.1 *In vivo* dimerization of BTB domain proteins . . . 85
5.2.2 BTB monomers adopt a closed state at the ribosome . . . 86
5.2.3 BTB closed states resist unfolding . . . 87
5.2.4 BTB monomers populate a small core fold . . . 88
5.2.5 Temporal assembly control at the ribosome . . . 90
5.2.6 Assembly control across the BTB proteome . . . 92
5.3 Discussion . . . 94
5.4 Methods . . . 96
5.5 Author Contributions . . . 101
5.6 Supplementary Figures . . . 102

6 Conclusion and Outlook 111

Bibliography 117

List of Publications 133

Acknowledgments 135

About the Author 149

SUMMARY

Proteins rarely act alone. A complex network of protein–protein interactions is essential for maintaining cellular health and, by extension, the health of the entire organism. Given the vast complexity of the proteome, which in humans is estimated to contain over 100,000 different proteins, it is clear that maintaining a well-regulated balance of each step of every protein's lifespan, from translation to degradation, is a grand challenge. Furthermore, disruptions in this balance, known as proteostasis, are linked to aging and a plethora of diseases. Yet, remarkably, the majority of organisms experience the joy of remaining healthy in their day-to-day lives.

Understanding how the proteome is kept in balance has been a central research question for decades, spanning multiple disciplines. At its core, this is a question of protein folding: only proteins that adopt their correct structure can perform their functions and interact faithfully with other proteins. While significant insights have been gained from studying small globular proteins, the mechanisms governing protein complex assembly and cellular influences on folding remain elusive. Studying these processes experimentally is inherently difficult due to their highly dynamic and heterogeneous nature. Overcoming these challenges will be crucial to deepening our understanding of proteostasis and its role in health and disease.

This thesis contributes to the broader goal of understanding how protein folding and complex assembly are guided by interactions with other proteins, such as ribosomes and chaperones. However, these complex folding dynamics cannot be understood without the fundamental insights gained from decades of preceding meticulous research.

Thus, **Chapter 1** provides an overview of key findings from recent years and discusses future directions of protein folding research. Additionally, it introduces Optical Tweezers as the principal experimental method used within this thesis. Optical Tweezers are a single-molecule technique that uniquely addresses the challenges of deciphering the dynamic and heterogeneous nature of protein folding and protein–protein interactions.

Chapter 2 further illustrates the power of single-molecule studies like optical tweezers in unveiling the intricate dynamics of chaperone-mediated protein folding, focusing on the bacterial chaperone Trigger Factor, through a literature review. Initially thought to merely prevent aggregation, recent studies have revealed that Trigger Factor actively reshapes the folding landscape both on and off the ribosome, stabilizing intermediates, modulating energy barriers, and steering proteins toward their native state.

The many insights gained from previous studies suggest that Trigger Factor plays a far more complex role than initially believed, with its function depending on both the timing and location of its interaction with substrates. Since Trigger Factor is the only known chaperone that directly associates with the ribosome in bacteria, its role during translation is particularly critical to elucidate. However, how Trigger Factor modulates the folding pathway of nascent chains during translation remains poorly understood. In **Chapter 3**, we address this question by combining selective

ribosome profiling with optical tweezers and correlated single-molecule fluorescence to investigate chaperone-induced conformational changes in nascent polypeptides at two distinct translational stages. We find that Trigger Factor binding compacts nascent chains and stabilizes partial folds, while nascent chain compaction prolongs TF binding. These cooperative effects are regulated by ongoing translation, with Trigger Factor-accelerated folding depending on the emergence of key peptide segments. This previously unobserved acceleration of nascent chain folding, dependent on the stage of their synthesis, expands the functional repertoire of Trigger Factor and influences processes such as co-translational protein assembly, aggregation, and translational pausing.

Beyond chaperone-modulated co-translational folding, another exciting discovery has recently further expanded our knowledge about co-translational folding mechanisms in protein biogenesis. Co-co assembly is a newly discovered pathway for protein complex formation, where two nascent proteins from nearby ribosomes begin to interact already during translation. Disome selective profiling results highlight the significance of this biogenesis route, revealing over 800 co-co assembling homodimers. However, the folding of interacting nascent chains remains unexplored. In **Chapter 4**, we develop an integrated single-molecule fluorescence and force spectroscopy approach to probe the folding and assembly of two nascent chains extending from nearby ribosomes, using the intermediate filament lamin as a model system. We show that co-translational ribosome pairing allows their nascent chains to 'chaperone each other', thus enabling the formation of coiled-coil homodimers from subunits that misfold individually. Moreover, ribosome proximity in early translation stages was found to be critical: when interactions between nascent chains are inhibited or delayed, they become trapped in stable misfolded states that are no longer assembly-competent. Taken together, this study provides deeper insight into how protein complex formation is enabled by ribosome cooperation and why co-co assembly constitutes an important new pathway in protein biogenesis.

In **Chapter 5**, we further explore the critical role of timing in interactions between nascent chains from nearby ribosomes and its impact on faithful complex assembly. The formation of intertwined protein complexes poses additional challenges, as structural rearrangements are often required, necessitating the disruption of already established intramolecular contacts. By studying the BTB domain, which forms an intertwined dimer, we reveal a "temporal control" mechanism driven by translation that overcomes these challenges. Early interactions between nascent dimerization partners during translation open up otherwise inaccessible folding-assembly pathways that bypass unproductive monomeric states. Notably, further analysis suggests temporal assembly control is relevant across the BTB proteome and works in concert with a dimerization quality control pathway. More broadly, we propose that the ability to regulate key folding and assembly events over time may be central to maximizing the spectrum of protein complexes that can be synthesized.

Finally, in **Chapter 6**, we provide an outlook on future directions and experiments inspired by the findings of this thesis. By bridging molecular-level folding mechanisms with large-scale proteome screenings performed by our collaborators

B. Bukau and G. Kramer at Heidelberg University, our results pave the way for exploring even more complex dynamics and protein–protein interactions, which shape protein folding and, consequently, help to explore how the proteome is kept in a well-regulated, balanced state.

SAMENVATTING

Eiwitten werken zelden alleen. Een complex netwerk van interacties tussen eiwitten is essentieel voor het gezond houden van cellen en uiteindelijk het gehele organisme. De enorme complexiteit van het proteoom, dat naar schatting uit meer dan 100.000 verschillende eiwitten bestaat bij mensen, maakt het correct balanceren van de verschillende stappen in de levenscyclus van een eiwit, van translatie tot afbraak, een grote uitdaging. Bovendien worden verstoringen in deze balans in verband gebracht met veroudering en een scala aan ziekten. Het is daarom verbazingwekkend dat de meeste organismen gezond blijven in hun dagelijks leven.
Hoe dit proteoom in balans wordt gehouden is al decennialang een belangrijke onderzoeksvraag binnen verschillende disciplines. Centraal in deze vraag is het vouwen van de eiwitten: alleen eiwitten die correct gevouwen zijn, kunnen hun functies goed uitvoeren en interacties aangaan met andere eiwitten. Hoewel er al veel inzichten in eiwitvouwing zijn verkregen door onderzoek naar globulaire eiwitten, blijven de onderliggende mechanismen grotendeels onbekend, met name de mechanismen achter de vorming van eiwitcomplexen en de invloed van de cellulaire omgeving. Het experimenteel bestuderen van eiwitvouwing blijft een uitdaging, omdat eiwitten inherent dynamisch en heterogeen zijn. Het overwinnen van deze uitdagingen zal dan ook cruciaal zijn om de eiwitbalans en de rol ervan in gezondheid en ziekte beter te begrijpen.
Dit proefschrift draagt bij aan het beter begrijpen van hoe eiwitvouwing en complexe eiwitassemblage gestuurd worden door interacties met andere eiwitten zoals ribosomen en chaperonnes. Om deze complexe vouwingsdynamiek te kunnen begrijpen, zijn de fundamentele inzichten uit decennia van onderzoek essentieel. In **Hoofdstuk 1** wordt een overzicht gegeven van onze huidige kennis over eiwitvouwing. Daarnaast introduceert dit hoofdstuk ook optische pincetten, die als belangrijkste experimentele techniek gebruikt worden in dit proefschrift. Optische pincetten zijn een single-molecule techniek die de unieke mogelijkheid biedt de dynamische en heterogene aard van eiwitvouwing en interacties tussen eiwitten te ontrafelen.
Hoofdstuk 2 gaat dieper in op single-molecule technieken zoals optische pincetten voor het bestuderen van de complexe dynamiek van eiwitvouwing begeleid door chaperonnes, waarbij specifiek gefocust wordt op het bacteriële chaperonne Trigger Factor. Initieel werd gedacht dat Trigger Factor enkel eiwitaggregatie verhinderde, maar dit proefschrift toont aan dat het actief het vouwingslandschap herstructureert, zowel op als buiten het ribosoom. Het stabiliseert intermediaire structuren, moduleert energiedrempels, en leidt eiwitten naar hun originele toestand.
Omdat Trigger Factor het enige gekende chaperonne is dat directe interactie met het ribosoom aangaat in bacteriën, is het belangrijk de rol van Trigger Factor in translatie te begrijpen. Hoe Trigger Factor de vouwingsroute van nascente ketens tijdens translatie beïnvloedt, blijft echter nog grotendeels onduidelijk.
In **Hoofdstuk 3** gaan we op deze vraag in door 'selective ribosome profiling' te combineren met optische pincetten en gecorreleerde single-molecule fluorescentie. Met deze methode kunnen wij de conformationele veranderingen in nascente

polypeptiden te onderzoeken die chaperonnes induceren in verschillende translatiestadia. We hebben ontdekt dat Trigger Factor de nascente ketens compacter maakt, en gedeeltelijke vouwingen stabiliseert, terwijl door deze compactie Trigger Factor weer langer bindt. Deze coöperatieve effecten worden gereguleerd door de voortgaande translatie, en de synthese van peptidesegmenten die een belangrijke rol in de structuur spelen. Deze versnelde ketenvouwing, breidt het functionele repertoire van Trigger Factor uit en kan daarnaast verschillende processen beïnvloeden, onder andere co-translationele eiwitassemblage, aggregatie en translatiestagnatie.
Naast chaperonne-gereguleerde co-translationele eiwitvouwing, heeft een andere recente ontdekking ons begrip van co-translationele vouwingsmechanismen verder vergroot. Deze 'co-co assembly' is een nieuw mechanisme voor eiwitcomplexvorming, waarbij twee eiwitketens die gesynthetiseerd worden door naburige ribosomen al tijdens de translatie interactie aangaan. Resultaten van 'disome selective profiling' welke 800 co-co-assemblerende homodimeren aan het licht bracht, benadrukken het belang van deze biogenese route. De vouwing van co-co-assemblerende homodimeren is echter nog grotendeels onbekend. In **Hoofdstuk 4** ontwikkelen we een geïntegreerde single-molecule fluorescentie- en kracht-spectroscopiebenadering om de vouwing en assemblage van twee nascente ketens te onderzoeken die uit naburige ribosomen groeien, gebruik makend van het intermediaire filament lamine als modelsysteem. We tonen aan dat co-translationele ribosomen hun nascente ketens in staat stelt voor elkaar als chaperonne te fungeren, waardoor 'coiled-coil' homodimeren kunnen vormen uit monomeren die zonder dit effect individueel misvouwen. Bovendien blijkt ribosoomnabijheid in vroege translatiestadia cruciaal, wanneer interacties tussen nascente ketens worden geremd of vertraagd, raken ze 'gevangen' in stabiele misvouwingsstaten en zijn ze niet langer in staat tot assemblage. Alles bij elkaar biedt deze studie verdere inzichten in hoe de vorming van eiwitcomplexen mogelijk wordt gemaakt door samenwerking tussen ribosomen en waarom co-co-assemblage een belangrijke nieuwe route vormt in de eiwitbiogenese.
In **Hoofdstuk 5** onderzoeken we verder de kritieke rol van timing in interacties tussen nascente ketens van naburige ribosomen en de impact ervan op eiwitcomplex-assemblage. De vorming van verweven eiwitcomplexen brengt extra uitdagingen met zich mee, omdat structurele herschikkingen vaak vereist zijn, wat het verbreken van al bestaande intermoleculaire contacten vereist. Door het BTB-domein te bestuderen, dat zo'n verweven dimeer vormt, beschrijven we een translatie-gedreven controlemechanisme gebaseerd op timing. Vroege interacties tussen dimerisatiepartners tijdens de translatie openen vouwings-assemblagepaden die niet-productieve conformaties van monomeren omzeilen. Verdere analyse suggereert dat temporele assemblagecontrole relevant is in het hele BTB-proteoom en samenwerkt met een kwaliteitscontrolemechanisme voor dimerisatie. In bredere zin stellen wij voor dat het vermogen om cruciale vouwings- en assemblageprocessen in de tijd te reguleren belangrijk is in het vergroten van het spectrum van eiwitcomplexen dat gesynthetiseerd kan worden.
Tot slot biedt **Hoofdstuk 6** een vooruitblik op toekomstige onderzoeksrichtingen en experimenten die voortkomen uit de resultaten in dit proefschrift. Door moleculaire vouwingsmechanismen te koppelen aan grootschalige screenings, uitgevoerd

door onze samenwerkingspartners B. Bukau en G. Kramer aan de Universiteit van Heidelberg, leggen onze resultaten de basis voor verdere verkenning van complexe dynamieken en eiwit-eiwitinteracties. Dit zal bijdragen aan een beter begrip van hoe het proteoom in een goed gereguleerde en gebalanceerde staat wordt gehouden.

Chapter 1

INTRODUCTION

Proteins are the molecular machines of life, yet their function depends entirely on their ability to fold into precise three-dimensional structures. Since the first protein structure was unveiled in 1958, researchers have been riveted by a remarkable puzzle: How does a one-dimensional amino acid chain fold rapidly and reliably into its unique native structure? The search for answers created an entire research field, combining physics, chemistry, and molecular biology. This introduction highlights the progress made in understanding life at its most fundamental level. However, it also underscores the vast challenges that remain, marking the dawn of an exciting new era in tackling the so-called protein-folding problem.

1.1 The protein-folding problem, an enigma solved?

In 1958, John Kendrew of the Cavendish Laboratory in Cambridge (UK) and co-workers published the 3-dimensional structure of myoglobin, the first protein to have its structure determined. Five years later, in 1962, Kendrew and Max Perutz received the Nobel Prize in Chemistry for their work on protein structure determination. [1, 2] In his further research, Max Perutz preceded to explore the connection between structure and function.[3] His findings lay the foundations for what is now well-established knowledge: the structure of a protein sets the ways of how it can interact with other molecules and thus determines its function. Proteins have become known as the principal molecular machines in the cell, capable of performing the many complex processes which enable life.

In 1961, Christian Anfinsen showed that ribonuclease A could be refolded after denaturation while preserving its enzyme activity. This led him to formulate the following statement: "[...] the three-dimensional structure of a native protein in its normal physiological milieu [...] is the one in which the Gibbs free energy of the whole system is lowest, that is, the native conformation is determined by the totality of interatomic interactions and hence by the amino acid sequence, in a given environment." [4] He thereby postulated that the 3D structures of small globular proteins are uniquely connected to their amino acid sequences. Now known as the *Anfinsen's Dogma*, his "thermodynamic hypothesis" became a paradigm in molecular biology and the connected research awarded him, together with Stanford Moore and William Howard Stein, the Nobel Prize in Chemistry in 1972. [5]

However, this hypothesis could also be considered the starting point of decades of research aiming to understand the *how*: How can a protein structure be predicted by its amino acid sequence, how does a stable native fold result from the interatomic forces acting on an amino acid sequence and how can a protein find its native folded state so fast by a random search among all the possible configurations. Taken together, these are the central questions of what is considered the protein-folding problem. [1, 2, 6] Urgency to find answers to those questions is highlighted by the fatal consequences in cases where proteins fail to fold correctly. Incorrectly folded proteins give rise to a wide variety of pathological conditions, as they can no longer perform their functions properly. In fact, protein misfolding is involved in the majority of diseases not caused by infectious agents. [7]

Where are we now, more than 50 years later? Research has advanced our understanding considerably and resolved many of the seeming paradoxes. Nevertheless, the 2024 Nobel Prize in Chemistry awarded for the achievements in computational protein design and the use of artificial intelligence to predict the structure of almost all known proteins, evidences the potential for further new and important discoveries, but also the existence of many remaining unknowns in the protein folding field. To determine the next steps, a thorough understanding of the existing knowledge is essential. A brief summary of some key findings:

1.1.1 Forces governing protein folding

Anfinsen's "thermodynamic hypothesis" states that a protein's native structure corresponds to the lowest Gibbs free energy (G) of the system. [4] This principle initially seemed paradoxical because protein folding reduces conformational entropy, which thermodynamically opposes the folding process. [2, 8] However, this unfavorable entropy loss during folding is compensated by favorable intra- and intermolecular interactions, which collectively result in a negative Gibbs free energy change (ΔG) and promote the formation of the native structure. ΔG is given by:

$$\Delta G = \Delta H - T\Delta S < 0 \tag{1.1}$$

where H, S and T are the enthalpy, entropy and temperature. The enthalpy change (ΔH) reflects the stabilizing interactions formed during folding. The unique physical and chemical properties of each amino acid, determined by its side chain, enable a variety of non-covalent and covalent interactions, including hydrogen bonds, disulfide bonds, van der Waals forces, and electrostatic attractions. Collectively, these interactions contribute to the structural stability of the folded protein. The most dominant contributor to protein folding, next to hydrogen bonding, was found to be the hydrophobic effect, whereby nonpolar residues are preferentially sequestered within the protein's core. [5, 6, 9] This process also increases solvent entropy by displacing ordered water molecules, further stabilizing the folded state [8].
Even though the forces governing protein folding have been extensively explored, their relative contributions remain debated. [10] Moreover, the free energy difference between folded and unfolded states is relatively small (10-15 kcal/mol), making proteins inherently prone to misfolding and aggregation [7, 11, 12]. This highlights the need for a deeper understanding of the molecular interactions and forces that govern protein stability.

1.1.2 Folding speed and mechanism

A polypeptide chain can adopt an astronomically large number of conformations at the atomic level. For a 100-residue protein, the number of possible conformations is estimated to be around 10^{70}. If protein folding occurred through a random search of all possible conformations, it would take an impractically long time to reach the native structure. However, the typical folding timescales are more on the order of milliseconds to seconds. Thus, how does a protein find its native structure so quickly? First highlighted by Cyrus Levinthal in 1969, this conundrum later became known as the *Levinthal Paradox*. [13, 14]
This paradox suggests that proteins must fold through a more directed mechanism rather than blindly searching all possible conformations. An explanation was given using the concept of folding funnels. Protein folding is driven by the formation of stabilizing interactions, such as hydrophobic contacts, hydrogen bonds, and van der Waals forces, which progressively lower free energy. As energy decreases, the number of accessible configurations, which determine the conformational entropy, is also decreased leading to a funnel-shaped protein-folding energy landscape. (**Fig. 1.1a**)[1]

While the folding funnel model describes the energetic landscape of folding, it does not describe the microscopic folding routes that proteins follow. Despite numerous proposed protein folding models (**Fig. 1.1b**), no universal mechanism has been established that applies broadly across all proteins. This indicates that folding pathways can be highly unique and different folding mechanisms may be applicable to varying degrees depending on the protein in question. However, many of the proposed models follow some general principals. Based on local conformational preferences in the chain, such as helices and turns, secondary structure may form first. This is followed by the growth into more global structures by including increasingly more surrounding chain. Each folding step must overcome an entropy-driven barrier, as forming new contacts restricts conformational flexibility. However, once partially folded structures stabilize, subsequent steps can become increasingly directed. Thus, this "local first, global later" process speeds up conformational searching as not all accessible conformations get sampled through a random search. [2, 5, 6, 13]. This serves as one unifying idea among other theories to describe different microscopic folding pathways.

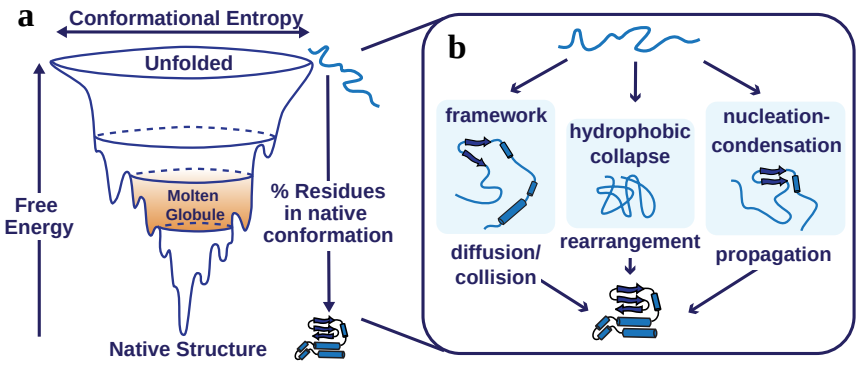

Figure 1.1 | Folding funnel free-energy landscape and different protein folding models. **(a)** A schematic representation of the protein folding funnel, illustrating the progressive decrease in conformational entropy and free energy as a polypeptide transitions from an unfolded state to its native structure. The rugged landscape reflects the presence of intermediate states and kinetic traps. The molten globule state represents an ensemble of folding intermediates for a protein that has undergone hydrophobic collapse but still lacks many interactions of its final native state. Proposed folding mechanisms, aiming to explain the microscopic folding routes between the unfolded state and the native structure, are shown in (b). **(b)** Schematic representation of protein folding mechanisms. **Framework model**: Secondary structure is formed first. Through interactions or collisions further advanced folding intermediates are formed, followed by side chain packing. **Hydrophobic collapse**: Folding starts with a collapse of the chain driven by its hydrophobic regions, which is followed by the formation of secondary and/or tertiary structure. **Nucleation-condensation model**: Folding starts with the formation of a nucleus, from which secondary and tertiary structures are propagated in parallel. This mechanism predicts a lack of intermediate states. Thus, it is best applied to the folding of small, single-domain proteins.

Funnel-shaped energy landscapes predict that folding doesn't follow a single microscopic pathway and different individual molecules of the same protein sequence may follow different routes to the same native structure. (**Fig. 1.1a**) Protein folding becomes even more complex in the crowded cellular environment, where interactions with other molecules can alter the folding landscape. Ongoing research explores how the folding funnel is shaped by the crowded cellular environment and how this differs from folding in dilute conditions. [15, 16]

1.1.3 Computational protein structure prediction from amino acid sequences

Predicting a protein's three-dimensional structure from its amino acid sequence has been a long-standing challenge. The long history of these efforts is exemplified by CASP (Critical Assessment of Protein Structure Prediction), a biennial competition initiated in 1994. This community-wide blind competition challenges researchers to predict unknown protein structures based solely on amino acid sequences. [2] In the 2020 14th CASP assessment unparalleled levels of accuracy were achieved with Google's AlphaFold2 deep learning mechanism. [17]
All successful structure-prediction algorithms are based on the assumption that similar sequences lead to similar structures. [2] AlphaFold2 follows the same fundamental assumption but achieves unprecedented accuracy through artificial intelligence and advanced neural network architectures. With an average root-mean-square deviation (RMSD) of approximately 1.6 Å, AlphaFold2 achieves accuracy approaching experimental resolution in many cases [17].
This led many to declare the protein-folding problem solved, but limitations quickly became apparent. AlphaFold2 is not able to reveal folding pathways, misfolding, dynamic conformational changes, or the molecular interactions critical for biological mechanisms and drug design. Structural heterogeneity, a key factor in many biological processes, remains difficult to capture through structure prediction alone. Thus, while AlphaFold2 represents a significant step forward, the protein-folding problem is far from fully solved. [18–22]

1.2 | What's next? The new era of the protein-folding problem

Section 1.1 gives insights into the tremendous advances made in regard to solve the protein-folding problem. Nowadays, many conceptual aspects of protein folding are considered well understood and established. However, decades of research have revealed something else as well: despite initially being regarded as a question belonging to the realm of biochemistry, protein-folding quickly evolved into an entire research field, demanding input from physicists, chemists and biologists equally. [2, 23] Naturally, the research itself became increasingly complex. Starting off by studying small model proteins in isolation, nowadays the focus has shifted toward understanding how folding is orchestrated within more complex systems and how it is influenced by interactions with other molecular factors.
For example, chaperone-mediated and cotranslational folding can lead to a radical reshaping of the conformational space explored by the polypeptide chains. How interactions with other cellular components and cotranslational folding reshapes

the folding funnel energy landscape and thus ultimately influences the success or failure of protein folding is among the central research questions in the field today. [16]
In the end, the protein-folding problem should no longer be viewed as a question with simple binary answers. [1, 2] It has grown far beyond that, serving as a beautiful example of how scientific progress unfolds. Often, understanding the foundations of a problem opens up even more possibilities for exploration rather than narrowing them down. The interdisciplinary nature of protein-folding research, which has shaped the field so profoundly, now finds its counterpart in the research subjects themselves: proteins act solely alone, nor are they always able to fold completely independently. 30-50% of all proteins have been estimated to oligomerize, but how individual subunits assemble remains incompletely understood [24–26]. Similarly, the impact of chaperone-assisted and cotransnational folding is not to be underestimated and still holds many unknowns and potential for new discoveries.
Thus, even though some of the original questions surrounding the protein-folding problem have been answered, they have also given rise to many new ones. An exciting new era has emerged, focusing on the complexity of inter-molecular interactions. With this we are only now starting to get closer to deciphering the fundamental mechanisms essential for maintaining proteome homeostasis and with this the overall cellular and organismal health. The following sections aim to highlight some of the recent findings in this context.

1.2.1 The Ribosome: Significant beyond protein synthesis

Folding often begins cotranslationally, meaning it occurs simultaneously with the synthesis of polypeptides on the ribosome. In this process, the ribosome actively shapes the energy landscape of the growing polypeptide chain, modulating its folding pathway.[27–30] The significance of cotranslational folding is highlighted in the striking differences observed between protein folding on the ribosome and free solution. After unfolding, many proteins are not able to refold, misfold or aggregate in solution. [31, 32]. These folding pathway differences remain incompletely understood. However, several factors have been determined which uniquely regulate cotranslational folding. These include the vectorial nature of nascent peptide synthesis (from the N- to the C-terminus), the geometry and physico-chemical environment of the exit tunnel, interactions at the ribosome surface, and the non-uniform rate of translation. [27, 33]

Translation rates and rhythm

Usually, the time it takes for tertiary structure to form is significantly shorter (μs-s) than the translation process, which occurs at a rate of 1–20 amino acids per second, depending on the organism. Due to these large timescale differences, cotranslational folding is often thought to take place under quasi-equilibrium conditions. Thereby, at early stages of translation the chance of aberrant interactions between amino acids is reduced. Additionally, the possibility of other cotranslational processes to occur is provided, such as chaperone binding, which further assist structure formation in the crowded cellular environment. [27, 28] Moreover,

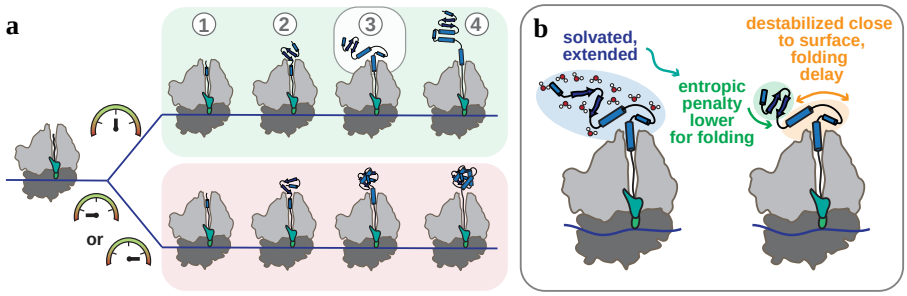

Figure 1.2 | Modulation of protein folding by the ribosome **(a)** Altered translation kinetics (bottom, red), e.g. being slower or faster compared to an optimal translation rate (top, green), can lead to protein misfolding. Top: Vectorial translation and interactions with the ribosome shape the folding pathway. (1) Confinement of the exit tunnel promotes formation of secondary structure. (2) The nascent chain can compact to small tertiary structure at the ribosome's wider vestibule. (3) The negatively charged ribosome surface destabilizes folding intermediates, but also promotes cotranslational folding (see (b)), preventing premature folding. (4) With increased distance to the ribosome surface the protein can stably fold into its native structure. Figure adapted from Komar *et al.* [27]. **(b)** Close to the ribosome surface the nascent chain is extended leading to high solvation by water, which reduces the entropy of the water molecules. Hence, the entropic penalty of folding is lowered, promoting the formation of folding intermediates, though the native state remains destabilized close to the ribosome surface due to space constraints and electrostatic interactions. [34]

the rhythm of translation influences protein production and folding. Synonymous codon usage, mRNA secondary structures and charged patches in the amino acid sequence can lead to non-uniform local translation kinetics modulating the pace of protein synthesis with specific pause sites to guide the folding pathway towards the native structure. Deviations from the natural translation rhythm may lead to misfolding and trapped intermediate states. (Fig. 1.2a) The substitution of synonymous variants encoding the same amino acid can lead to proteins with different structural and functional properties. [27, 35, 36] In some cases, naturally occurring single synonymous codon mutations were found to be linked to disease [37–39]. Similarly, patches of charged amino acids can alter the translation rate and play an important role in modulating protein folding. [40] Depending on their location in the exit tunnel positively and negatively charged amino acids have different effects. The ribosomal exit tunnel is lined with negative charges causing a non-uniform negative electrostatic potential inside the tunnel. The electrostatic interactions between nascent polypeptides and the tunnel may delay tertiary structure formation and stretches with negatively charged residues can even cause translation arrest, premature termination and ribosome destabilization.[41, 42]

Ribosome exit tunnel and surface

The ∼100 Å long and 10-20 Å wide exit tunnel modulates, together with the ribosome surface, the dynamics of the nascent chain. [29] Initially, the roughly cylindrical tunnel provides a confined folding space for the newly synthesized polypeptide.

The confinement was shown to promote compaction as early as a nascent peptide length of 13 amino acids and to facilitate secondary structure formation by entropically destabilizing the coiled state, favoring the formation of α-helices [43–46]. As the tunnel gradually widens (reaching >20 Å at the vestibule), long-range interactions become possible, allowing the formation of tertiary structure intermediates. [47, 48] (**Fig. 1.2a**) Moreover, the tunnel's environment has been suggested to accelerate folding and stabilize partially folded states, preventing premature aggregation. [49]

Beyond the exit tunnel, the ribosome surface introduces additional complexity. Its negatively charged environment has multiple effects on nascent chains: it can destabilize native states while promoting cotranslational folding intermediates. These seemingly contradictory effects arise from complex enthalpy-entropy compensation considerations.

It was shown that on the ribosome, the nascent polypeptide is structurally expanded, forming fewer long-range contacts partly due to steric exclusion and tethering effects. This expansion results in increased solvation compared to isolated polypeptides off the ribosome, which form more compact conformational ensembles in solution. Water molecules bound to the polypeptide have lower entropy than free water molecules, which leads to a destabilization of the nascent chain on the ribosome. The highly solvated state is entropically more unfavorable than the less solvated free polypeptides. Since the nascent chain has a lower entropy, the entropic penalty of folding is also lowered, which in turn promotes partially folded intermediates. However, native states remain enthalpically destabilized close to the ribosome surface probably due to space constraints of the ribosome's vestibule and electrostatic effects. Thus, the ribosome stabilizes intermediate states and pushes folding to occur sequentially, but simultaneously destabilizes the native state close to the ribosome surface. (**Fig. 1.2b**) In this way, the ribosome introduces intermediates that are not observed in solution, potentially mitigating harmful misfolding events. [34, 50, 51]

Emerging role in protein complex formation

Beyond modulating the folding of individual proteins, recent findings indicate that complex formation is also facilitated by coupling protein synthesis with assembly. [52–54] Until recently, the prevailing assumption was that protein complex formation is driven by diffusion and random collisions between fully synthesized and folded partner subunits, a mechanism known as post-translational assembly (**Fig. 1.3a**). However, this pathway faces significant challenges in the crowded cellular environment, such as increased risk of aggregation and degradation. [52, 55]

The discovery of mechanisms that directly couple assembly with translation may offer several advantages over the post-translational assembly pathway. For instance, unstable subunits are thought to spend less time unengaged by their interaction partners, which could help to reduce nonproductive interactions and would allow for folding and assembly to occur in a synchronized and timely manner. [56, 57]

Two main mechanisms of translation-coupled protein complex assembly have been identified. In the co-post-translational assembly pathway, a nascent ribosome-bound protein subunit was shown to interact with a fully synthesized and folded partner

[53, 58] (Fig. 1.3b). However, this sequential process is also thought to pose specific challenges, particularly in achieving the necessary spatial coordination between subunits. In prokaryotes, colocalized translation and assembly may be supported by the ordered arrangement of genes into operons [53]. In contrast, the corresponding mechanisms in eukaryotic cells remain largely unclear. Given that eukaryotic cells lack polycistronic mRNAs, alternative regulatory mechanisms, such as electrostatic interactions between nascent chains and the ribosomal surface, translation elongation rates, and interactions with molecular chaperones, have been proposed to facilitate assembly. [54, 56, 57, 59]

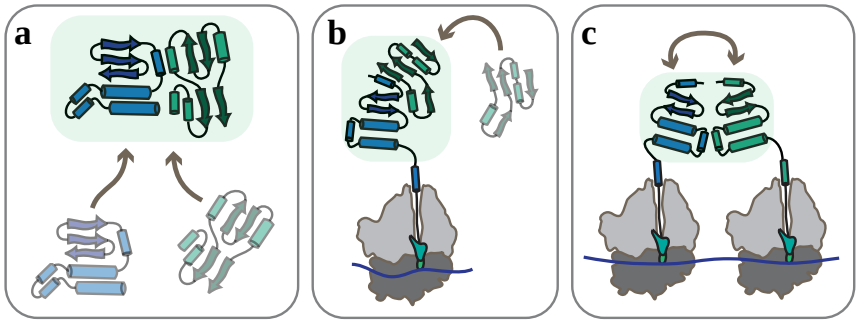

Figure 1.3 | Mechanisms of protein complex formation. **(a) Post-translational assembly**: Fully synthesized and folded partner subunits diffuse and form a complex by random collision. **(b) Co-post-translational assembly**: One fully synthetized protein subunit interacts with a nascent, ribosome-bound subunit. **(c) Co-co assembly**: Two nascent subunits begin to interact during their concurrent translation.

A second, more recently uncovered mechanism, termed co-co-assembly, represents another pathway of protein complex formation at the ribosome (Fig. 1.3c). Here, two nascent subunits begin to interact already during their concurrent translation by neighboring ribosomes. This interaction can either occur in cis, if the subunits are synthesized on the same mRNA, or in trans, if nascent chains are synthesized on different mRNA molecules. [60]
These mechanisms add yet again to the ribosome's extensive role in protein folding and complex assembly. They also raise numerous new questions, especially as emerging evidence suggests that translation-coupled assembly mechanisms are more prevalent than previously thought. [56] Understanding how faithful complex assembly is coordinated, and identifying which proteins particularly rely on these mechanisms is now a central focus of research [55, 61], and will also be one of the major focal points of this thesis. More detailed discussions will follow in the subsequent chapters.

1.2.2 Chaperones: Major regulator of proteostasis

The folding pathway of proteins often entails a series of intermediate states before the native structure is achieved. The likelihood for proteins to populate globular

intermediates increases with larger, topologically more complex domain folds. For multidomain proteins it can take minutes to hours to fold [62] and sometimes they fail to fully reach their native state *in vitro*. In the highly crowded cellular environment, the folding task becomes even more challenging. Incompletely synthesized polypeptide chains can also experience delay in folding until their translation is complete. Generally, nascent chains remain in an unfolded conformation for longer on the ribosome than off. [63] These unfolded or partially folded states are potentially problematic, as they expose hydrophobic residues to the solvent, increasing the risk of misfolding and nonspecific association with other polypeptide chains. This can lead to the formation of toxic oligomers or ordered amyloid fibrils. Many diseases, like neurodegenerative disorders, are associated with these aberrant protein conformations. [64, 65]

The cell addresses these challenges through a complex network of protein machinery known as chaperones. Molecular chaperones are proteins that interact with, stabilize, and assist other proteins in attaining their functional conformation without becoming part of their final structure. Chaperones support *de novo* folding, oligomeric assembly and refolding of stress-denatured proteins. Consequently, the chaperone machinery is quintessential for minimizing protein aggregation and thereby for the maintenance of the whole proteome. Deletion of their genes is often lethal or causes severe cellular defects. [65–67]

In human cells, this extensive network entails around 200 chaperones, which can be found in all cellular compartments, where conformational rearrangements of proteins occur. Several classes of molecular chaperones exist and are usually classified according to the molecular weight. [65] Due to the vast diversity of proteins, a detailed description of every functional aspect of each chaperone is not feasible in this context. However, most molecular chaperones exhibit common functional characteristics in which they operate and influence the folding energy landscape. [66]

Functional Properties of Molecular Chaperones

In general, chaperones are thought to associate with unfolded conformers and partially folded states. During those folding stages, the hydrophobic residues of the protein are partially exposed to the solvent. The low specificity of the hydrophobic interaction enables chaperones to bind to a wide range of polypeptides, regardless of differences in amino acid sequence or conformation. Through binding hydrophobic regions, chaperones fulfill a so-called 'holdase' function, blocking aggregation with other molecules. Furthermore, chaperones can induce conformational changes. By unfolding protein substrates in an 'unfoldase' function, chaperones can reverse non-native contacts, preventing misfolding and allowing another opportunity for proper folding upon release. In contrast, cylindrical chaperonins facilitate folding by enclosing single protein molecules in a cage. (**Fig. 1.4**) Chaperones with distinct functions often act sequentially, either interacting upstream with nascent and newly synthesized polypeptides or downstream to assist final folding of proteins that have failed to achieve their native state so far. Another feature of chaperones is the controlled release of substrates, typically achieved by transitioning to an alternate state with reduced affinity for hydrophobic polypeptides. This state change requires

energy, which often comes from the hydrolysis of ATP. The formation of the native state, and with it the burial of hydrophobic regions, can also lead to substrate release for ATP-independent chaperones. [65, 66]

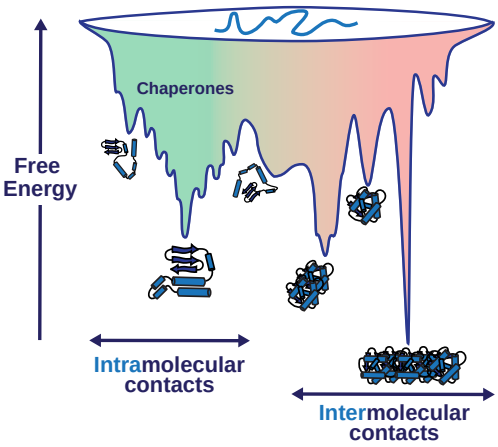

Figure 1.4 | Folding funnel energy landscape with chaperones. The ruggedness of the free-energy landscape can lead to kinetically trapped conformations. Partially folded intermediate states may promote intermolecular aggregation *in vivo* by interacting with other concurrently folding protein substrates, leading to the formation of amorphous aggregates, toxic oligomers, or structured amyloid fibrils (red). Molecular chaperones help to prevent harmful polymerization and support the folding process towards the native structure in various ways. Figure adapted from Hartl *et al.* [65].

These descriptions barely do justice to explain the complex mechanics of chaperone-assisted protein folding. Additionally, many aspects, including substrate specificity, the role in mediating the assembly of oligomeric complexes and functional variation across different cellular contexts, are still not fully understood. For example, functions might differ when substrates are engaged cotranslationally compared to free in solution. [68] This is illustrated in chapter 2, which dives deeper into the diverse set of functions of the bacterial ATP-independent chaperone Trigger Factor.

1.3 | Optical tweezers: A tool to unveil detailed folding dynamics

Protein folding is an inherently dynamic process. Thus, it can be understood best when all the steps between the unfolded conformation and the native structure of the protein become apparent. Full understanding of the folding pathways would additionally allow to determine when and how folding fails and how other factors like the ribosome and chaperones shape the folding process and help to avert misfolding. However, as we have seen from the previous sections, gaining a detailed mechanistic insight into the underlying molecular processes is often the most difficult and challenging. This is mainly because intermediate folding states are often transient and very short lived making it hard to study them, especially for many structural methods which rely on a stable state of the protein. [69] Other methods that aim to follow dynamic molecular processes over time have largely depended on traditional ensemble approaches, where the native state of the protein is disrupted by introducing chemical denaturants like urea. Consequently, the obtained folding pathways inevitably include the asynchronous contributions of all molecules in the ensemble, resulting in an average of their behavior. [70, 71]

The aim of obtaining more detailed molecular trajectories, has given rise to single-molecule methods, where one molecule at a time is studied. Among those, optical tweezers are part of the most frequently used techniques and are also the main technique used within the work presented in this thesis.

How to exploit the power of light?

Optical tweezers rely on the fact that every photon carries a momentum. This momentum only has little effect on the macroscopic world, but if light is focused into tiny volumes it can exert a force on micrometer scale objects towards the point of the highest intensity. In 1970, Arthur Ashkin was the first to exploit this fact and demonstrated how tightly focused laser beams could be used to trap and manipulate the movement of micron-sized spheres suspended in water.

The physical description of this phenomenon depends on the size of the trapped object relative to the wavelength of the trapping light. If the object is much smaller than the wavelength, it can be treated as a Rayleigh or Mie scatterer. However, if its diameter is comparable to the wavelength of the trapping light, the principles of ray optics can be applied. Since most biological optical tweezers applications fall into the latter category, this case will be explored in greater detail below.

A trap is formed by tightly focusing a Gaussian beam with a high numerical aperture objective lens into a transparent sphere with a refractive index higher than its surroundings. When the focus is precisely at the center of the sphere, symmetry ensures that the light exits the sphere unchanged, keeping it stationary (Fig. 1.5a).

However, if the sphere is displaced laterally or axially from its equilibrium position, the momentum of the light leaving the sphere changes, which generates a restoring force. If the sphere is displaced axially, the divergence of the laser beam is altered. A divergent beam has many rays at large angles to the optical axis, reducing the axial component of its momentum, which leads to an axially acting restoring force (Fig. 1.5b,c). In contrast, if the bead is displaced laterally, the light is deflected in the direction of the displacement, causing a force that pulls the sphere back laterally to its equilibrium position. (Fig. 1.5d) [72]

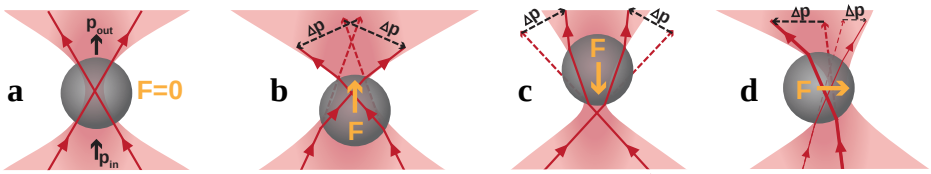

Figure 1.5 | Ray optics sketch of optical tweezers forces due to refraction. **(a)** The trapped sphere is at its equilibrium position, in the center of the trap. Light passes through the sphere unchanged, thus the light's momentum is not changed and the trapped sphere experiences no force. **(b)**, **(c)** Axial displacements alter the divergence of the laser beam, which changes the light's axial momentum, resulting in an axial restoring force. **(d)** Lateral displacement leads to deflection of the light passing through the sphere, changing the light's momentum, resulting in a laterally acting restoring force.

Thus, any displacement of the sphere leads to a change in momentum flux, resulting in a restoring force known as the gradient force. The potential energy of a nearly Gaussian beam is locally harmonic, allowing the trap to be modeled as a Hookean spring. Thus, the gradient force acting on the sphere can be determined by

$$F(x) = -\kappa(\Delta x) \tag{1.2}$$

where κ is the trap stiffness matrix and Δx is the displacement of the sphere. The trap stiffness is critical to determine the force accurately. It is inverse proportional to the sphere radius and influenced by the used laser power. [72–74]
Not all light transmits through the sphere, it also gets partly reflected. Hence, in addition to the gradient force, a scattering force occurs. This force pushes the particle in the direction of light propagation and is proportional to the laser intensity. For stable trapping, the gradient force must be strong enough to counteract the scattering force, but in most cases the scattering force only causes the particle to be positioned slightly behind the focal point. Additionally, gravitational and buoyancy forces also play a role. The equilibrium trapping position is determined by the balance of all these forces. [72]

Optical tweezers for protein folding

In 2018, Ashkin was awarded half of the Nobel Prize for his invention of optical tweezers, but also for his breakthrough work on their application to biological systems. Since his success in trapping bacteria without harming them, the application field of optical tweezers has broadened tremendously. Now we are able to manipulate matter as small as proteins with optical tweezers. [75]
But how? Typically, two optical traps are created within the focal plane of a single inverted microscope objective, with one trap capable of being moved or steered relative to the other. Proteins can be "tethered" between two optically trapped beads using DNA molecules, for example. As one trap is moved, the distance between the trapped beads increases, exerting pN-level forces on the tethered molecule and gradually stretching it. The force gradually increases as the beads are being pulled apart or decrease as the beads are being brought closer together, resulting in typical force-extension traces. Sudden extension jumps indicate unfolding events, while abrupt contractions signify a compaction event. [70] (**Fig. 1.6**) Hence, conformational changes and folding intermediates can be detected, which is otherwise difficult to achieve. Such experiments provide valuable insights about the energy landscape of the folding process. Apart from the here described experimental approach, multiple other measurement modes and trapping geometries exist, which are explained in great detail elsewhere. [70, 73]
Analysis and interpretation of optical tweezers data is often not straight forward. Applied forces change the protein's free-energy landscape. Although models exist to describe how kinetic rates depend on force, they are not always sufficient to describe experimental data. [70, 71] Moreover, it is often difficult to infer which structural elements of a protein fold or unfold during state transitions, especially if heterogeneous unfolding and refolding pathways are observed. Moreover, like any method, optical tweezers have inherent limitations. Tethering of molecules can be rather complex and not without effect on the studied molecule. For example,

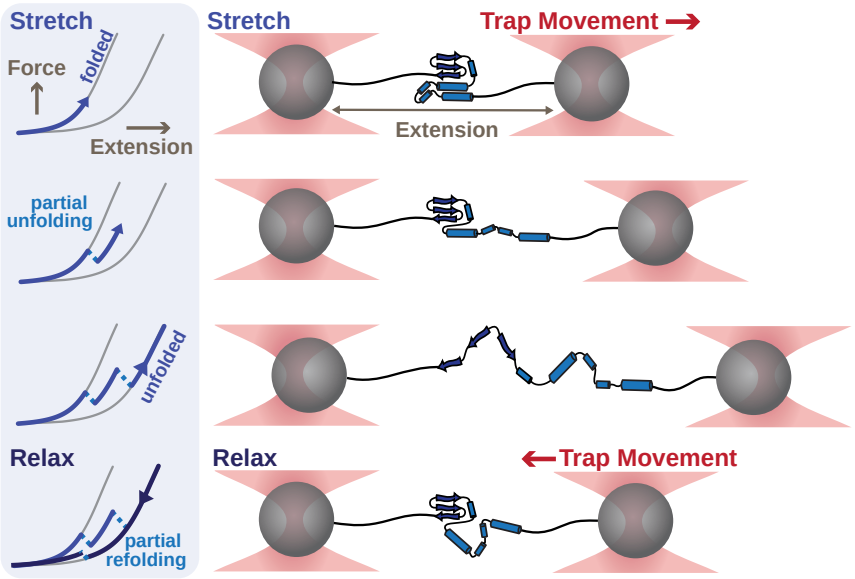

Figure 1.6 | Schematic of a typical force spectroscopy measurement (right) and corresponding data (left). Measurement procedure: Protein of choice is tethered between two optically trapped beads. By moving one trap, the distance between the beads (extension) is increased and a force is exerted on the protein. Unfolding events are visible in the force-extension trace as a sudden jump in the extension (left). After a 'stretch' cycle, the distance between beads is decreased again in the 'relax' cycle. Refolding events are observable by a sudden jump in the extension again. Grey lines in the force-extension data depiction (left) indicate the theoretical forces and extensions for a compact folded state and an extended unfolded state of the protein derived through the worm-like chain (WLC) model. Thereby, conformational changes and intermediate states are detectable within the protein (un-)folding pathway. After the relax cycle usually a waiting time at 0pN follows to allow for folding without force (not shown), before stretch-relax cycling is repeated.

despite constituting a small contribution compared to other relevant energies, DNA linkers can reduce the chain entropy. High forces can lead to melting of the DNA handles, whilst at small forces the measurement signal is likely to be drowned in Brownian noise. As a result, most measurements are conducted within a range of approximately 2 to 60 pN. [76] Thus, optical tweezers can be integrated with other techniques like integrated simultaneous fluorescent measurements and bulk studies. Once again we see that, even within the applied method, protein folding is best explored by multiple interdisciplinary approaches. The following experimental chapters are aimed to illustrate how different methods can be combined in order to achieve a better understanding of the folding pathways. They also entail a more detailed description of the optical tweezers assays and diverse analysis methods, hence this section only aimed to provide a brief overview of what will be following.

Chapter 2

UNVEILING FUNCTIONS OF TRIGGER FACTOR WITH SINGLE-MOLECULE STUDIES

F. Wruck, M.J. Avellaneda, M.M. Naqvi, E.J. Koers, **K. Till**, L. Gross, F. Moayed, A. Roland, L.W.H.J. Heling, A. Mashaghi, S.J. Tans
Royal Society of Chemistry **29**, (2023)

Proteins begin folding as they emerge from the ribosome, often guided by molecular chaperones like Trigger Factor (TF). Once thought to merely prevent aggregation, TF dynamically reshapes the folding landscape, stabilizing intermediates, modulating energy barriers, and steering proteins toward their native states. Recent single-molecule optical tweezer studies reveal a far more intricate role than previously imagined. This chapter explores the evolving picture of TF and how single-molecule studies have helped to unravel the intricate dynamics of TF-mediated protein folding.

2.1 | Trigger Factor: A more versatile chaperone than previously thought

As soon as they exit the ribosomal tunnel, nascent chains can interact with a plethora of proteins that could affect their folding pathway and dynamics, which optical tweezers can uniquely address. In bacteria, the chaperone trigger factor (TF) is directly associated with the ribosome, at the tunnel exit, and hence it is typically the first chaperone that nascent chains interact with [77, 78]. Discovered in 1987 [79], TF is not essential as deletion of the TF-encoding gene *tig* seems to be compensated by enhanced action of the chaperones DnaK and GroEL [78]. However, a combined deletion of TF and DnaK was found to be lethal above ~30 °C, causing misfolding and aggregation of several hundred cytosolic proteins [77]. Despite sharing a lot of overlapping functions with DnaK and GroEL, the ATP-independent TF appears to engage with protein chains in a unique way, which leaves many open questions about how TF affects the folding process.Over the last decades, a wide range of techniques ranging from structural to single-molecule studies have been employed to decipher the function of TF.

2.1.1 Trigger Factor Structure

The 48 kDa TF protein consists of three domains, the N-terminal, C-terminal and the PPIase domain, namely because this domain displays catalytic activity as peptidylprolyl cis/trans isomerase. [78] Together these domains adopt a dragon-shaped structure, where the N-terminal domain forms the "tail", the PPIase domain the "head" and the C-terminal domain a central body, constituting nearly half of the TF molecule and residing between N-terminal and PPIase domains with two protruding "arms" [77] (Fig. 2.1). TF binds to the ribosome via its N-terminal domain, using the ribosomal exit-site proteins L23 and L29 as major docking sites [80]. Ribosome binding stabilizes TF in an open conformation, creating a cradle-like cavity between the ribosomal surface and the N-terminal tail and the C-terminal arms of TF, which is about 40 Å deep and 35 Å wide [81, 82]. The open cavity is thought to be linked to the function of TF, which is incompletely understood however [77].

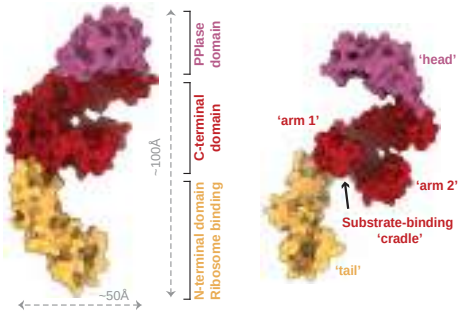

Figure 2.1 | Trigger Factor structure (pdb:1W26). Different colors indicate separate domains.

2.1.2 Ribosome-independent functions of Trigger Factor

For a long time, it has been thought that the open cradle-shaped cavity provides a protective environment for emerging nascent chains, shielding them from unwanted

interactions with their hydrophobic segments as well as with other cellular components, thereby preventing aggregation and protein degradation [83–85]. Thus, TF was believed to fulfill a classic holdase function that stabilizes unfolded states [86]. However, single-molecule studies revealed several other functions, including the ability to bind and stabilize partially folded states and promote correct folding [87, 88]. The first studies focused on fully synthesized protein substrates, away from the ribosome. In cells, TF is present in a two- to threefold excess relative to ribosomes, suggesting that it may also play a role when not bound to the ribosome [77].

In one study, optical tweezers were used to study the impact of TF on folding pathways [87]. In data from repeated relax-wait-stretch cycles, unfolding and folding transitions are observed as increases and decreases in the extension, respectively, noting that chain segments that are extended by tension can be orders of magnitude longer than folded ones. The maltose binding protein MBP was found to show a distinctive (un)folding pathway, which was significantly altered in the presence of TF. Partially folded states were "visited" more frequently, for longer, and resisted higher forces, suggesting that TF directly binds the folded part of the protein chain, not just the unfolded chain [87]. At zero force, the protein chain continued to fold, observable by reductions in measured extension, and hence was not irreversibly stabilized by TF. Within tandem-repeated MBP constructs, TF increased the probability of each MBP copy to adopt the native core structure, while decreasing the probability to engage with neighboring MBP copies to form aggregated structures. Together, these data indicated that by binding partially folded structures, TF shields them from non-native interactions with distant sites along the protein sequence [83, 87] (**Fig. 2.2**).

Notably, a subsequent magnetic tweezer study showed that the interaction of TF depends on the extension of the substrate chain, as modulated by mechanical tension [88]. Here, the experimental procedure differs slightly, and for instance allows extended and unfolded proteins to rapidly jump to a particular force, after which folding is monitored as extension decreases in time. Specifically, for the small globular protein L, it was found that the folding probability for an intermediate force regime (5-9 pN) is increased by up to ∼40% in the presence of TF. At zero force the chaperone appeared to hinder the refolding transition, fulfilling potentially a stabilizing function [88].

Taken together, these single-molecule results provided insights into how TF reshapes the folding free energy landscape (**Fig. 2.2a**) away from the ribosome. The stabilization of partially folded states indicates the formation of energy minima in between the unfolded and fully folded states, or a deepening of existing ones. Such minima may in fact decelerate folding within individual substrate repeats. But at the same time the 'spatial separation' of different substrate repeats by TF raises kinetic barriers towards aggregated states, as revealed by the tandem MBP repeats [83]. Increased folding rates mediated by TF may also be caused by an overall lowering of the folding energy barrier, which we here refer to as folding acceleration, and hence also impacts single substrates in the absence of aggregation. Folding energy barriers can be effectively reduced by lowering the entropy of the unfolded chain, which may be achieved by multiple contact sites on the chaperone

surface, even as contacting must remain dynamic and thus preserve entropy to continue folding, yielding what has been termed a 'fuzzy complex' [89, 90]. The inner surface of the TF cradle exposes hydrophilic and hydrophobic residues and continuous hydrophobic patches, which may enable TF to interact in this fashion, with substrates of diverse compositions and sizes [85, 91]. Stabilization of partially folded states cannot be explained by binding to unfolded substrate segments, however. TF may instead interact with patches on the folded substrate surface, which are exposed when partially folded and not accessible when fully folded. This idea is supported by the observation that TF does not interact with fully folded substrates in optical tweezers experiments [87]. Additionally, simulations showed that TF

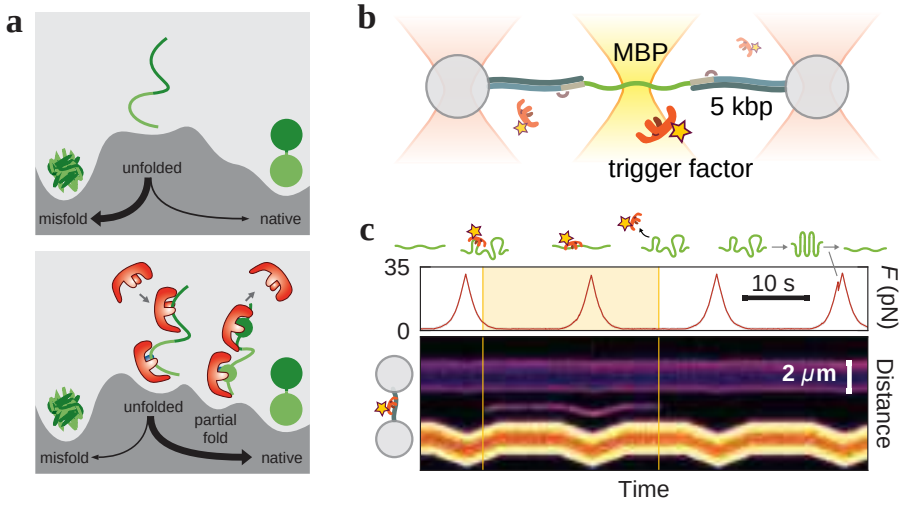

Figure 2.2 | Trigger factor mechanisms revealed by substrate manipulation studies. **(a)** Cartoon of how folding landscapes can be reshaped by trigger factor, as observed in optical tweezers studies of single-domain and engineered multi-domain substrates [87]. Top: without chaperone, interactions between domains lead to efficient misfolding. Bottom: trigger factor binds and stabilizes not only the unfolded chain, but also intermediate states with stable tertiary structure, which corresponds to the formation of energy valleys or the deepening of existing ones. Owing to the resulting protection against interactions between domains, the folding barrier against misfolding is increased, thus limiting interdomain misfolding. Hence, native folding is promoted indirectly by limiting misfolding pathways. Trigger factor can also be seen as setting a length scale for native folds, as its binding effectively promotes local over distant intra-chain interactions. **(b)** chematic of combined optical tweezers and fluorescence study of chaperone–substrate interactions. A key technical challenge is to attach long DNA handles efficiently and stably, in order to increase the distance between the substrate and the bead surface. The bead surface is typically highly fluorescent and thus perturbs fluorescence detection at the substrate location [92]. **(c)** Corresponding kymograph during stretching and relaxation cycles shows a single fluorescently labelled trigger factor binding to and unbinding from the tethered MBP protein (thin line in the center) [92]. The data is consistent with MBP refolding less frequently when trigger factor is bound [87]. Here, MBP does refold when unbound, as seen by the unfolding feature at the end of the force–time trace [92].

employs the flexible arms and polypeptide loop at its tips to interact with its substrates forming "touching" and "hugging" complexes in a dynamic way [91].

2.1.3 Functions of Trigger Factor at the ribosome

First single-molecule results on TF roles at the ribosome have been reported recently [84]. A newly synthesized unfolded nascent chain segment of the multidomain protein elongation factor G was found to denature an already synthesized, and folded domain. While the ribosome alone did not protect against this denaturation, TF did, presumably by limiting interactions between the different domains. TF was also found to prevent interdomain misfolding and as a result speeds up folding, in line with the 'spatial separation' model discussed above (**Fig. 2.2**). The data also showed intermediate states with altered molecular extension in the N-terminal G-domain folding pathway in presence of TF. Considering the flexibility of TF it was suggested that these altered molecular extensions stem from binding of the nascent chain to several sites within TF's inner surface, which would reduce the extension of the protein while keeping it largely unfolded and entropy lowered, thus reducing inter-domain misfolding and promoting domain folding. It was also hypothesized that by forming multiple contacts spaced apart along the client protein chain, entropy is reduced, which in turn may also facilitate subsequent folding [84]. These novel single-molecule findings thus extend the picture that TF acts as an unfolded chain holdase that decelerates folding. NMR relaxation experiments had indeed shown binding to several distinct regions within TF's inner surface, suggesting TF keeps substrate proteins in an extended, unfolded conformation [85]. Earlier crosslinking studies had indicated that growing nascent chains initially follow a predefined, domain-wise, path through the entire interior of TF in an unfolded conformation, which indicated that TF can act as a holdase [78]. Another NMR study even indicated an unfoldase role of TF. By using all its substrate binding sites, TF may be able to unfold transiently formed structures [81, 85]. However, since TF cannot use ATP, it is assumed that its unfolding activity is restricted by the intrinsic thermodynamic stability of the substrate [81].
The ability of TF to form dimers has been highly debated [81, 93, 94]. The dimers may represent an inactive storage, as it occludes substrate binding and prevents promiscuous binding of TF [94–96]. TF dimerization could also impose a substrate-selection filter, with only high-affinity clients able to bind. Depending on size, folding state and amino acid composition, the emerging nascent chains increase the affinity of TF for ribosomes by about 2 to 30-fold (KD ∼40-700 nM) [83, 95, 97].
In conclusion, single-molecule optical tweezer studies have added a new dimension to the bulk-biochemical, NMR, and structural insights, thanks to their ability to follow large conformational changes and folding pathway dynamics. Since TF acts in a dynamic reaction cycle governed by translation, with a half-life of TF–ribosome nascent chain complexes of about 15 to 50 s, the detailed dynamics of how TF engages nascent chains are difficult to unveil [81, 83, 84, 93, 94]. Optical tweezers combined with fluorescence detection of chaperone binding will be a useful tool to address these questions.

I feared the fear
So I started holding it dear

Artist impression of trigger factor bound to a nascent chain
Fineliner, 2025
Katharina Till

Chapter 3

TRIGGER FACTOR ACCELERATES NASCENT CHAIN COMPACTION AND FOLDING

K. Till, AB. Seinen, F. Wruck, V. Sunderlikova, C.V. Galmozzi, A. Katranidis, B. Bukau, G. Kramer, S.J. Tans
PNAS **122**, (2025)

Conformational control of nascent chains is poorly understood. Chaperones are known to stabilize, unfold and disaggregate polypeptides away from the ribosome. In comparison, much less is known about the elementary conformational control mechanisms at the ribosome. Yet, proteins encounter major folding and aggregation challenges during translation. Here, using selective ribosome profiling and optical tweezers with correlated single-molecule fluorescence, with dihydrofolate reductase (DHFR) as a model system, we show that the Escherichia coli chaperone trigger factor (TF) accelerates nascent chain folding. TF scans nascent chains by transient binding events, and then locks into a stable binding mode as the chain collapses and folds. This interplay is reciprocal: TF binding collapses nascent chains and stabilizes partial folds, while nascent chain compaction prolongs TF binding. Ongoing translation controls these cooperative effects, with TF-accelerated folding depending on the emergence of a peptide segment that is central to the core DHFR beta-sheet. The folding acceleration we report here impacts processes that depend on folding occuring co-translationally, including co-translational protein assembly, protein aggregation, and translational pausing, and may be relevant to other domains of life.

3.1 Introduction

Elucidating the principles of protein conformation control is a major challenge in molecular biology [98]. Chaperones alter folded states throughout the proteome, which is key to efficient folding and aggregation suppression, and hence of general relevance to cellular function and malfunction. Determining the underlying effects on folding pathways is nontrivial, owing to the inherent dynamics, heterogeneity, and small length scales. Several chaperones are known to bind unfolded and partially folded conformers [65, 87, 99], which can suppress aggregation and unproductive interactions between domains – and hence indirectly promote folding. Direct folding acceleration of single-domain proteins was shown more recently for ATP-driven chaperone systems, either by limiting the entropic folding penalty [100] or by increasing the collapse energy of polypeptide chains [101]. Folding acceleration may be important to limiting the exposure of hydrophobic internal protein segments to the cytosol [102]. However, chaperone-induced conformational changes have been studied almost exclusively for fully synthesised proteins, while the most acute folding risks arguably arise co-translationally [103–107]. Moreover, recent work suggests chaperone interactions with nascent chains are far more prevalent than assumed [108–110].

In Escherichia coli, trigger factor (TF) is thought to be the only general chaperone that binds ribosomes directly. Its flexible protrusions form a cradle-like structure across the ribosome tunnel exit, yielding interactions with a large part of the proteome [78, 111–114]. Functionally, TF is generally thought to bind and stabilize unfolded conformers, and hence shield nascent chains from aggregation [115, 116]. Consistently, NMR showed fully synthesised unfolded proteins bound to TF, either as a conformational ensemble or in a single dominant conformation [85, 89, 117, 118]. Single-molecule techniques have shown that TF also suppresses misfolding interactions between domains [84, 87] and promotes folding of multi-domain protein constructs [88] away from the ribosome, and can rescue interdomain misfolding at the ribosome [84]. Whether TF induces conformational changes within nascent chains to accelerate their folding is unknown.

To address these issues, we used selective ribosome profiling to determine chaperone binding during different phases of translation *in vivo*, and employed optical tweezers with correlated single-molecule fluorescence to study how TF affects co-translational folding and stability *in vitro*. We identified E. coli dihydrofolate reductase (DHFR) as a model substrate: it has a small single-domain structure, yet is large enough to bind TF, but as we show does not interact significantly with the other major chaperones DnaK and GroEL during translation – which may confound TF-mediated effects. We found that TF triggers compactions in nascent DHFR, and thus strengthens the collapse of nascent chains. The resulting partially folded states are stabilized by TF against forced unfolding, indicating direct interactions between TF and the surface of partially folded nascent structures [87, 91]. Stabilization is not observed when a key beta strand within the DHFR structure remains untranslated or is still inside the ribosomal tunnel, indicating that specific surface features of the nascent protein are bound by TF or a minimum intrinsic stability is required. Simultaneous single-molecule fluorescence detection showed

increased TF binding times when the nascent chain was folded, consistent with TF binding to the partially folded structures. The findings indicate a reciprocal dependence, with TF interactions yielding nascent chain compactions, and in turn, nascent chain compactions yielding stabilized TF binding.

3.2 | Results

3.2.1 DHFR interacts with trigger factor late in translation

Selective ribosome profiling (SeRP) [114] was employed to assess TF binding during translation and to identify a protein substrate for single-molecule investigation. In this method, co-translational chaperone binding is studied by purifying chaperone-bound ribosomes and sequencing their mRNA footprints. We focused on the protein DHFR as it has a single domain, is comparatively small (159 residues), and is known to bind TF co-translationally [116, 119]. Consistently, the SeRP data showed significant co-translational TF association (**Fig. 3.1a**). The profile starts low, rises after 75 translated codons, and levels off after about 130 codons (**Fig. 3.1a**). TF binding thus increases strongly only after a nascent chain of significant length has emerged [114]. A continuously increasing profile would have suggested that TF binds with increasing number or strength as the nascent chain grows and additional binding sites become available. Conversely, the observed sigmoidal shape that levels off may indicate that one TF molecule binds, and does not dissociate until translation is completed. We surmise that the ribosome binding site for one TF molecule contributes to this sigmoidal binding profile. SeRP did not show significant binding of the chaperones DnaK and GroEL at any phase of DHFR translation (**Fig. 3.1a**), even as DnaK and TF can bind similar substrates and are known to partially compensate for each other's deletion [120, 121]. The chaperone SecB was recently also shown to not engage co-translationally with DHFR [109], showing that DHFR selectively interacts with TF during translation.

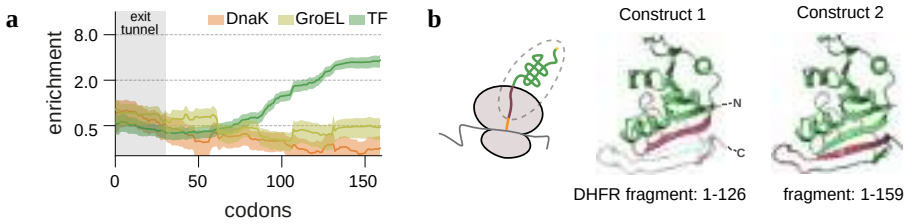

Figure 3.1 | DHFR interacts with trigger factor late in translation (a) Selective ribosome profiles of DHFR for DnaK (orange), GroEL (light green) and TF (dark green). Grey marks the size of the ribosome tunnel. **(b)** Constructs used. Orange: SecMstr arrest peptide (19 aa) at the C-Terminus. Shown are protein segments that are inside (red) and outside (green) the ribosome tunnel, or not translated (grey). A segment of 37 aa spans the ribosome tunnel [122]. Yellow: N-terminal biotin tag for DNA tethering. A beta stand (red in construct 1 image) that is key to stabilizing N-C-terminal contacts emerges when translating from construct 1 to 2. DHFR is fully translated for construct 2. Crystal structures: PDB 1RG7.

The SeRP data thus identified DHFR as a suitable model system and showed that TF interacts predominantly late during translation.

3.2.2 TF promotes partially folded states during translation

To study how DHFR nascent chain conformations are affected by TF we used optical tweezers. We defined two stalled constructs that interact with TF, as indicated by SeRP (**Fig. 3.1a**), while following these structural considerations (**Fig. 3.1b**). In construct 1, the first N-terminal part of the protein has emerged from the ribosome tunnel exit, but a beta strand that stabilizes interactions between the C- and N-termini has not. In construct 2, translation has progressed such that this key C-terminal beta strand is exposed. Note that the 18 most C-terminal amino acids reside inside in the ribosome tunnel at the end phase of translation, and hence are never exposed during translation.

To study constructs 1 and 2 with optical tweezers, we generated stalled ribosome-nascent chain complexes (RNCs) using a modified *in vitro* transcription-translation reaction with ribosomes that were biotinylated at the uL4 ribosomal protein on the large subunit [123]. The biotin tag allowed tethering of the ribosomes to micron-sized beads via DNA handles, with its placement ensuring unimpeded TF binding to its docking site near L23 and L29 [112]. A second biotin tag at the N-terminus of the nascent chain was co-translationally incorporated with an amber stop codon using suppressor tRNAs pre-charged with biotin. We used the secM strong stalling sequence [124] to stably attach the nascent chain to the ribosome [124, 125].

Two types of micron-sized beads were flown into a microfluidic chamber: one had RNCs attached via DNA handles and the other had solely DNA handles with a neutravidin at the opposing end attached (**Fig. 3.2a**). One of each was trapped by the optical tweezers, and then brought together, such that the biotinylated nascent chain N-terminus could link up to the neutravidin – thus forming a molecular 'tether' (**Fig. 3.2a**). Note that the RNC density was titrated down to achieve single rather than multiple tethers between the two beads. Next, the tethered nascent chain was subjected to repeated stretching-relaxation cycles, including a 5 second waiting time between relaxation and stretching at 0 pN, to allow for the chain to refold in absence of force (**Fig. 3.2a**). As is typical [49, 99], the measured force and extension (the distance between the beads) showed curved segments that indicated different stable folded states, as well as transitions between them that indicated folding and unfolding events (**Fig. 3.2b**).

Nascent chains in different folded states were characterized by their contour length, which is defined as the length of the unfolded part of the nascent chain. This contour length was determined by fitting the curved data segments to two worm-like chain (WLC) models in series, using the model of an extensible polymer for the DNA [126] and the Odijk inextensible WLC model [127] for the protein (**Fig. 3.2c**). Different RNC tethers were probed for both constructs in absence and presence of TF, each for several cycles, thus yielding histograms of folded states observed during these cycles, where a contour length of 0 nm thus denotes a fully compacted state (**Fig. 3.2d**).

In the absence of TF, the distributions for both constructs peaked at the end

of the length range, indicating that in most cases, the nascent chains were predominantly unfolded (**Fig. 3.2d**, top). Yet, the data revealed a broad distribution that extended to more compacted states, while at lower frequency (**Fig. 3.2d**, top). Hence, while DHFR nascent chains most often remain unfolded in absence of TF, a sub-population forms small partially folded structures. In presence of TF, construct 1 was again predominantly unfolded (**Fig. 3.2d**, bottom left). The population mean contour length increased somewhat, from 36 to 41 nm ($p < 0.05$, Mann-Whitney U test), indicating the nascent chain is less folded on average – consistent with the model that TF stabilizes unfolded states [85, 115]. Notably however, the distribution for construct 2 now peaked towards compacted states, at a contour length of about 10 nm (**Fig. 3.2d**, bottom right). Thus, TF interactions rather led to more compact folded states for construct 2.

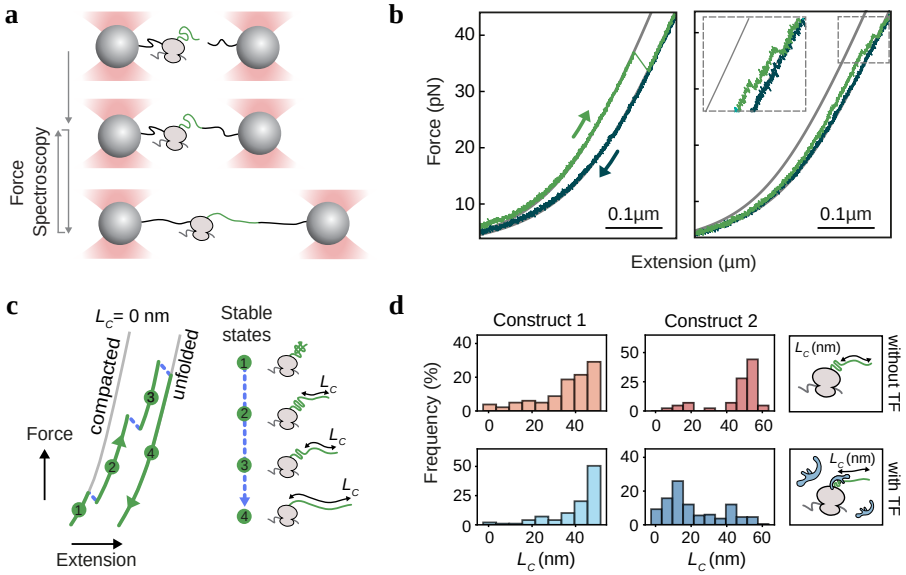

Figure 3.2 | TF promotes partially folded states during translation **(a)** Diagram of optical tweezer approach allowing nascent chain folding studies. DNA handles (black) tether stalled ribosomes and nascent chain N-terminus to two laser-trapped polystyrene beads. By changing their distance, nascent chains are exposed to stretch wait-relax cycles, with folding occurring in the 5 second waiting time at 0 pN, and stretching allowing probing of refolded states. **(b)** Example force-extension traces, for construct 1 in absence of TF. Grey lines: behavior for the fully compacted (left) and fully unfolded (right) states. Stretch-relax cycles showing the chance-based formation of fully (left graph) and partially folded (right graph) nascent protein states, and their unfolding as sudden decreases in the measured force. **(c)** Cartoon of stretch-relax cycle. Grey curves: stretching behavior for fully compacted and fully unfolded states. Numbers: distinct folded states. Dotted blue lines: unfolding transitions. Force-extension data quantifies the contour length of the unfolded part of the protein (L_C), and hence its folded state. **(d)** Contour length histogram for both constructs in absence (red) and presence (blue) of Trigger Factor. For n-values see Methods, section Data analysis.

Overall, these findings show that TF not only stabilizes unfolded states, but can also promote the presence of partially folded DHFR states, provided that a key C-terminal beta strand is synthesized and has emerged from the ribosome tunnel. To gain structural insight we performed a residue-residue contact analysis (**Fig. S3.1**). It suggested that the observed partial folds at the end of the length range **Fig. 3.2d** consist of up to three of the top-most beta stands as visualized in **Fig. 3.1b** (**Fig. S3.1b**), which is consistent with recent structural work [128]. These partial folds are encoded in the C-terminal end of the exposed nascent chain for construct 1, while the N-terminal end remains unfolded, and in the middle of construct 2 (**Fig. S3.1a**). The more compact partial folds at the beginning of the length range, observed in particular for construct 2 with TF (**Fig. 3.2d**), are suggested to consist of the 6 top-most beta strands visualized in **Fig. 3.1b**, in which the key C-terminal beta strand forms interactions with an N-terminal beta strand (**Fig. S3.1b**).

3.2.3 TF enhances nascent chain collapse and accelerates partial folding

To understand how TF promoted folding, we analyzed the associated preceding length changes. Notably, we found that nascent chains started compacting already during relaxation when the force was decreasing, as gradual or sudden decreases in the measured extension (**Fig. 3.3a,b** and **Fig. S3.2**). The gradual decreases were characterized by a continuous (rather than a step-wise) changes in length that occurred as the force relaxed to 0 pN. Chain compactions also occurred during the subsequent 5 second waiting time at 0 pN, as quantified by the measured extension during ensuing stretching (**Fig. 3.3b** and **Fig. S3.2**). We quantified the fraction of cycles showing a total compaction of 20 nm or more during relaxation and the waiting period at 0 pN (**Fig. 3.3c** and **Fig. S3.3a**), as this is substantially larger than the approximately 10 nm that TF measures along its longest axis [77]. For construct 1, the 20 nm compaction frequency was low without and with TF (6% and 9% respectively). In contrast, TF substantially increased the 20 nm compaction frequency for construct 2 (from zero to 28%).

Whether chaperones accelerate folding or limit aggregation is difficult to determine in bulk, as both can promote the presence of folded monomeric conformations. Given the absence of aggregation in our assay, the data (**Fig. 3.3c**) directly showed that TF accelerates the co-translational formation of partially folded states. Note that during translation, if folding occurs it is necessarily partial as not all the residues are exposed. The TF-mediated stimulation of large (over 20 nm) compactions occurred in construct 2 only and hence depends on translation, which is consistent because key residues for large-scale (high contact order) folding emerge when translating from construct 1 to 2 (**Fig. S3.1**).

If this reasoning is correct, we conjectured that TF may also stimulate compactions in construct 1 – as long as they are small in scale (and contact order). Hence, we identified the gradual and discrete compactions during relaxation (showing length decreases of minimally 2.5 nm, **Fig. S3.3b**), and analyzed the forces at which these compactions started (**Fig. 3.3d**). TF indeed increased these compaction forces for construct 1 (from 7 pN to 21 pN on average, $p < 0.05$), as well as for construct 2 (from 0 pN to 8 pN on average, $p < 0.05$) (**Fig. 3.3e**). The forces were broadly

distributed, ranging from 0 to about 50 pN. Note that collapsed conformation can start locally within the chain involving a small number of residues, and correspondingly small length decreases. The collapsed part can grow by adding residues from the extended part of the chain, thus leading to further length decreases as the force is decreased during relaxtion. These data show that TF increases the driving force of the nascent chain collapse – and hence directly increases the chain collapse energy (**Fig. S3.4**).

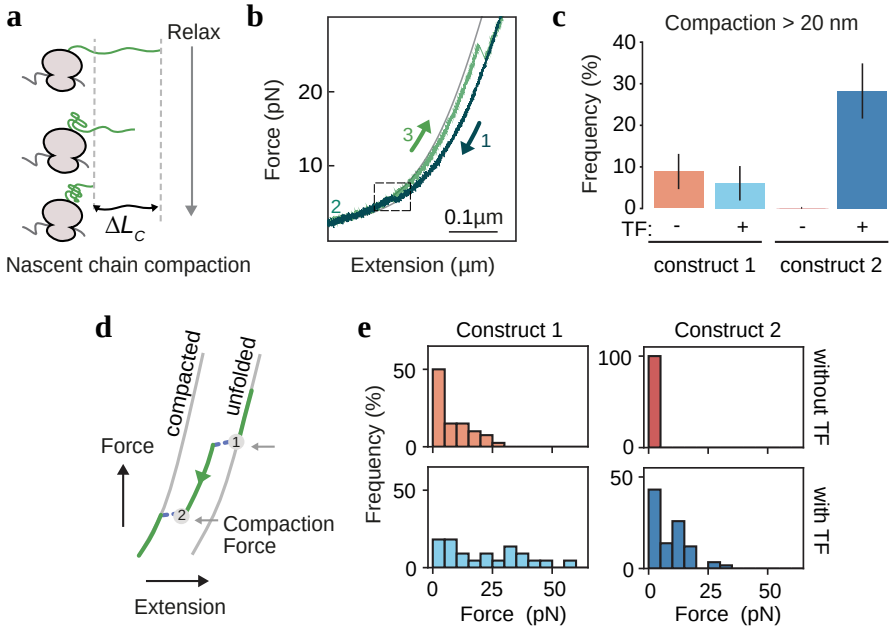

Figure 3.3 | TF enhances nascent chain collapse and accelerates partial folding **(a)** Cartoon of the nascent chain compaction analysis. As the force is relaxed on unfolded nascent chains, the latter collapse and fold partially, detected as a decrease in the contour length of the unfolded part of the chain (ΔL_C). Further compactions can occur during the subsequent waiting time of 5 seconds at 0 pN, detected by the subsequent stretching curve. **(b)** Force-Extension trace showing a compaction step (dashed box) during relaxation (1). After the waiting time at 0 pN (2), the first observed contour length in the consecutive pull (3) quantifies further possible compactions at 0 pN. **(c)** Frequency of cycles showing compactions with $\Delta L_C <$ 20 nm during relaxation and waiting time at 0 pN (see panel (a)). **(d)** Cartoon of the refolding force analysis. As the force is relaxed, sudden or gradual decreases in the measured extension (dashed lines) start at a certain folding force (arrows), which indicate nascent chain compaction events. Contour length changes of 2.5 nm and higher are analyzed. **(e)** Histogram of compaction forces (see panel (d)). TF increases the compaction force for both constructs, showing that for TF increases the forces that drive the nascent chain collapse and folding, and hence increases the collapse energy. For n-values see Methods, section Data analysis.

3.2.4 TF accelerates folding by stabilizing collapsed states

Mechanistically, folding acceleration can be achieved by entropy reduction of the unfolded state [100], inhibiting unproductive kinetically trapped conformers [129] and by enhancing polypeptide collapse [101]. The latter is driven by the stabilization of collapsed and folded states while the former two are not. Note that polypeptide collapse can accelerate folding by bringing residues in close proximity while providing the conformational dynamics required for adopting native folding. The increased compaction forces we observed (**Fig. 3.3e**) were in line with such stabilization.

To further probe the stability of TF meditated compacted conformations, we quantified the force at which they unfolded when stretched (**Fig. 3.4a,b**). In cases where unfolding did not occur below 60 pN, when the DNA handles begin to melt, that maximum force was scored. Construct 2, which displayed an increased compaction frequency (**Fig. 3.3c**), indeed showed a marked shift to higher forces due to TF (**Fig. 3.4b**). The unfolding forces were broadly distributed, increased from 43 pN to 52 pN ($p < 0.05$) on average, with a major peak above 50 pN and a narrow tail extending to 0 pN (**Fig. 3.4b**). The unfolding force histogram for construct 1 did not show a noticeable change (**Fig. 3.4b**). However, analysis of nascent chains of similar compactness did reveal a shift to higher unfolding forces (from 31 to 43 pN on average) for the smaller structures, which thus have a larger contour length for the unfolded part of the nascent chain (above 40 nm, **Fig. S3.6**). These findings are consistent with the observed TF-mediated compaction force (**Fig. 3.3e**). Thus, while entropy reduction and suppressing unproductive conformations may also contribute, our data indicates that folding acceleration by TF (**Fig. 3.2** and **Fig. 3.3**) is mediated by the stabilization of compacted states (**Fig. 3.4b** and **Fig. S3.6**).

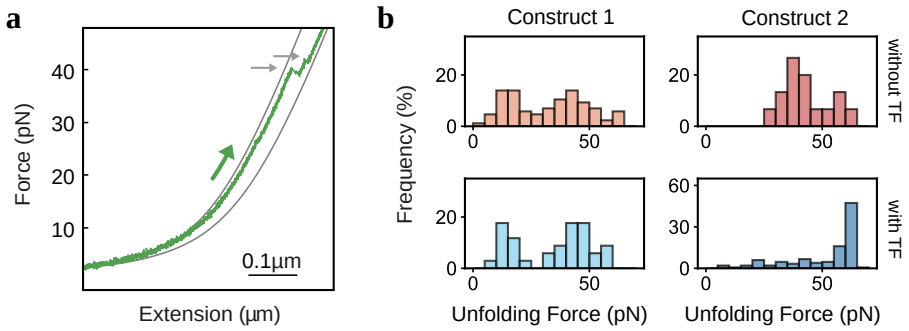

Figure 3.4 | TF stabilizes nascent partial folds against forced unfolding
(a) Example force-extension trace with two discrete unfolding events (arrows).**(b)** Unfolding force histogram. A wide distribution of unfolding forces is observed. For construct 2, TF increases the unfolding force, which shows TF stabilizes nascent partial folds against unfolding. When analyzing unfolding forces for partial folds of similar size, TF also increases the unfolding force of smaller folds for construct 1 (**Fig. S3.6**). For n-values see Methods, section Data analysis.

3.2.5 TF binds longer to compacted nascent chains

Finally, to further test compacted state stabilization by TF, we surmised that the compacted chains and TF may then form a stable complex, and hence increase the TF binding duration. To study TF binding durations directly, we combined optical tweezers with simultaneous detection of fluorescently labelled TF (Fig. 3.5a). We note that this assay is experimentally highly challenging and has important limitations. Background fluorescence and fluorescence intensity from the beads that are also bound by TF interfere with detection of ribosome-bound TF. We partially mitigated these issues by using long DNA tethers (5 kbp) and low TF concentrations (500 nM), though the latter renders the assay unsuitable to study on-rates and practically limits the probability of observing bound TF. TF detection is further limited by chance-based imperfect RNC positioning in the fluorescence imaging plane and incomplete TF labelling. However, the assay does uniquely provide TF binding durations and their dependence on folded states, which is our central aim. TF was Atto532 labeled at a site (L99C) not involved in ribosome docking or nascent chain binding [130]. While performing RNC stretch-relaxation cycles, a fluorescence excitation beam was repeatedly scanned along it. These experiments

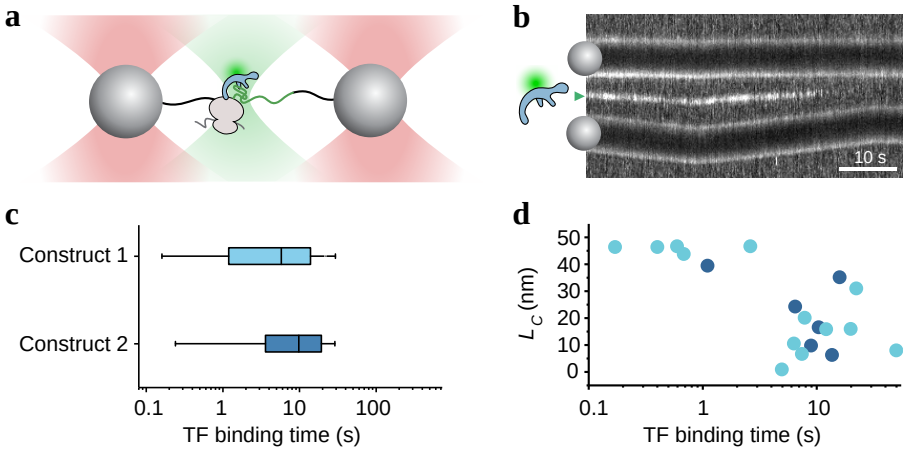

Figure 3.5 | TF binds longer to compacted nascent chains **(a)** Cartoon of correlated optical tweezers and single-molecule fluorescence measurements. A RNC tether between two bead is prepared (Fig. 3.2). The bead pair is moved into a side channel within the flow chamber, 500 nM of TF labeled with Atto532 is introduced. Stretch-relax cycles are performed, while a 532 nm fluorescence beam is repeatedly scanned along the tether to detect the fluorescence signal of bound TF. **(b)** Kymograph showing the TF-Atto532 fluorescence signal as a bright line (green triangle) between the two beads during stretching and relaxation. **(c)** TF binding durations. The binding durations for constructs 1 and 2 differed not significantly (p-value: 0.34, Mann-Whitney U). For n-values see Methods, section Data analysis. **(d)** Binding duration vs. measured contour length. More compacted states (smaller L_C) showed longer TF binding durations. The number of binding events is lower than in panel (c) to allow accurate L_C determination. For n-values see Methods, section Data analysis.

yielded kymographs that show these scans side-by-side, where bound TF was detected as a bright line in between the beads (**Fig. 3.5b**). The resulting TF binding times varied widely from below 0.5 seconds to well above 10 seconds (**Fig. 3.5c**). Importantly, binding times were longer when the nascent chains were more compacted (**Fig. 3.5d**, $p < 0.05$). Note that folding is a chance-based process in which smaller or larger parts of the chain can be compacted in different cycles. We also found instances of nascent chain folding or unfolding while bound TF was detected by fluorescence (**Fig. S3.7**), indicating that the system is dynamic and TF does not need to dissociate to accommodate nascent chain structural changes. Overall, these data show that the effect between TF and nascent chain is reciprocal: TF stimulates the formation of compact nascent chains while stabilizing them, and conversely, compaction stabilizes the nascent chain-TF complex and increases TF binding duration.

3.3 | Discussion

We combined *in vivo* selective ribosome profiling with *in vitro* optical-tweezers and single-molecule fluorescence to study nascent chain conformational control by TF. We showed TF interacts efficiently with DHFR during translation without interference or assistance from the other main chaperones DnaK and GroEL. TF binding is undetectable early in translation and increases after about 75 residues are translated (**Fig. 3.1a**). Single TF chaperones were found to bind from the lower detection limit of 0.1 s for unfolded nascent chains, to well over 10 s for folded nascent chains (**Fig. 3.5c**). The data indicated a model in which TF scans RNCs through a process of rapid binding and unbinding, and locks into a stable binding mode upon (partial) nascent chain folding, which in turn depends on the residues that are available for folding and hence translation. TF continues to bind until completion of translation, which takes about 10 s for DHFR [131, 132]. (**Fig. 3.6**)

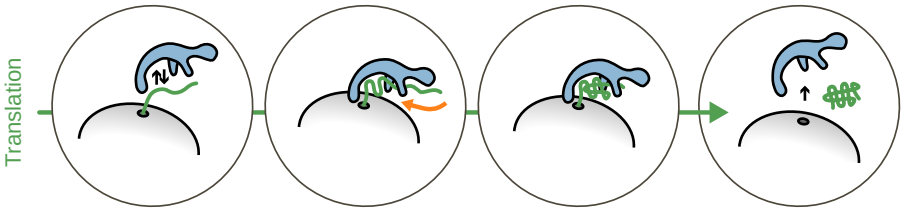

Figure 3.6 | Resulting model. Circle 1: TF scans ribosome nascent chain complexes by transient binding events early in translation. Circle 2: TF increases the forces that drive nascent chain collapse and folding (thick orange arrow). Circle 3: TF locks into a stable binding mode when the nascent chain has collapsed and folded. The interplay is thus reciprocal: TF binding compacts nascent chains, while compacted nascent chains prolong TF binding. Circle 4: After translation is finished, the nascent chain in the ribosome tunnel is released, which allows the protein to dissociate and folding to be completed.

The interplay between TF binding and nascent chain conformations is reciprocal: not only do nascent chain compaction and folding increase TF affinity, TF binding promotes nascent chain collapse and folding. Due to inherent limitations of our fluorescence assay including the high background, it is unsuitable to study how the finger-like protrusions of TF [91] structurally adapt to ongoing folding, or to quantify TF binding on rates. The reciprocal nature of the interaction suggests that TF binding and nascent chain compaction may occur at the same time. TF was also found to increase the forces that drive the compaction process (**Fig. 3.3c**, **Fig. 3.3e** and **Fig. S3.4**), by showing that mechanical work is performed. These findings are reminiscent of recently observed higher refolding and unfolding forces of ADR1A inside the ribosomal tunnel [49], and folding promotion at the ribosome by entropy reduction [34], even as underlying mechanisms may differ. Our observations indicate that TF offers an adaptable extension of the ribosome tunnel – not only to shield nascent chains against unwanted interactions, but to accelerate tertiary structure formation. Hence, they show that the functional repertoire of ribosome-bound TF goes beyond that of a protective holdase [85].

Direct folding acceleration (as opposed to indirect folding promotion like aggregation suppression) was long demonstrated only for GroEL-GroES [100, 133], and hence is associated with enclosure in a chamber. However, open GroEL was recently shown to increase the collapse energy of unfolded clients and stabilize partial folds to accelerate folding [101]. Polypeptide collapse is thought to involve the local nucleation of a compact yet still dynamic state along the chain, which can grow in size at the expense of the unfolded conformation. This collapse has long been thought to be relevant to autonomous folding (in absence of chaperones), by bringing residues together that must contact each other in the native structure [134]. Our work highlights that chaperones can modulate the collapsed state to regulate folding. The underlying collapse enhancement mechanism may be related to the ability of small osmolytes to stabilize collapsed conformations of hydrophobic polymers, by structuring water molecules that can otherwise solvate and stabilize their unfolded conformation [135]. TF may exploit similar mechanisms to accelerate folding of nascent chains at the earliest moment after synthesis. Several findings were consistent with TF accelerating folding by stabilizing collapsed and partly folded states: As also seen for GroEL [101], compacted states unfolded and refolded at higher forces (**Fig. 3.3**, **Fig. 3.4** and **Fig. S3.4**, **Fig. S3.6**), TF bound longer to compacted states (**Fig. 3.5**), and the emergence of a key beta-strand for higher-order C- and N-terminal contacts yielded larger stabilized partial folds (**Fig. 3.1**, **Fig. 3.4** and **Fig. S3.6**). Chaperone-mediated stabilization of partial folds thus occurs co-translationally, prior to post-translational conformational control by chaperones [83, 87, 136, 137]. Our model of TF mediated folding acceleration and stabilization also provides a mechanistic explanation for recently resolved structures of TF engaged co-translationally with partially folded nascent chains [128, 138].

At the structural level, the early folded states suggested by our data on construct 1 are consistent with HDX-MS work [128] (**Fig. 3.2d**, **Fig. S3.1**). Conversely, we find that the partially folded states of DHFR in later stages of translation observed with construct 2 (**Fig. 3.2d**, **Fig. S3.1**), which was not studied directly using struc-

tural methods, are promoted by TF presence. Once DHFR is no longer nascent (translation stage after construct 2), DHFR can dissociate rapidly from both the ribosome and TF, allowing rapid docking of the last two beta strands on the already formed beta sheet. More generally across the proteome, proteins may experience post-translational folding delays, which can be mitigated by other chaperones like DnaK and GroEL-ES, as has been studied extensively [65, 98]. The ability of TF to interact with partial nascent structures of diverse size and sequence may benefit from the structural flexibility of its finger-like protrusions, as well as from the mixed hydrophobic-hydrophillic nature of its internal suface [85, 89, 118, 128, 139]. These TF features may generate a local environment that contracts unfolded nascent chains, thus promoting their accelerated co-translational folding.

The acceleration of co-translational folding impacts diverse downstream processes. Protein folding delays, which for many proteins including DHFR [140] is over minutes *in vitro*, can push folding events to occur after translation is completed. In addition, folding was shown to be delayed by the ribosomal surface [107], and by TF in a holdase role [81]. The folding acceleration observed here rather acts in the opposite direction, thus shifting folding to (earlier) translation. Hence, the TF-mediated folding acceleration reported here increases the prevalence and efficiency of cellular processes that depend on folding to take place during translation. This includes many actively studied functions, such as the assembly between nascent and fully synthesized proteins [54], the assembly between two nascent proteins [60], the mitigation of translation arrests by folding induced nascent chain forces [141], and the mitigation of aggregation by folding-induced protection of hydrophobic nascent chain segments [102]. Co-translational folding acceleration by TF may thus be critical to limiting overall protein biosynthesis errors. It could also be relevant to understanding chaperone interplay [142]. For instance, GroEL and DnaK could engage with and act on nascent chains already partially folded by TF, or may themselves have co-translational folding acceleration functions. Finally, chaperone-mediated acceleration of co-translational folding may be of direct relevance to faithful protein biosynthesis across all domains of life [143].

3.4 Methods

Selective Ribosome Profiling (SeRP)

TF-SeRP [114] was performed without chemical crosslinking to improve the resolution. Cells encoding Avi tagged TF (Δtig::tig-TEV-AviTag) were cultured in media supplemented with 40 µg/ml of D-biotin and harvested by rapid filtration. Frozen cells were mixed with frozen lysis buffer (50 mM HEPES-KOH pH 7.0, 100 mM NaCl, 10 mM $MgCl_2$, 1 mM Chloramphenicol, 1 mM PMSF, 0,4% Triton X-100, 0.1% NP-40, 5 mM $CaCl_2$, 0.2% glucose, protease inhibitor mix (cOmplete^{TM} EDTA-free, Roche) and RNase-free DNase I 0.1 U/µl, and lysed by mixer milling (2 min, 30 Hz, Retsch MM400). The pulverized cells were thawed in a 20 °C water bath for 1 to 3 min and incubated for 10 min in an ice-water bath. Subsequently, ribosomes were collected by centrifugation through a 20% sucrose cushion prepared with cushion buffer (50 mM Tris KOH pH 7.5, 100 mM NaCl, 10 mM $MgCl_2$, 1 mM chloramphenicol, 1 mM PMSF, 0,4% Triton X-100, 0.1% NP-40, protease inhibitor mix (cOmplete^{TM} EDTA-free, Roche). The pelleted ribosomes were resuspended in cushion buffer. For each 200 ml of filtered cell culture, 750 µl of a 50% slurry of Strep Tactin sepharose was washed three times with 1.5 ml of cushion buffer. The resuspended ribosomes were incubated with the slurry for 30 min at 4 °C under gentle shaking. The slurry was washed three times for 15 min with constant shaking with cold wash buffer (1x TBS, containing 1 mM chloramphenicol, 10 mM $MgCl_2$, 0.1% Triton X-100). The RNA extraction by phenol-chloroform, the ribosome-protected footprints purification and library preparation was performed as described in (Becker et al., 2013) [122].

SeRP alignment and preprocessing of short reads

We first used cutadapt to remove adapter sequences and discard short (< 20 nt) and long (>45 nt) reads. The exact command was:
cutadapt -u 2 –nextseq-trim 20 –discard-untrimmed -m 20 -M 45 -O 6 -a NNNNNATCGTAGATCGGAAGAGCACACGTCTGAACTCCAGTCAC -o <outfile><infile>
Trimmed FASTQ files were aligned against an rRNA/tRNA reference using bowtie to exclude these contaminants from further processing. The exact command was:
bowtie -t -n 2 –best <indexdir>-q <infile>/dev/null –un <outfile>
Unaligned reads from the previous step were aligned against the E. coli MC4100 reference genome using bowtie. The exact command was:
bowtie -t -n 2 -m 1 –best –strata <indexdir>-q <infile><outfile>–un <outfile_unaligned>–max <outfile_multialigned>
P-site positions were assigned using a fixed offset of 15 nt from the 3'-end of a read. P-sites at each position within a CDS were counted and these counts were used for further analysis. We excluded four genes from analysis: The genes of the elongation factor tufA and tufB due to high sequence similarity and resulting alignment gaps. DnaK and GroEL because the IP-antibody also recognized nascent DnaK and GroEL, causing artificial enrichments. To calculate the chaperone enrichment scores [109], for each transcript a sliding window of 15 codons was applied. Then,

the 95% confidence interval (CI) according to Agresti and Coull of the enrichment ratio (factor-bound translatome to total translatome) was calculated. This calculation was performed for each biological replicate separately and then the average of both replicates was formed.

Trigger Factor Purification and Labeling

The *tig* mutant gene encoding the TF^{L99C} mutant was constructed using the QuikChange – Site-Directed Mutagenesis method and the plasmid pCA528-tig [116]. Overexpression and purification of untagged Trigger Factor was performed as described in (Hoffmann et al. 2012) [116]. For TF labeling, the purified TF^{L99C} was dialyzed overnight at 4 °C in PBS buffer supplemented with 1 mM Tris(2-carboxyethyl)phosphin (TCEP). Before starting the labeling, the TCEP concentration was increased to 5 mM. Fluorescent dyes were dissolved in N, N-Dimethylformamide (DMF) and labeling was started by mixing the chaperones with an about 10 fold excess of the dye. Labeling was performed for 2 hours at 25 °C in the dark and stopped by adding 10 mM DTT. Excess label was removed by size exclusion chromatography using a Sephadex 75 10/300 GL column.

Plasmid Construction

The gene of full-length E.coli DHFR (construct 1: 1-159) was ligated to a NcoI/XhoI restricted pRSET vector (Invitrogen) and modified. An amber stop codon was added upstream and the SecMstr arrest peptide (FSTPVWIWWWPRIRGPP) [125] downstream of the gene, as previously described65. To generate the shorter version of DHFR (construct 2: 1-126), part of the gene, coding for the last 33 amino acids of the protein, was removed by inverse PCR and following the In-Fusion seamless cloning protocol (Takara). pRSET plasmids containing either construct 1 or construct 2 were used for transformation into Top10 E.coli competent cells and selected on dYT-agar plates supplemented with ampicillin. Plasmids were subsequently isolated using the QIAprep Spin Miniprep Kit (QIAGEN).

Coupling of ribosomes to beads with DNA handles

5kbp long double-stranded DNA (dsDNA) molecules were prepared by PCR amplification using digoxigenin (DIG) and biotin 5'-end-modified primers. Neutravidin (NTV) (ThermoFisher, 31000) was added in a 200 times excess ratio to the PCR fragments (Bio-DNA-DIG) and incubated overnight at 4 °C in a rotary mixer. 2.1 µm diameter carboxyl polystyrene beads (Spherotech, CP-20-10) were covalently coupled with sheep anti-digoxigenin antibody (anti-DIG) (Roche,11333089001) using the carbodiimide crosslinker EDAC to create an active ester that is reactive toward primary amines in the anti-DIG and buffers from a coupling kit (PolyLink Protein Coupling Kit, 24350). Before each measurement two batches of around 1.4 nM NTV-Bio DNA-DIG and 4.5 µl/ml of anti-DIG coated beads were incubated in 140 µl TICO buffer (20 mM HEPES-KOH pH 7.6, 10 mM $(Ac)_2Mg$, 30 mM $AcNH_4$, 4 mM β-mercaptoethanol as an additional oxygen scavenger) for 20 min at 4 °C

on a rotary mixer. To remove unbound DNA, beads were pelleted and washed twice with TICO buffer. One of the bead batches was resuspended in 20 µl and the other in 300 µl TICO. Within the 20 µl, 350 nM ribosomes, which were biotinylated *in vivo* [123] at the uL4 ribosomal protein and subsequently isolated [144] from Can20/12E [145], were added together with 1.76 U/µl RNase Inhibitor, Murine (New England BioLabs, M0314S) and incubated for 45 min at 4 °C degrees on a rotary mixer. Excess unbound ribosomes were removed by pelleting the beads and washed twice with TICO buffer before directly resuspending it the cell free transcription/translation mix described below. The other batch of prepared bead bound NTV-Bio-DNA DIG is used later in the flow chamber to link up the biotinylated nascent chain on the ribosome.

Cell-free protein synthesis

A variation omitting the ribosomes of the cell-free transcription/translation mix of the PURE system [146] (New England BioLabs, E3313S) is used to synthesis the DHFR constructs. The system was supplemented with 10 µM of modified tRNA precharged with biotinylated lysine (Hölzel, PRX-CLD04). 5.5 nM linearized plasmid was added to the reaction mixture after mixing it with the biotinylated ribosome bound beads. Synthesis was carried out at 37 °C for 20 min. The bead-tethered RNCs were resuspended in TICO buffer and injected in the microfluidic chamber.

Optical tweezers assay

Data was recorded at 500 Hz as described before [49] using a C-Trap instrument (Lumicks) equipped with a powerful intensity- and polarization stable single 1064 nm laser, which is split in two orthogonally polarized beams, and with two fluorescent excitation lasers (532 nm and 638 nm). This allows for correlated single molecule force spectroscopy and multi-color confocal laser scanning spectroscopy measurements. Single photon sensitivity is assured by APDs. Measurements were performed in a monolithic laminar flow cell with five separated by flow channels with an advanced microfluidic system. This allows to keep the beads with RNCs and bead-tethered NTV-Bio-DNA-DIG separate. For tethering of individual molecules, a bead from each channel is trapped and moved into a separate measurement side channel with a P2O oxygen scavenging system (3 units per ml pyranose oxidase, 90 units per ml catalase, and 50 mM glucose, Sigma) together with 1mM Trolox [147], in order to reduce damage by reactive oxygen species induced by the trapping laser [148], to keep the pH stable [149] and prolong fluorescence lifetime. Within this side channel Trigger Factor is added for a subset of the experiments as well. The inter-bead distance is reduced to link up the biotinylated end of the nascent chain to the neutravidin-capped end of the DNA. A slight increase in force while increasing the bead to bead distance again signals tether formation. Measurements were taken in a cycling force spectroscopy mode, where the steerable trap was moved at a constant rate of 0.1 µm/s between a minimum bead separation of 2 µm and a maximum force of up to 65 pN.

Data analysis

Optical traps were calibrated using power spectral analysis. The power spectrum obtained from the beads undergoing Brownian motion in the optical traps is fitted with a Lorentzian, which allows to determine the corner frequency, which is proportional to the trap stiffness. The trap stiffnesss was around 350±50 pN/µm throughout measurements, since the laser intensity was kept constant. Custom scripts in Matlab and python were used to analyze force-extension curves by fitting two worm-like chain (WLC) models in series using the approximation of an extensible polymer for the DNA [126] and the Odijk inextensible WLC model [127] for the stalled nascent chain contribution. Checks were performed to show that a single RNC tether was established, which included consistency with the WLC model, overstretching at about 65 pN, and final tether breakage in a single clean step. For tethered RNCs, multiple force-extension curves were measured during consequtive stretch-relax wait cycles, until the thether broke. We note that tether stability, which in turn determines the number of stretch-relax cycles per tether, depends on the used force range, with higher forces leading to lower number of cycles. In this study TF is shown to mechanically stabilize nascent chain folded states, and hence we performed experiments with high applied forces (60 pN) during those cycles. Tether stability further depends on the stability of the biotin-Neutravidin and Dig-AntiDig linkages. Our tethers have two of each, and each can be the weakest link in the chain that breaks. N-values for data shown in **Fig. 3.2d**, construct 1, -TF: 17 molecules, 72 cycles, +TF: 12 molecules, 45 cycles, and for construct 2, -TF: 6 molecules, 28 cycles, +TF: 19 molecules, 119 cycles. N-values for data shown in **Fig. 3.3c**, construct 1, -TF: 45 cycles +TF: 33 cycles; construct 2, -TF: 20 cycles, +TF: 46 cycles. N-values for data shown in **Fig. 3.3e**, construct 1, -TF: 40 compaction events in 45 cycles, +TF: 22 compaction events in 33 cycles, construct 2, -TF: 6 compaction events in 20 cycles, +TF: 58 compaction events in 46 cycles. N-values for data shown in **Fig. 3.4b**, construct 1, -TF: 86 unfolding events, +TF: 34 unfolding events, construct 2, -TF: 15 unfolding events, +TF: 150 unfolding events. N-values for data shown in **Fig. 3.5c**, construct 1: 57 binding events, construct 2: 14 binding events. N-values for data shown in **Fig. 3.5d**, construct 1: 13 binding events, construct 2: 6 binding events. N-values for data shown in **Fig. S3.3a**, construct 1, -TF: 32 compactions +TF: 15 compactions. Construct 2, -TF: 6 compactions, +TF: 49 compactions. N-values for data shown in **Fig. S3.3b**, construct 1, -TF: 40 compactions, +TF: 22 compactions. Construct 2, -TF: 6 compactions, +TF: 58 compactions. N-values for data shown in **Fig. S3.4a**, construct 1, -TF: 72 cycles, 21 compactions at force +TF: 45 cycles 18 compactions at force, and for construct 2, -TF: 28 cycles, 0 compactions at force +TF: 120 cycles , 33 compactions at force. N-values for data shown in Figure **Fig. S3.4b**, construct 1, -TF: 40 compactions, +TF: 22 compactions. Construct 2, -TF: 6 compactions, +TF: 58 compactions. N-values for data shown in **Fig. S3.5**, 112 events for construct 1, 154 events for construct 2. N-values for data shown in **Fig. S3.6**: construct 1, -TF: 34 unfolding events, +TF: 17 unfolding events. construct 2, -TF: 10 unfolding events, +TF: 14 unfolding events.

Error bars (**Fig. 3.3c** and **Fig. S3.4a**) are standard error of proportion calculated by following formula:

$$\sigma = \sqrt{\frac{p(1-p)}{N}} \tag{3.1}$$

where p is the sample proportion and N is the total number of observations.

Contact map with high-energy contact regions

Two residues were considered to be in contact using a threshold of 7 Å in spatial distance between the residue's C_α atoms of the 3D DHFR (PDB 1RG7) structure. The lowest contact order interactions, between residues spaced less than 10 residues along the polypeptide, were not considered. The stability of inter-residue contacts was estimated using the empirical Thomas–Dill energies [150] (**Fig. S3.1a**). Contact regions were determined based on contact cluster regions, the largest of which corresponded to beta sheet contacts. When formed, these contacts define sub-structures of DHFR that reduce the measured length, and hence correspond to putative partial folds (**Fig. S3.1b**). Lengths of the polypetide segments in between the contact regions were determined, in order to quantify the corresponding reduction in measured length. Note that the order of structure formation may differ, in particular between substructure 1 and 2.

3.5 | Author Contributions

Conceptualization: K.T., A.S., F.W., S.J.T. Methodology: K.T., A.S., F.W., C.G., B.B., G.K., S.J.T. Biotinylated ribosomes: A. K. Ribosome Profiling Experiments: C.G. Single-molecule experiments: A.S., K.T. Single molecule data analysis and visualization: A.S., K.T., F.W., S.J.T. Writing: A.S., K.T., F.W., C.G., B.B., G.K. and S.J.T. Supervision: S.J.T., B.B. and G.K.

3.6 | Supplementary Figures

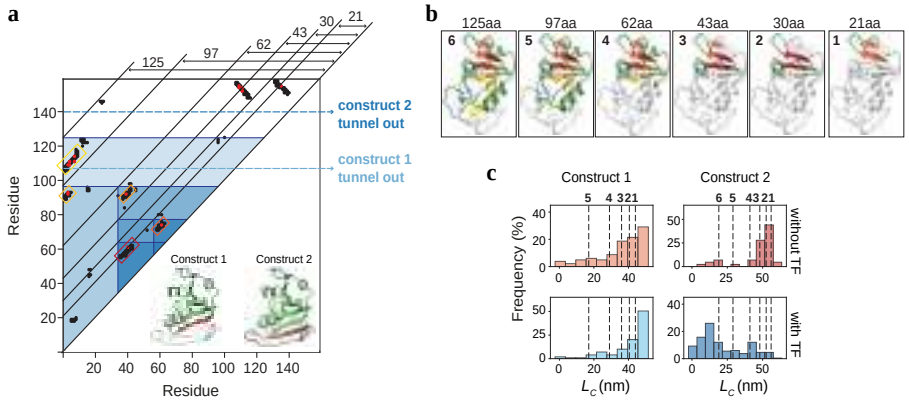

Figure S3.1 | Contact map analysis of DHFR and comparison to observed partial folds. **(a)** Contact map of DHFR (PDB 1RG7), showing residue pairs within 7 Å distance in the crystal structure. Low contact order contacts along the diagonal are excluded for clarity. Dashed horizontal lines indicate estimated last residues of the nascent chain outside the ribosomal tunnel for both constructs. Insets show corresponding structures in green, with residues in the tunnel in red (taken from **Fig. 3.1b**). Red points show most stable contacts estimated by empirical Thomas–Dill energies [150]. Partial fold regions (blue shaded triangles) are determined based on contact cluster regions (red/yellow boxes). Black diagonal lines indicate the polypeptide length corresponding to the partial fold. **(b)** Structures of corresponding partial folds, based on the polypeptide segments in panel (a). **(c)** Comparison to data. Each partial fold can be characterized by the contour length (L_c) of the unfolded part of the chain, and hence is mapped onto the contour length histograms (taken from **Fig. 3.2d**). Note that nm-scale variation along the L_c axis is possible depending for instance on the number of residues residing in the ribosomal tunnel. As the analysis shows, structures 1-4 overlap with the observed states at the right of the length histogram for both constructs without TF (top-row), suggesting these are sufficiently stable to form. The match is not perfect, as the histogram lengths are somewhat larger than those of partial fold structures 1-4. However, unfolded states also appear at significant frequency on the far-right of the histogram for structure 1 (top-left, last bar beyond partial fold 1). For construct 2 without TF, the length peak at about 50 nm also overlaps with structures 1-3 (predominantly structures 1 and 2). Structure 6 overlaps with data for construct 2 with TF. Structure 5 does not show much overlap with data for any condition, suggesting it is not stable. For construct 1 it may require the next beta strand that has not emerged yet, while for construct 2, it may be out-competed by the more stable construct 6. Note that the observed lengths between below 12 nm suggest additional compaction, possibly by the C-terminal end of the nascent chain within the ribosomal tunnel, which has been shown to promote secondary structure formation. The analysis further shows how TF can contribute to promoting the formation of the compact structure 6, as evidenced by the increased frequency in the presence of TF for construct 2.

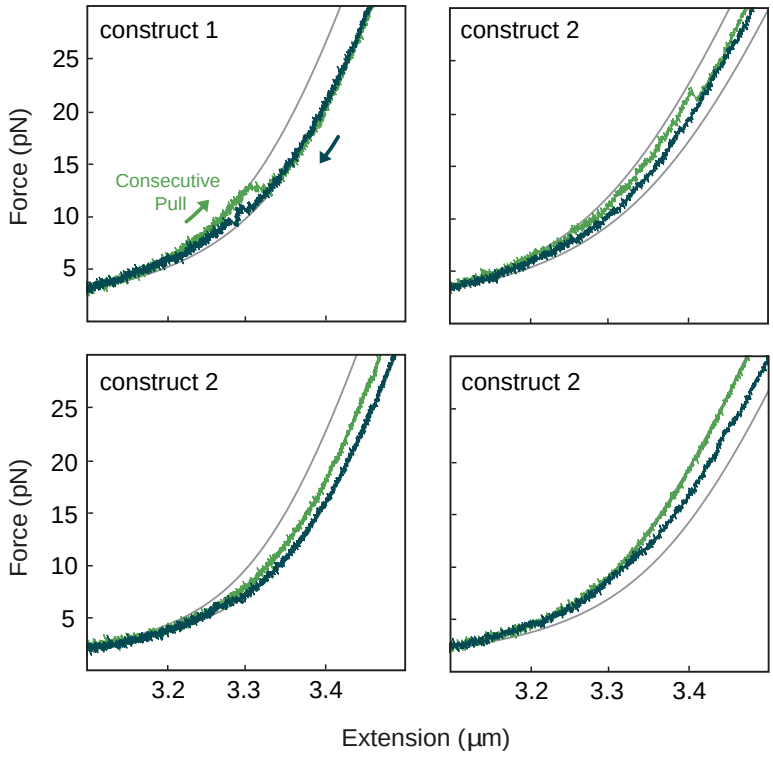

Figure S3.2 | Force-extension traces showing nascent chain compaction during relaxation. Example force-extension traces showing compaction events during relaxation (dark green trace). Left black line: theoretical WLC curve indicating the stretching behavior of the molecular construct in the fully compacted state. Right black line: theoretical WLC curve indicating the stretching behavior of the molecular construct in the fully unfolded state. The (dark green) trace is seen to move towards more compacted states as the force decreases in time. Light green: the consecutive pulling trace. At lower forces the difference in extension between compacted and unfolded states becomes smaller. However, the light green pulling trace allows one to determine compaction down to the fully relaxed state at 0 pN, and to assess the stability of formed compacted states. Traces show smaller gradual compaction, as well as larger gradual compactions (bottom right trace).

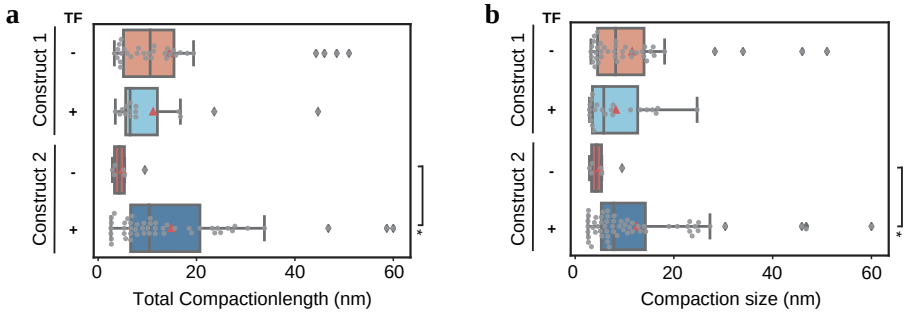

Figure S3.3 | Compacted length. **(a)** Total compacted length in relax-wait-pull cycles. Indicated is the maximum observed cumulative reduction in the measured contour length during relaxation, waiting at 0 pN, and stretching. Construct 2 shows a larger total compacted lengths with TF present, as compared to without TF present (star: $p < 0.05$, Mann-Whitney U), indicating its ability to compact the nascent chain. Construct 1 did not show a significant difference. Construct 1, -TF: 32 compactions +TF: 15 compactions. Construct 2, -TF: 6 compactions, +TF: 49 compactions. **(b)** Individual compaction lengths within relax-wait-pull cycles. Compaction lengths are indicated for events during relaxation, and during the waiting time at 0 pN. Majority of compactions are under 10 nm for all cases. Consistent with panel (a), the data suggests that for construct 2 TF causes an increase in compaction length. For construct 1 the nascent chain may form transient contacts that do not lead to a stable tertiary structure. Construct 1 does not show a significant difference with TF, while construct 2 does (star: $p < 0.05$, Mann-Whitney U). Construct 1, -TF: 40 compactions, +TF: 22 compactions. Construct 2, -TF: 6 compactions, +TF: 58 compactions. The box shows the quartiles of the dataset while the whiskers extend to show the lowest (highest) data point still within 1.5 IQR of the lower (upper) quartile. Line indicates median and orange triangle the mean.

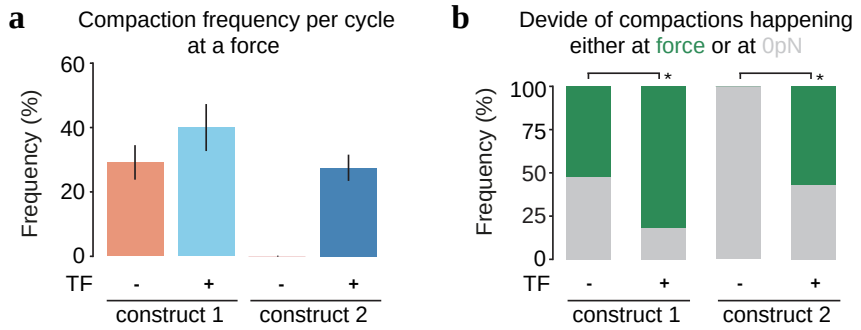

Figure S3.4 | Trigger Factor increases the frequency of compactions occurring at an applied force. **(a)** Frequency of compactions occurring at a counteracting force (during relaxation) per cycle. Construct 1 does not show a significant increase in this frequency when adding TF ($p = 0.23$, Fisher's exact test). In contrast, construct 2 does show a significant increase when adding TF ($p < 0.05$, Fisher's exact test). N-values: construct 1, -TF: 72 cycles, 21 compactions at force +TF: 45 cycles 18 compactions at force, and for construct 2, -TF: 28 cycles, 0 compactions at force +TF: 120 cycles , 33 compactions at force. **(b)** The fraction of compaction events happening at a force during relaxation (green) or at 0 pN (grey). Both constructs show that this fraction increases when adding TF (construct 1: $p < 0.05$ ($p=0.03$), construct 2: $p < 0.05$ ($p=0.009$), Fisher's exact test). Construct 1, -TF: 40 compactions, +TF: 22 compactions. Construct 2, -TF: 6 compactions, +TF: 58 compactions.

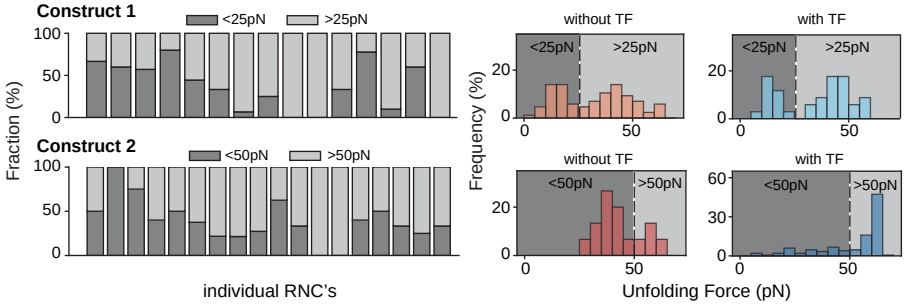

Figure S3.5 | Mode analysis of unfolding forces. For the distributions of **Fig. 3.4b** (right), two modes are defined: events above and below 25 pN (construct 1), and events above and below 50 pN (construct 2). Stacked bars (left) represent the fractions of events contributing to each mode, as observed for individual tethered RNC's showing at least 3 events in subsequent stretch-relax cycles in presence or absence of TF. N-values: 112 events for construct 1, 154 events for construct 2. The data shows that individual nascent chains sample both modes in subsequent cycles.

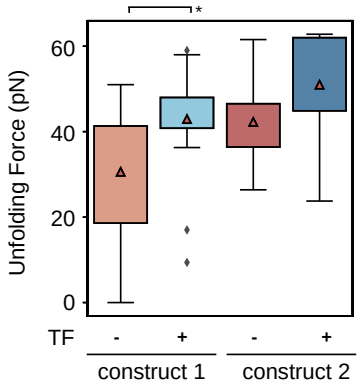

Figure S3.6 | Trigger Factor protects compacted states against forced unfolding. Unfolding force for small compacted states, with L_C larger than 40 nm. The mean (orange triangle) increased for both constructs when Trigger Factor is added, indicating that TF stabilizes partially folded states for both constructs. For construct 1, the mean force increases significantly from 31 pN to 43 pN ($p < 0.05$, Mann-Whitney U). For construct 2, the mean force increases from 42 pN to 51 pN, though the increase is just not significant (p=0.065, Mann-Whitney U). Construct 1, -TF: 34 unfolding events, +TF: 17 unfolding events. Construct 2, -TF: 10 unfolding events, +TF: 14 unfolding events. The box shows the quartiles of the dataset while the whiskers extend to the lowest (highest) data point still within 1.5 IQR of the lower (upper) quartile, except for the displayed outlier points.

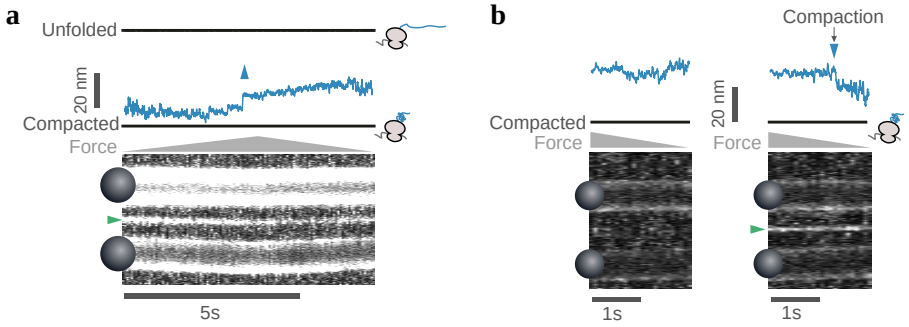

Figure S3.7 | Example fluorescence data of Trigger Factor bound to single tethered RNC. **(a)** Top: Contour length of nascent chain held by optical tweezers in time, in between the fully compacted and fully unfolded states (black lines, see **Fig. 3.5**). Bottom: Simultaneously measured fluorescence signal. Displayed is the fluorescence emission detected for consecutive scans along the two trapped beads. Green triangle: fluorescence signal from Atto532 labelled TF bound by the RNC tethered in between the two beads. Grey triangle indicated increasing and decreasing force on the tether. Blue triangle: small unfolding event while TF is bound. **(b)** Left: Data taken as in panel (a), for a case in which no fluorescence signal is detected nor compaction events. Right: Data taken as in panel (a), showing nascent chain compaction (top blue trace) while TF is bound (bottom white line marked by green triangle).

I sought to be strong on my own
But found to be stronger not alone

Artist impression of co-co assembly of the lamin dimer
Fineliner & Pencil, 2025
Katharina Till

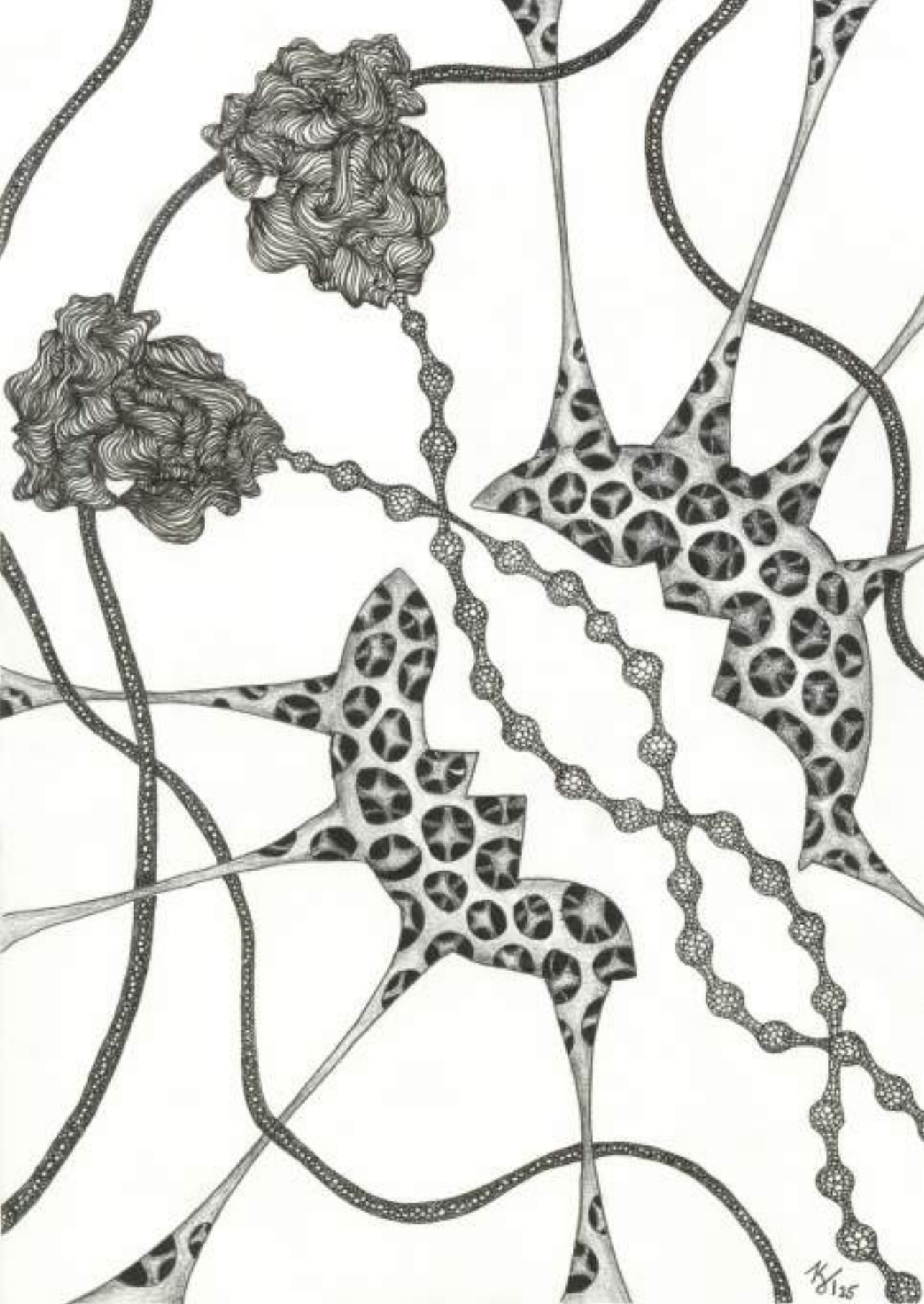

Chapter 4

CO-TRANSLATIONAL RIBOSOME PAIRING ENABLES NATIVE ASSEMBLY OF MISFOLDING-PRONE SUBUNITS

F. Wruck, J. Schmitt*, **K. Till***, K. Fenzl*, M. Bertolini*, F. Tippmann, A. Katranidis, B. Bukau, G. Kramer, S.J. Tans
Nature Communications **16**, (2025)

Protein complexes are pivotal to most cellular processes. Emerging evidence indicates that pairs of ribosomes ubiquitously drive the synchronized synthesis and assembly of two protein subunits into homodimeric complexes [60, 151–154]. These observations suggest protein folding mechanisms of general importance enabled by contacts between nascent chains [56, 155] – which have thus far rather been considered detrimental [156, 157]. However, owing to their dynamic and heterogeneous nature, the folding of interacting nascent chains remains unexplored. Here, we show that co-translational ribosome pairing allows their nascent chains to 'chaperone each other', thus enabling the formation of coiled-coil homodimers from subunits that misfold individually. We developed an integrated single-molecule fluorescence and force spectroscopy approach to probe the folding and assembly of two nascent chains extending from nearby ribosomes, using the intermediate filament lamin as a model system. Ribosome proximity in early translation stages was found to be critical: when interactions between nascent chains are inhibited or delayed, they become trapped in stable misfolded states that are no longer assembly-competent. Conversely, early interactions allow the two nascent chains to nucleate native-like quaternary structures that grow in size and stability as translation advances. We conjecture that protein folding mechanisms enabled by ribosome cooperation are more broadly relevant to intermediate filaments and other protein classes.

* These authors contributed equally

4.1 | Introduction

Cells rely on the faithful production of protein complexes. According to textbook models, newly translated polypeptides first undergo a conformational search for the native tertiary structure [107, 159, 160], and then a diffusion-driven assembly into larger complexes [161, 162]. This paradigm is challenged by mounting evidence of co-translational assembly, either between a fully-formed diffusing subunit and a nascent chain [53, 54, 58, 155, 163, 164] (termed "co-post assembly"), or between two nascent chains [151–154] (termed "co-co assembly"). We recently revealed over 800 co-co assembling homodimers, thus showing the general nature of this biogenesis route [60]. However, the biochemical methods and disome selective ribosome profiling (DiSP) [60] employed thus far do not detect the nascent chain structures nor the conformational changes during the folding and assembly process. Single-molecule fluorescence and optical-tweezers methods have made important advances in studying nascent chain folding but remain limited to single ribosome-nascent chain complexes (RNCs) [47, 107, 165]. As a result, we lack insight into the conformational basis and functional relevance of protein complex assembly enabled by coupled ribosomes.

Here, we study these issues using the human intermediate filament lamin, whose homodimeric coiled-coil structure represents the largest co-co assembly class [60]. Lamins form a scaffold for the nuclear envelope that spatially organizes chromatin [166, 167], with mutants being the root cause for diseases including premature ageing and cardiomyopathies [168]. Lamin A and its splice variant lamin C contain three domains [169–171]: the N-terminal unstructured head domain, the central α-helical rod domain that mediates dimer formation (Fig. 4.1, Fig. S4.1), and the C-terminal tail domain with an immunoglobulin-like fold [172]. Lamin polymerization occurs in the nucleus by head to-tail assembly of lamin homodimers [173]. The lack of lamin heterodimers [174], even though

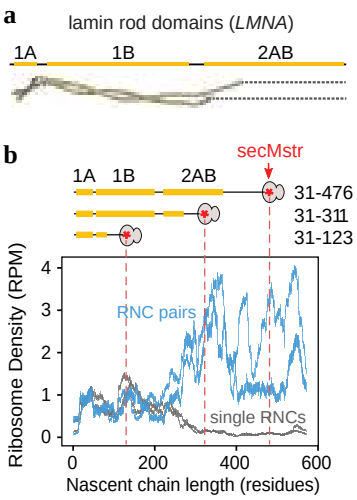

Figure 4.1 | (a) Structure of the lamin A/C homodimer showing the coiled-coil rod domains 1A, 1B and a part of domain 2AB (PDB code: 6JLB [158]). **(b)** Lamin RNC pairing *in vivo*. Bottom: Ribosome density along the LMNA mRNA for RNC pairs (pairing via the nascent chains, blue) and for single RNCs (grey), as obtained by DiSP for U20S cells, with 150 mM KCl and (Bissulfosuccinimidyl suberate) crosslinker present upon cell lysis. Two replicate data sets are shown, as bars representing the position wise 95% Poisson confidence intervals corrected for library size and smoothed with 15-codon wide sliding window [60]. RPM: reads per million. Top: Lamin nascent chain fragments for optical tweezer experiments. Dashed lines: ribosome stalling positions. SecMstr: peptide sequence for efficient translation stalling. Yellow bars: coiled-coil domains. Also indicated are the amino acids of the three fragments.

lamin A and C have identical dimerization domains, led to suggestions of a post-translational sorting mechanism that recognizes the different tail domains [175]. Co-co assembly can alternatively promote isoform-specific homomer formation, and more generally avoid promiscuous interactions between conserved oligomerization domains [176].

4.2 | Results

4.2.1 In vivo detection of lamin nascent chain interactions

We first studied lamin co-co assembly *in vivo*, including the dependence on cell type (U2OS and HEK cells) and DiSP conditions that can potentially influence the detected assembly onset (**Fig. 4.1b**, **Fig. S4.2**). The DiSP method is based on isolating RNC pairs that are coupled via their nascent chains (disomes), as well as uncoupled RNCs (monosomes), followed by sequencing their protected 30 nucleotide-long RNA footprints as in standard ribosome profiling. Consistent with co-co assembly, the number of mRNA reads for lamin RNC pairs increased after synthesis of coil 1B, as the reads decreased for the uncoupled RNCs [60]. This lamin dimerization transition was robustly observed, and did not depend on factors that can affect nascent chain interactions, such as the salt concentration (150 mM or 500 mM KCl) or presence or absence of a protein-protein crosslinker (BS3 and EDC, see **Fig. S4.2**). The robustness of the lamin nascent chain interactions may originate from the comparatively large dimer interface of its coiled-coil structure. Co-translational dimerization is an alternative mechanism to classical post-translational dimer formation, in which monomers find each other by diffusion through the cytosol. However, pull-down experiments on TwinStrep-tagged lamin showed that no wild-type lamin was co-purified [60], further supporting the notion that lamin co-co dimerization occurs *in vivo*.

4.2.2 In vitro formation of lamin RNC pairs

Approaches to purify RNC pairs from cells, like our DiSP method, are less suited to study nascent chain conformations [60, 177, 178], due to RNC heterogeneity and the difficulty of incorporating measurement probes. Hence, we aimed to construct RNC pairs *in vitro*, stalled at key phases of translation identified by the DiSP data: before the onset of dimerization, with only the small α helical coil 1A fully translated, after the dimerization onset with coils 1A and 1B fully translated, and finally after translation of coil 2AB, with the full-length rod domain translated and ribosome exposed (**Fig. 4.1b**).

To construct pairs of RNCs coupled by their nascent chains, we first linked biotinylated ribosomes to polystyrene beads via 5 kb DNA handles (**Fig. 4.2a**). Synthesis of lamin nascent chains by the bead-tethered ribosomes was performed by *in vitro* transcription-translation, using the 'SecM strong' [124] sequence to stall translation at positions indicated above (**Fig. 4.1b**, **Fig. S4.3**). Two such beads were captured by two optical traps, repeatedly brought together, within about 200 nm for about 5 seconds, and separated again. We quantified the fraction of approach-retract cycles

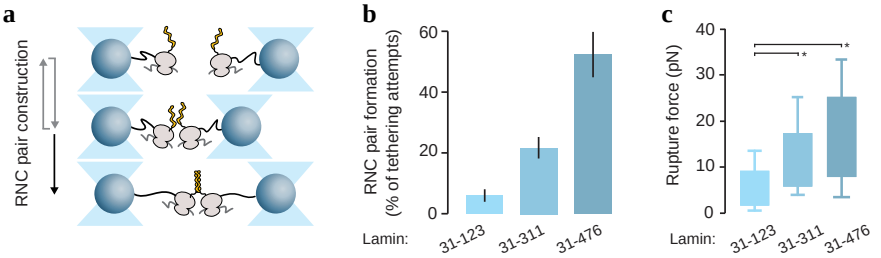

Figure 4.2 | Formation of lamin RNC pairs. **(a)** Optical tweezer approach to constitute RNC pairs. Ribosomes, coupled to beads via DNA handles, translate lamin fragments until a secMstr mediated translation arrest using *in vitro* transcription translation. Next, the beads are repeatedly brought together for 5 seconds, to let nascent chains interact and dimerize, and separated again (grey arrows). A stable tether upon pulling, of twice the DNA handle length, indicates dimer formation (black arrow), while no tether is formed when the chains do not dimerize. **(b)** The fraction of dimerization attempts yielding dimer formation, determined as depicted in panel (a), for three lamin fragments ($n = 136$ $LMNA_{31-123}$, $n = 140$ $LMNA_{31-311}$, $n = 46$ $LMNA_{31-476}$ cycles). Error bars are standard error of proportion. **(c)** Rupture force of nascent chain dimer tethers, as measured by ramping up the tether tension, for three lamin fragments ($n = 8$ $LMNA_{31-123}$, $n = 30$ $LMNA_{31-311}$, $n = 24$ $LMNA_{31-476}$ rupturing events). Boxes indicate 25th and 75th percentiles, error bars are the S.D. Star: significant difference, $p < 0.05$ (two-sided Mann-Whitney U test, $LMNA_{31-123}$/$LMNA_{31-311}$: $p = 0.036$, $LMNA_{31-123}$/$LMNA_{31-476}$: $p = 0.017$).

in which a tether formed between the beads that was twice the length of a single DNA handle (Fig. S4.4), and hence indicated the coupling of two RNCs via their nascent chains (Fig. 4.2a). This fraction increased from below 10% to above 50% with increasing fragment length (Fig. 4.2b). Such an increasing trend agrees with the lamin DiSP data (Fig. 4.1b), and with coupling taking place via the nascent chains, rather than via other (ribosomal) components. While rare, we did detect dimerization events already for the shortest fragment, indicating an earlier assembly onset than detectable by DiSP (Fig. 4.1b). Interactions between shorter nascent chain dimers may be detected less efficiently by DiSP, while the polysome structure may also reduce their interactions. To probe the stability of the nascent chain dimers against dissociation, we measured the force required to rupture the tether by increasing the distance between the beads. The tethers ruptured in a single step, in line with coiled-coils unfolding and dissociating discretely during pulling [179]. The rupture force indeed increased with fragment length, from about 5 pN to over 15 pN (Fig. 4.2c), consistent with a progressively larger coiled-coil dimer interface. Based on the DiSP data alone, one cannot formally exclude that lamin nascent chains do not homodimerize, but instead form complexes with other nascent chains. Thus, the *in vitro* experiments presented here provide direct support for the ability of lamin nascent chain homodimerization. Overall, the data indicated that lamin nascent chains dimerized when brought in close proximity, with associations that start at short chain lengths and become more resistant against forced dissociation with increasing chain length.

We studied how these findings related to coiled-coil structural features, in order to obtain further mechanistic insight (Fig. S4.5, Fig. S4.6). Coiled-coil structures are based on interactions between heptad sequences in each coil, denoted as: $(abcdefg)_n$. Residues at positions a and d are mainly hydrophobic and make up the core of the coiled-coil interface. Coiled-coils have a packing arrangement termed knobs-into-holes (KIH) [180–182], with certain residues like Leucine, Valine, and Isoleucine packing particularly well within this arrangement considering their side chain packing geometries [183, 184]. A tabulation of these interactions indicated that going from the short to the intermediate fragment increased the stability the most, while the longest fragment gained less in comparison (Fig. S4.5a,b,c). The same is concluded when computing the cumulative residue-residue contact energy [185] along the lamin dimer interface (Fig. S4.5d, Fig. S4.6). These computations agree with our measurements of the mean rupture force, which doubles from construct 1 to construct 2 (from 7 pN to 14 pN, $p < 0.05$), but increases only marginally to construct 3 (18 pN, $p = 0.5$). Overall, this analysis indicated that most of the lamin dimer stability is contributed by coil 1B, as it has the most heptad repeats and more ideal packing amino acids at the a and d positions, when compared to coils 1A and 2B.

We note that the applied force acts on the inter-chain contacts, as both are perpendicular to the helical axis in our assay (Fig. 4.2a). Hence, substantial α-helical unfolding likely does not occur before inter-strand contacts are broken. This is in line with previous work, which suggests that mechanical unfolding of coiled-coils involves the simultaneous breakage of many intra- and inter chain contacts [186–189]. We also note that rupture forces between 8 and 15 pN were observed, which is in the same range as the rupture forces observed here (Fig. 4.2c). In contrast, when the force acts in parallel to the helical axis, helices can elongate before the strands separate [188, 190, 191].

4.2.3 Nascent lamin complex formation observed by fluorescence

To test whether the observed nascent dimers are consistent with the native coiled-coil lamin structure, we integrated fluorescence detection into the optical tweezers assay (Fig. 4.3a). We inserted a pair of adjacent cysteines at the lamin N-terminus and reasoned that two such pairs should co-localize in the native parallel coiled-coil conformation. Hence, a bipartite tetra-cysteine motif would form that can bind the FlAsH dye [192], which becomes fluorescent upon binding, and detectable by confocal fluorescence imaging. We performed the above approach-retraction protocol to form a lamin RNC pair and exposed it to FlAsH in solution. To detect bound FlAsH, a confocal fluorescence excitation beam was scanned across the beads and along the connecting tether. A fluorescent signal indeed appeared in-between the beads, visible as an additional line in kymographs that display the subsequent fluorescence emission scans (Fig. 4.3b). Consistent with the formation of an in-register parallel coiled-coil, we detected a FlAsH signal when tethers were formed. As in the measurements without the FlAsH dye (Fig. 4.2b), the longer fragments again showed higher dimer formation frequency (Fig. S4.7a).

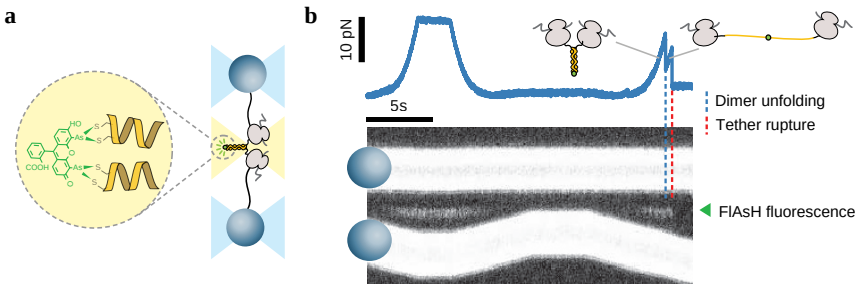

Figure 4.3 | Fluorescent detection of nascent lamin dimers. **(a)** Approach for visual verification of N-terminal co-localization. Two nascent chains can be linked by the FlAsH dye, which binds to a bipartite tetracysteine motif formed by two cysteines at each N-terminus, if they co-localize as in the native coiled-coil dimer structure (Fig. 4.1a). Bound FlAsH becomes fluorescent and is detected by scanning a confocal excitation beam (yellow beam) along the molecular tether, while the optical tweezers laser beams (blue) trap the beads.**(b)** Corresponding data. Bottom: detected fluorescence scans in time, showing bead movements in stretch-relax cycles and the FlAsH fluorescence signal between the two beads (green arrowhead). The FlAsH signal is only observed when the tether is under tension and hence stably in focus. RNC pair construct: $LMNA_{31-476}$. Top: corresponding measured force acting on the beads and tether. Blue dashed line: sudden drop in force indicates unfolding, while FlAsH keeps the N-termini connected (see panel (a)). Red dashed line: tether rupture, likely by dissociation of one of the DNA handles from the bead surface.

4.2.4 Delayed RNC interaction promotes non-native lamin dimer conformations

The above experiments showed that dimers of nascent lamin chains can be formed *in situ* but did not provide insight into unsuccessful assembly attempts or folding errors. We surmised the split FlAsH-tags may keep the N-termini connected after full unfolding, which could allow us to directly follow dimer formation and dissociation, including underlying conformational changes. Upon RNC coupling and FlAsH exposure, tethers indeed remained intact after lamin dimers were unfolded by stretching, as evidenced by a force drop to a non-zero level and the continued presence of the fluorescence signal (Fig. 4.3b). Note that the fluorescence signal is not visible at the lowest forces because the molecular tether may exit the confocal imaging plane. The force and fluorescence signals disappeared when the tether fully ruptured (broke), which could be due to FlAsH, Dig-

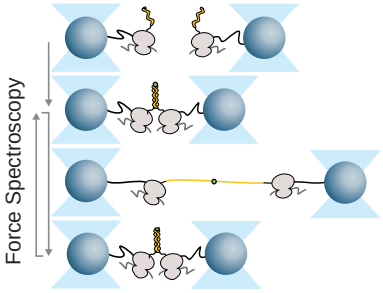

Figure 4.4 | Diagram of nascent chain dimer force spectroscopy approach. Lamin nascent chain dimers are formed as depicted in Fig. 4.2a, and subsequently exposed to repeated stretching and relaxation while the split-FlAsH-tag (green dot, see also Fig. 4.3a) keeps N-termini bound together upon unfolding.

AntiDig, uL4 or biotin-neutravidin dissociation, but whose rupture force should not depend on nascent chain length. Accordingly, we found similar rupture (or tether breaking) forces for all three constructs (**Fig. S4.7b**). In this manner, nascent chain dimers could be cyclically unfolded by stretching and then given a chance to reform by relaxation (**Fig. 4.4**).

The measured forces and extensions (bead-to-bead distance) during the stretch-relax cycles report on the degree of nascent chain compaction. In principle, nascent chain compaction during relaxation and decompaction during stretching can reflect various underlying conformational changes. Details of the Force-Extension data can be used to distinguish these possibilities. For instance, a sudden and discrete increase in extension during stretching typically indicates an unfolding transition. In turn, this shows that a folded state had formed in the previous relaxed state. We note that the FlAsH moiety may not always bind, for instance, if the two coils would initially not be in register. Stretching would then lead to simple tether breakage, as we have observed in the absence of FlAsH (**Fig. 4.2**, **Fig. S4.7b**). Out-of-registry rupture and assembly therefore cannot be studied in higher detail with our method. Four classes of behaviour were observed (**Fig. 4.5a**, **Fig. S4.8**), with individual RNC pairs showing different classes from one cycle to the next (**Fig. S4.9**). The chains were for the largest part either: (1) initially unfolded, and remaining so throughout the stretch-relax cycle, (2) initially compact and gradually decompacting during stretching (or conversely becoming gradually more compact during relaxation), with the data resembling previous pulling experiments on stretched linear α-helices [193, 194] (3) initially compact and unfolding discretely, consistent with the formation and unfolding of the coiled-coil dimer [186] (see also **Fig. 4.3b**), or (4) initially compact and remaining so throughout the cycle, with the applied force unable to unfold the structure.

The compacted states (4) indicated the formation of stable non-native conformations that differ from coiled-coil or linear α-helical structures [99]. These states were preserved for multiple cycles until the tether ruptured, indicating that the nascent chains could no longer form coiled-coil-like dimers. Conversely, unfolded (1) and α-helix-like states (2) could transition at 0 pN to the coiled-coil-like state that unfolded in discrete steps (3) (**Fig. S4.9**). In line with these data and the increased dimerization propensity with nascent chain length (**Fig. 4.2b**), class (3) was found to increase in frequency with nascent chain length, while classes (1) and (2) decreased (**Fig. 4.5b**). Notably, class (4) was only observed for the longest fragment (**Fig. 4.5**, **Fig. S4.8**). Note that these stretch-relax assays with different fragment lengths thus allow one to study the conformational consequences for nascent chains that start interacting during different phases of translation. Also note that unfolded polypeptides may be in different rotational states that can affect the ability to form secondary and tertiary structure. Overall, these data indicated that two neighbouring nascent chains can adopt α-helical and coiled-coil dimer structures early during translation, which grow as translation progresses. Alternatively, however, non-native states are promoted when the interactions between chains are delayed until later phases of translation.

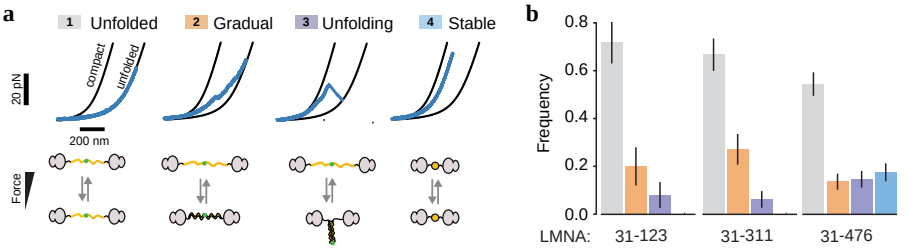

Figure 4.5 | Delayed RNC interaction promotes non-native lamin dimer conformations. **(a)** Classes of force-extension behaviour of lamin nascent chain dimers. Black lines are theoretical worm-like chain (WLC) curves for both nascent chains being compact (left) or fully unfolded (right). The position of the measured data (blue) in between these two reference curves indicates what fraction of the nascent chain (how many amino acids) is in the compact state, and what fraction is in the extended state. During stretch-relax cycles four classes are observed, with the majority of the chain: (1) remaining unfolded, (2) initially compact and extending and compact gradually under tension, as expected for linear α-helices, (3) initially compact and unfolding discretely below 45 pN, as expected for coiled-coil dimer structures, (4) initially compact and remaining so up to 45 pN , typically for multiple stretch-relax cycles, indicative a kinetically trapped misfolded state (3). Data is shown for $LMNA_{31-476}$ fragments. **(b)** Frequency of stretch-relax cycles with observed force-extension features (see panel (a)), for lamin nascent chain dimers of three nascent chain lengths. $n = 14$ $LMNA_{31-123}$ molecules, 24 pulling cycles $n = 29$ $LMNA_{31-311}$ molecules, 43 pulling cycles, $n = 54$ $LMNA_{31-476}$ molecules, 100 pulling cycles. Dimer formation and misfolding increases in frequency with increasing nascent chain length, at the expense of unfolded states. $LMNA_{31-311}$ and $LMNA_{31-476}$ are significantly different ($p = 0.002$, χ^2-test). Error bars: standard error of proportion. Colours are as in panel (a).

4.2.5 Co-co assembly suppresses intra-chain lamin misfolding

A key question concerns the conformational competition that determines the different observed folding pathways. Native complex formation can be in competition with aggregation interactions between the chains, or misfolding interactions within chains – both of which could yield the observed non-native states (**Fig. 4.5**). To address this issue, we probed single ribosome-associated lamin nascent chains, in the absence of partnering RNCs (**Fig. 4.6a**). First, we generated stalled ribosomes tethered to beads via 5 kb DNA handles as before, using suppressor tRNAs to biotinylate the nascent chains N-terminally. After trapping one bead, the biotinylated nascent chain was linked to a second trapped bead via another 5 kb DNA handle. Next, we cyclically first separated and subsequently approached the two optical traps, thus stretching and relaxing the α-helical lamin rod domains by their N- and C-termini, for all three lamin fragments (**Fig. 4.6a**).

With single RNCs, we observed three of the four classes (**Fig. 4.6b,c**, **Fig. S4.10**): (1) unfolded, (2) α-helix-like, and (4) non-native. As expected, observations of the discrete unfolding corresponding to the coiled-coil-like dimer class (3) were negligable. The data indicated that a second nascent chain is not required, but

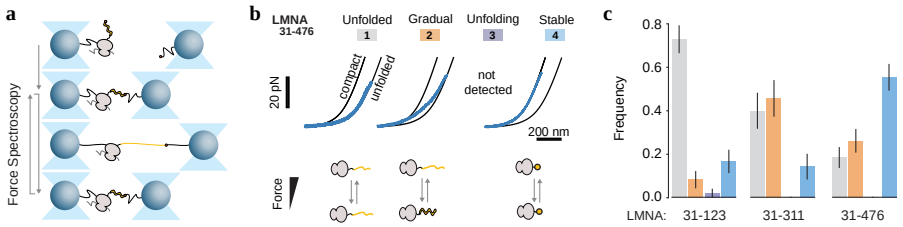

Figure 4.6 | Lamin misfolds when interactions with other nascent chains are denied. **(a)** Diagram of optical tweezer approach to probe single monomeric lamin nascent chains. Stalled ribosomes, coupled to beads via DNA handles, translate lamin nascent chain fragments, incorporating biotin N-terminally. This biotin is coupled to a second trapped bead via another DNA handle. The nascent chain conformations are hence probed by repeated stretching and relaxation (grey arrows). Indicated is the transition between the unfolded and linear α-helical conformations. **(b)** Classes of observed force-extension behaviour for monomeric lamin nascent chains. Black lines indicate reference behavior for a single nascent chain being compact (left) or fully unfolded (right). During stretch-relax cycles four classes of conformational states may be distinguished, with the majority of the chains: (1) remaining unfolded, (2) initially compact and extending gradually under tension, as expected for linear α-helices, (3) initially compact and unfolding discretely, typical for a dimer state that cannot form here, (4) initially compact and remaining so up to 45 pN, typically for multiple stretch-relax cycles, indicative of a kinetically trapped misfolded state. Data is shown for LMNA_{31-476} fragments. **(c)** Frequency of stretch-relax cycles with specific force-extension features (see panel (b)), for lamin nascent chain monomers of three nascent chain lengths (n = 14 LMNA_{31-123} molecules, 45 pulling cycles, n = 13 LMNA_{31-311} molecules, 32 pulling cycles, n = 17 LMNA_{31-476} molecules, 65 pulling cycles). Error bars are standard error of proportion. LMNA_{31-311} and LMNA_{31-476} are significantly different (p = 0.0003, χ^2-test). Error bars: standard error of proportion. Colours are as in panel (b).

may promote α-helix formation. However, most notable was the prominence of the non-native class (4). This class was observed for all fragments, at frequencies ranging from 20% for the shortest to 60% for the longest (Fig. 4.6c), while for the RNC pairs it was detected for the longest fragment only, and at a low frequency of 20% (Fig. 4.5b). These data indicate that in the absence of another lamin nascent chain, the individual lamin nascent chains were prone to form compact and stable non-native structures. Indeed, polypeptides that can form α-helices can also form misfolds that have high contact-order and are hence compact [195]. Conversely, the presence of a second nascent chain suppressed this lamin misfolding while enabling the coiled-coil-like assembly. Hence, native structure formation here is not inhibited, but instead promoted by interactions between nascent polypeptide chains.

4.2.6 Ribosome pair asymmetry and proximity

We thus far paired two identical RNCs (Fig. 4.3, Fig. 4.4 and Fig. 4.5) in order to study the interaction between two nascent chains in similar phases of translation. Alternatively, one ribosome may have translated substantially further than the

other. To study this assymetric scenario, we performed RNC pairing assays as before (Fig. 4.4, Fig. 4.5), but now using one bead with an intermediate-fragment RNC ($LMNA_{31-311}$) and one bead with a long-fragment RNCs ($LMNA_{31-476}$). These conditions indeed produced tethers and showed the previously observed classes during stretch-relax experiments: (1) unfolded, (2) α-helix-like, (3) coiled-coil-like, and (4) non-native (Fig. S4.11a,b). These data thus showed that asymmetric RNC pairs also can generate lamin dimers *in vitro*. The intermediate-long asymetric RNC pairs displayed a higher frequency of non-native cases than the symmetric intermediate RNC pairs, which did not show these states (Fig. S4.11c). This is consistent, as the longer nascent chain of the leading ribosome provides more opportunities for non-native interactions. These experiments *in vitro* show that ribosomes being in similar phases of translation and in close proximity on the RNA message is not strictly required but may be beneficial for co-translational lamin dimerization.
It has been shown that ribosomes can favor unfolded over folded states of nascent chains [107]. A similar or even stronger effect might occur here, as two ribosomal surfaces are brought in close proximity to the lamin dimer when it forms co-translationally. To test the potential difference in lamin dimer stability on and off the ribosome, we purified lamin dimers of the intermediate construct, after engineering ybbR tags for DNA handle attachment, and performed similar single molecule stretching and relaxation experiments in the absence of ribosomes (Fig. S4.12). Strikingly, the purified dimers could not be unfolded even when stretched to the maximum force of 65 pN in our assay. While small unfolding events were observed, for the majority of curves they totaled less than 30 nm (Fig. S4.12d). Such a destabilizing effect of ribosome proximity may be beneficial to co-co assembly, by allowing more options for finding the lowest-energy dimeric state.

4.2.7 Proteome-wide considerations

To assess the importance of interfacial contacts for co-translational dimer formation throughout the proteome, we analyzed the inter- and intra-molecular contacts of co-co candidates from our DiSP study [60] (Fig. S4.13). We found that the relative abundance of inter- vs. intra-molecular contacts was similar for high and low confidence co-co assembling candidates (Fig. S4.13a). Two peaks were observed: A first subpopulation of nascent dimers that showed over 10-fold more inter- than intra-chain contacts (15% of dimers), suggesting an important role for the partner chain in stabilization. Coiled-coils including lamin are very dependent on inter-chain contacts, as they rely solely on an α-helix structure for intra-chain stabilization. The second sub-population showed less than 10-fold more inter- than intra-chain contacts at co-co onset (85% of dimers), which could indicate partial domain folding before dimerization. Dimers in this group may also employ self-chaperoning, in particular dimers with an inter- vs. intra-chain contact ratio of more than 1. For most proteins, the inter-chain contacts were more important at the co-co assembly onset than after translation, when considering the total dimer interface (Fig. S4.13c). This suggested that the stabilizing initial inter-chain contacts are further stabilized by intra-chain contacts later during translation. Thus, the self-chaperoning mechanism may be especially useful in early translation phases.

4.3 | Discussion

In this study, we report that by coupling co-translationally, RNC pairs can drive the assembly of coiled-coil homodimers composed of subunits that misfold in isolation. We find that physical RNC proximity and their translation progress along the RNA message biases the competition between native and non-native contacts, which both can form within single chains or between two chains (**Fig. 4.7a**, **Fig. S4.14**). Specifically, residues that are translated early can form non native contacts with chain segments that are translated later (**Fig. 4.7a**, red arrows), which compete with native coiled-coil contacts (**Fig. 4.7a**, green arrows). Timely formation of the latter native contacts between nascent chains allows the realization of partial coiled-coils, which grow in size and stability as translation proceeds (**Fig. 4.7b**). Conversely, non-native contacts are promoted when the RNCs either cannot interact, or interaction is delayed until later phases of translation. Lamin nascent chains then misfold and are no longer assembly-competent (**Fig. 4.6b,c**). These risks should be further aggravated when assembly is postponed until after translation, and the monomeric lamin subunits must diffuse through the cytosol in order to dimerize (**Fig. 4.7b**). Overall, nascent chain interactions during translation thus provide a

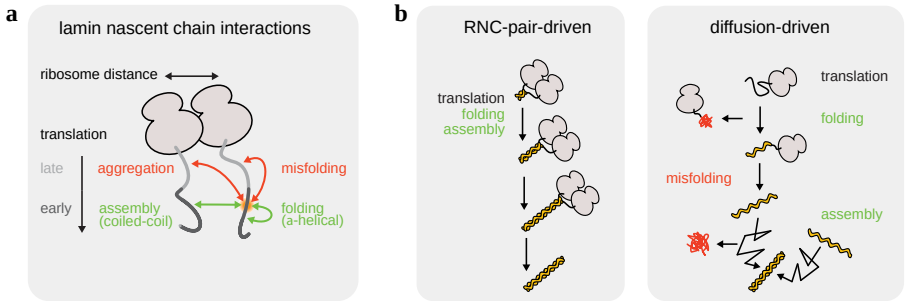

Figure 4.7 | Lamin misfolds when interactions with other nascent chains are denied. **(a)** Competition between initial lamin nascent chain interactions and factors that affect it. A given site (orange) can engage in non-native aggregation and misfolding interactions (red arrows), and native (α-helical) folding and (coiled-coil) assembly contacts (green arrows). The two lamin coils natively contact 'in-register', starting with the co-localizing N-termini (**Fig. 4.1a**) at an early time point of translation. Delay of inter-chain interactions until later phases of translation results in more competition from 'out-of-register' aggregation and misfolding interactions between earlier and later translated segments. Larger ribosome distances limit inter-chain interactions, which inhibits the stabilizing assembly interactions, and hence promotes intra-chain misfolding interactions. **(b)** Schematic representation of RNC-pair- and diffusion-driven complex formation. Two nascent chains may either be synthesized first and then dimerize by diffusion (right), or dimerize during translation by two proximal ribosomes (co-co assembly, left). The latter promotes proper folding and dimer assembly, by establishing native inter-chain contacts before non-native intra-chain contacts can form, and by limiting cytosolic exposure of protein chain monomers during translation and diffusion. Co-co assembly of lamin coiled-coils results in progressive dimer growth, in a process that merges α-helical folding and assembly and is driven by ongoing translation.

reciprocal chaperoning function that suppresses misfolding, in contrast with the view that high local nascent chains concentrations promote aggregation [196].
The ability to synthesise complexes composed of misfolding-prone subunits may be of broad relevance to cells, as it expands the range of possible protein structures and functions. Indeed, the elongated lamin shape renders the lamin subunits prone to misfolding in monomeric form, yet is also key to its unique mechanical properties [197]. The early and co-translational lamin dimerization we observed may be relevant to efficient subsequent import into the nucleus, where lamin dimers polymerize [198]. Importin-α, which binds the lamin nuclear localization signal and can inhibit premature polymerization [199], may hence provide co- and post-translational lamin chaperoning functions. Lamina-associated polypeptide 2α (LAP2α) may also help to maintain a soluble pool of lamin dimers in the cytosol [198].
Coupled folding and assembly by RNC pairs can impact other translational processes. For instance, peptide bond formation and translational pausing are known to be affected by co-translational folding and related generated pulling forces in the order of 10 pN [141, 200, 201], and may similarly be controlled by co-translational assembly transitions. While our data do not directly show the forces generated by lamin dimerization, the dimer disruption forces we measured (several tens of pN) are of similar order as co-translational folding events [49, 107], which suggests that they are large enough to modulate translational activity.
The mechanism we report is likely more widely relevant, given the recently observed prevalence of RNC pairing for coiled-coil and other homodimer classes, including BTB and Rel homology domain proteins [60], and may extend to heterodimers, higher-order oligomers, as well as membrane based biogenesis. For instance, it is an interesting question whether intermediate filaments with a heterodimeric coiled-coil structure also assemble co-translationally in trans, thus involving two rather than one mRNA strand, and hence rely on the self-chaperoning mechanism we report. Our mechanism may thus contribute to understanding the architecture and (mutation-induced) misfolding of proteins ranging from intermediate filaments to major regulatory and metabolic proteins such as initiation factor 2B and Fatty Acid Synthase. Furthermore, the findings raise the question of whether the formation and translation synchrony of RNC pairs is controlled. The latter may be achieved by sequence-induced translational pausing or regulatory factors, as recently studied in ribosome collision detection [202]. Finally, the results may open up new routes in artificial protein and mRNA therapy design.

4.4 | Methods

Disome Selective Profiling (DiSP)

U2OS (ATCC Cat# HTB-96, RRID: CVCL_0042) and HEK293-T cells (DSMZ Cat# ACC 635) were cultivated in high glucose DMEM media containing GlutaMAX and pyruvate (Gibco), which was freshly supplemented with 10% heat-inactivated FCS (Gibco), 100 U/ml penicillin and 100 µg/ml streptomycin (Gibco) and were grown in a humidified incubator with 5% CO2 at 37 °C (HERAcell 150i). Variations in the lysis protocol were implemented in different datasets. A lysis

buffer with physiological salt concentration (50 mM HEPES pH 7.0, 10 mM $MgCl_2$, 150 mM KCl, 1% NP40, 10 mM DTT, 100 µg/ml CHX, 25 U/ml recombinant Dnase1 (Roche) and protease inhibitor (cOmplete^{TM} EDTA-free, Roche)) was used for DiSP of HEK293-T and U2OS cells (**Fig. S4.2a,d**). A high-salt lysis buffer containing 500 mM KCl was employed for DiSP of HEK293-T cells to test possible effects on the detected onset of lamin disome formation (**Fig. 4.1b**). DiSP of U2OS cells was also performed by lysing cells in the presence of chemical crosslinkers (**Fig. S4.2c,d**). In this case, the lysis buffer was supplemented with 2.5 mM BS3 and 20 mM EDC. Cells were scraped in crosslinker-containing lysis buffer on ice, such that crosslinking occurred simultaneously with cell lysis. After lysis, DiSP samples were processed [60]. Briefly, clarified cell lysates were loaded on sucrose gradients (5% - 45%), centrifuged for 3.5 hours at 35.000 rpm, 4 °C (SW40-rotor, Sorvall Discovery 100SE Ultracentrifuge) and fractions corresponding to the monosome and disome peaks were collected. 30 nt long footprints were extracted from both monosome and disome fractions and deep sequenced. DiSP gene density profiles show the position-wise 95% Poisson confidence interval corrected for library size, and read counts are smoothed with a 15-codon wide sliding window [60].

Cloning

All primer sequences used for cloning are available in Table S1. LMNA corresponding to lamin C that lacks the unstructured head domain (residues 31-542), was PCR-amplified from a self made U2OS cDNA library (SuperScript^{TM} III first-strand synthesis kit, ThermoFisher). The employed PCR primers (MB143 + MB144) added an NdeI restriction site followed by a splitFlAsH tag (SF: MAGSCCGG) at the 5' end and a TwinStrep tag (TS: GGSGSAWSHPQFEKGGGSGGGSGG-SAWSHPQFEKGA) with a BamHI overhang at the 3' end of the construct (final sequence named SF-LMNC-TS). T4 DNA ligase was used to ligate the gel-purified PCR fragment into a BamHI/NdeI restricted pET3a vector. The resulting plasmid was confirmed by Sanger sequencing. Fragments for Gibson assembly were generated by PCR reactions on the SF-LMNC-TS amplicon (described above) using the primer combinations JS9 and JS10, JS9 and JS11, JS9 and JS12. Primers JS7 and JS8 were used to create the linear pRSET plasmid backbone, containing the SecMstrong sequence (FSTPVWIWWWPRIRGPP) at the 5' end and the T7 promoter at the 3' end. The LMNA containing fragments were assembled with the linear plasmid backbone by Gibson assembly. Plasmids were isolated using standard procedures and confirmed by Sanger sequencing. From these plasmids, the linear dsDNA templates for the *in vitro* transcription/translation reaction were amplified by PCR using primers JS28 and JS29.
Plasmids for post-translational lamin constructs (pJS81, pJS82) were cloned using homology based *in vivo* DNA assembly [203]. The pET3a backbone was linearized from stop to start by PCR using oligos JS169 and JS170. N-terminal extensions (M-HHHHHH-AGS-C/CC-GG) were added via primers JS315 (single Cys) or JS316 (double Cys), respectively, and the C-terminal ybbR-tag was introduced with JS318. After DpnI digestion, E. coli XL1 cells were transformed with backbone and insert for *in vivo* assembly. Plasmids were selected on ampicillin-containing LB plates

and confirmed by Sanger sequencing.

Purification of post-translational lamin constructs

BL21(DE3) + pRare (CamR) cells containing pJS81 (AmpR) or pJS82 (AmpR), respectively, were grown at 30 °C in 1 L 2xYT medium supplemented with 100 µg/ml ampicillin and 5 µg/ml chloramphenicol. When the OD600 reached 1, expression was induced with 1 mM IPTG for 4 hours. Cells were harvested by centrifugation at 4 °C, 4000 rcf for 15 min and snap frozen in liquid nitrogen. The pellet was resuspended in lysis buffer (50 mM HEPES-KOH pH 7.5, 150 mM KCl, 5% (v/v) glycerol, cOmplete^{TM} EDTA-free protease inhibitor cocktail (Roche)) to ∼100 OD/mL and lysed in a French pressure cell press at ∼16.000 PSI. The lysate was clarified by centrifugation at 4 °C, 30.000 rcf for 30 min. The supernatant was loaded onto a Protino Ni-NTA Agarose (MACHEREY-NAGEL) gravity flow column, washed (25 mM HEPES KOH pH 7.5, 500 mM KCl, 5% (v/v) glycerol) and eluted (25 mM HEPES-KOH pH 7.5, 150 mM KCl, 5% (v/v) glycerol, 250 mM Imidazole pH 8.0). The sample was concentrated with a centrifugal filter (MWCO 5 kDa) and dimers were isolated by size-exclusion chromatography (Akta Superdex200 pg) using coupling buffer (50 mM HEPES-KOH pH 7.5, 10 mM $MgCl_2$, 5% (v/v) glycerol). Pooled dimeric fractions were concentrated again and snap-frozen in liquid nitrogen.

Attachment of DNA handles to purified lamin dimers

Purified His-CC-LMNA$_{31-311}$-ybbR protein was coupled to 20 nt oligo modified with CoA (Biomers GmbH) in the presence of 50 mM HEPES, 10 mM $MgCl_2$ (both Merck) and 1 µM SFP synthase (addgene) at 4 °C overnight. The remaining oligos were removed by Ni-NTA purification (Protino, MACHEREY-NAGEL). The 1.3 kb DNA handles were created by PCR amplification from pUC19 plasmid (New England Biolabs) using primers modified with phosphate on one end and either biotin or digoxigenin on the other end (Eurofins, Germany). The DNA fragment was purified using Qiagen PCR Purification Kit (Qiagen). The DNA was subsequently digested with Lambda exonuclease (New England Biolabs) at 37 °C for 2 hours, followed by 10 min inactivation at 75 °C. Obtained ssDNA was purified with an Amicon 30 kDa column (Merck, Darmstadt, Germany). The second strand was completed using Deep Vent (exo-) DNA polymerase (New England Biolabs), dNTP mix (ThermoFisher) and a phosphorylated primer (Eurofins, Germany) starting 20 nt downstream to create the overhang. The final product was purified using PCR purification Kit (Monarch). The 1.3 kb DNA handles with 20 nt overhang complementary to the oligo attached to protein and biotin or digoxigenin was ligated to protein-oligo complex using T4 ligase (New England Biolabs) at 16 °C for 4 hours followed by overnight incubation on ice. The resulting DNA-LaminDimer-DNA complex was flash-frozen and stored at −80 °C for future analysis.

Coupling of neutravidin-DNA handles to beads

Double-stranded DNA (dsDNA) molecules were prepared by PCR amplification using digoxigenin (DIG) and biotin 5'-end-modified primers. 2DIGfw5kbp and 3BIOrev5kbp were used with pOSIP-TT as a template in a two-step Phire Green Hot Start II PCR (Thermo Scientific) reaction. The 5 kb PCR product was purified using the QIAquick PCR Purification Kit (QIAGEN). 10 nM 5 kb DNA was coupled to 2 µM neutravidin (Thermo Scientific) by incubation in 10 mM PBS overnight at 4 °C. 2.1 µm diameter carboxyl-functionalized polystyrene beads (Spherotech) were modified with anti-digoxigenin (anti-DIG, Roche), using the carbodiimide crosslinker EDAC, following the PolyLink protein coupling kit protocol (Polysciences). Subsequently, the resulting 5 kb neutravidin-DNA handles (1.7 µm contour length) were coupled to the anti-DIG beads at a reaction ratio of ∼10 neutravidin-DNA/bead for 30 min at 4 °C. The beads with the neutravidin-DNA handles were then washed several times with Tico buffer (20 mM HEPES-KOH pH 7.6, 10 mM $(Ac)_2Mg$, 30 mM $AcNH_4$, 4 mM β-mercaptoethanol) and split into two batches (modified protocol from [204]).

Coupling of ribosomes to beads with DNA handles

Ribosomes from an RNase deficient E. coli K-12 strain (Can20/12E7) were biotinylated *in vivo* at the uL4 ribosomal protein and subsequently isolated [165]. Biotinylated ribosomes were added to one batch of Tico-washed neutravidin-DNA modified beads at 350 nM, supplemented with murine RNase inhibitor (New England Biolabs) and incubated at 4 °C for 30 min. The remaining unbound ribosomes were then removed via pelleting and the beads were washed once with Tico buffer before they were resuspended directly into the cell-free transcription/translation mix described below.

Cell-free protein synthesis and co-translational labelling

The cell-free transcription/translation mix used in this study is a customized version of the bacterial PURE system without ribosomes (PURExpress Δribosomes, New England Biolabs). Biotin was incorporated co-translationally at the two N-terminal amber positions TAG using the suppressor tRNA technique [165]. The system was supplemented with 10 µM of a modified tRNA pre-charged with biotinylated lysine (Biotin-XX-AF_tRNA, amber, CloverDirect), 0.5-5 µM trigger factor, as well as murine RNase inhibitor (New England Biolabs). Synthesis was initiated by mixing the system with the E. coli ribosomes coupled to beads, and the 5.5 nM linear DNA template. The reaction mixture was incubated at 37 °C for 30 min. The resulting nascent chains remained attached to the ribosome due to the SecMstr arrest peptide at the C terminus [124, 125]. Following the transcription/translation reaction, the bead with their tethered and stalled ribosome nascent chain complexes (RNCs) were resuspended in TICO buffer (20 mM HEPES-KOH pH 7.6, 10 mM $(Ac)_2Mg$, 30 mM $AcNH_4$, 4 mM β-mercaptoethanol) at 4 °C. The RNC-coupled beads were diluted in 300 µl TICO buffer prior to their usage in the optical tweezers. As oxygen

scavenger the P2O system (3 U/ml pyranose oxidase, 90 U/ml catalase and 50 mM glucose, Sigma) was used.

Preparation of the FlAsH Dye

Stock solutions of 5 mM were prepared by dissolving FlAsH-EDT_2 (Carbosynth) in DMSO (Thermo Scientific) and stored in an inert atmosphere at −20 °C. For experimental use, the stock solutions were diluted in TICO buffer to a working concentration of 100 nM.

Optical tweezers assay and single-molecule data analysis

Correlated single-molecule force spectroscopy and multi-color confocal laser scanning spectroscopy measurements were carried out with the C-trap instrument (Lumicks, Amsterdam). This instrument features two optical traps formed by a high intensity- and polarization-stable single 1064 nm laser, which is split into two orthogonally polarized beams, one of which can be steered with a piezo mirror relative to the other. Two fluorescence excitation lasers (532 nm and 638 nm) allow for dual color confocal fluorescence, while the dedicated APDs assure single-photon sensitivity. Measurements were performed in a monolithic laminar flow cell with a stable passive pressure-driven microfluidic system with 5 separate flow channels. Data was acquired at a rate of 50 kHz, decimated/averaged down to 500 Hz, and was analysed using custom scripts in Matlab and python. Calibration of the two orthogonally polarized traps was performed using the power spectrum method, where the power spectra obtained from the beads undergoing Brownian motion in the optical traps are fitted with a Lorentzian to obtain conversion parameters for displacements and forces in nm and pN [205]. The trapping laser intensity was kept constant for all measurements, resulting in a trap stiffness of about 260±50 pN/µm. To tether individual molecules, the optically trapped beads were brought within close proximity for short time intervals, before separating them to an inter-bead distance of about 3 µm. A slight increase in the force would signal tether formation. Measurements were taken in a cycling force spectroscopy mode, where the steerable trap was moved at a constant rate of 0.2 µm/s between a minimum bead separation of 2 µm and a maximum force of up to 65 pN. The resulting force-extension curves for individual tethers were fitted with two worm-like chains (WLC) in series, one for the DNA handle contribution (extensible worm-like chain, eWLC) [206] and the other for the stalled nascent chain contribution (inextensible worm-like chain, WLC) [127], yielding an average DNA persistence length of 43±10 nm (SD of 5 nm) and a DNA stretch modulus of 1037±388 pN/nm (SD of 194 pN/nm). Tethered molecules undergoing only gradual transitions could not be fitted with the Odijk inextensible approximation WLC model, and hence WLC rulers were used corresponding to fully compacted and fully extended monomer and dimer chains as depicted in **Fig. 4.5a**, **Fig. 4.6b**, and **Fig. S4.4**, **Fig. S4.8**, **Fig. S4.9**, **Fig. S4.10**, **Fig. S4.11**, **Fig. S4.12** using the average DNA parameters obtained above. Four features were identified during the pulling-relaxation experiments of monomers and dimers. Most of the total chain was characterized as: (i) unfolded, (ii) extending or compacting

gradually, (iii) compacted and unfolding in discrete events, and (iv) compacted and not unfoldable. More specifically, the features were: (i) An unfolded state, in which more than half of the total monomer or dimer chain is unfolded, and remains so during a stretch-relax cycle. (ii) A compacted (or an extended) state composed of more than half of the total monomer or dimer chain, which displayed a gradual contour length increase (decrease) of more than half of the total chain length during a stretch-relax cycle. (iii) A compacted state composed of more than half of the total monomer or dimer chain, which displayed multiple discrete contour length changes totalling more than half of the total chain length during a stretch-relax cycle. (iv) A compacted state composed of more than half of the total monomer or dimer chain, which displayed no detectable contour length change during a stretch-relax cycle.

Estimation of lamin dimer stability

To assess the dimer stability of our constructs, we considered the following. Coiled-coil interactions involve heptad repeats $(abcdefg)_n$ in both monomers. Residues a and d are predominantly hydrophobic and make up the core of the coiled-coil interface, while e and g are typically charged or polar and occupy the region between the core and the solvent. (**Fig. S4.11a**). Structural stability is affected by the number of heptad repeats and the side chain packing at position a and d, with Leucine, Valine and Isoleucine most commonly observed at these positions [158, 182, 184, 207]. The packing is affected by van der Waals interactions between side chains, for instance [208]. The packing arrangement for coiled coils is termed knobs into-holes (KIH) (**Fig. S4.5c**). A 'knob' is defined as a side chain of position a and d residues that project from one helix and packs into a diamond-shaped 'hole' formed by four side chains of an adjacent helix. Three of the four residues of this diamond are themselves knobs, so that a complementary interlocking structure results [180, 181]. The a sites can accommodate more residue types than d, including the bulkier β-branched amino acids, like Val and Ile. The inward pointing orientation of the side chain at the d position is thought to best accommodate amino acids which are not branched at the β-carbon [182–184]. Side-chain mobility contributes significantly to the stability of the folded state. The number of side chain rotamers, can be an additional source of stability [209].
Hence, we counted the full heptads (abcdefg) for each construct and considered the a and d amino acid. Construct 2 has 15 more heptads than construct 1 (of which 5 had Val, Ile or Leu at site a and d, **Fig. S4.5b**). In contrast, construct 3 gains only 7 more full heptads compared to construct 2 (with less ideal amino acids at site a and d). Thus, we predict that construct 2 is significantly more stable than construct 1, while construct 3 is only slightly more stable than construct 2. Consistently, the calorimetric enthalpy of coil 1B (in construct 2 and 3) was measured as above 55 kcal/mol, while 2B (fully present only in construct 3) showed a smaller ∼3.7 kcal/mol [210]. These values agree with our mean rupture forces, which double from construct 1 (∼7 pN) to construct 2 (∼14 pN), but increase only marginally to construct 3 (18 pN, p-value: 0.5).
Next, we calculated inter-chain energies. Because side chains are key to the in-

teractions, we used side chain centroids to represent the residues. Residues were considered in contact if their centroids were closer than 6.5 Å, using Alphafold2 [21] for structure prediction (**Fig. S4.5d**, **Fig. S4.6a**). Cumulative effective contact energies were determined using the approach by Zhang C. et al. [185]. Consistent with the above estimates and our data, the largest energy drop is seen from construct 1 to construct 2 (**Fig. S4.6b**).
One may note the regions with few contacts (marked in pink, **Fig. S4.5d**,**Fig. S4.6**), which link the coils and hendecad patterns (abcdefghijk). The hendecad region in coil 1B (res 207-277) forms an untwisted helical section (**Fig. S4.5d**), which gives rise to mismatched inter-helical hydrophobic interactions and therefore to fewer contacts [158]. The fewer contacts within these regions are also reflected in plateaus within the cumulative contact energies plot (**Fig. S4.6b**).

Calculation of all-atom inter- and intra-molecular contacts for proteome-wide co-co assembly candidates

Initial structures of complexes were selected by aligning the amino acid sequences of high and low confidence co-co candidates to every protein chain larger than 25 amino acids from the PDB (January 3rd, 2023) using adlib (https://pypi.org/project/edlib/). Structural assemblies were a co-co candidate had at least 90% sequence similarity with at least two protein chains were kept (n = 503 for low-confidence and 95 for high-confidence genes, respectively). Then pair-wise permutated interfaces between protein chains were calculated. Interface contacts were defined as atom pairs of residues from different protein chains that had a distance of less than or equal to 5 Å. For these interface residues, intra-molecular chain contacts were calculated. These stabilizing contacts were defined as atom pairs of different residues from the same protein chain that had a distance of less than or equal to 5 Å and were at least 10 amino acids apart on the protein chain. Only inter- and intra-molecular contacts where both residues are emerged from the ribosomal exit tunnel at the co-co onset (30 amino acids before the co-co onset position) are considered and summed. Finally the ratio between ribosome exposed inter- and intra-molecular contacts for every chain is calculated. Then the ratios of all chains from a co-co candidate were averaged by the median.

4.5 | Author Contributions

Conceptualization: F.W., J.S., K.T, K.F., M.B., F.T., B.B., G.K., S.J.T. Methodology: F.W., J.S., K.T., K.F., M.B., F.T., B.B., G.K., S.J.T. Biotinylated ribosomes: A. K. Experiments: F.W., J.S, K.T. Formal analysis, and data visualization: J.S., F.W., K.T., K.F., M.B., B.B., G.K., S.J.T. Writing: all authors. Supervision: S.T., B.B. and G.K.

4.6 | Supplementary Figures

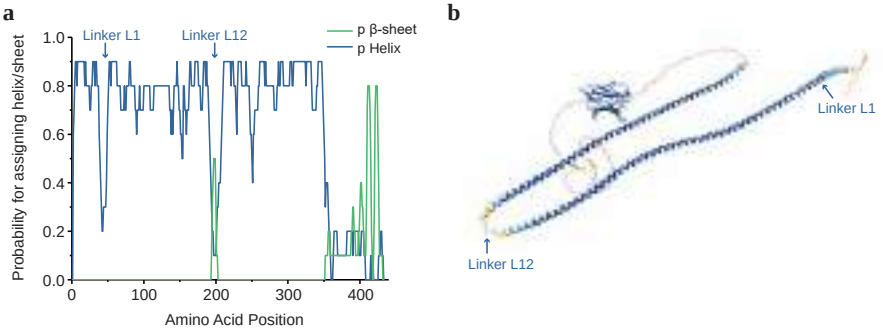

Figure S4.1 | Structure prediction of Lamin. **(a)** Estimation of the secondary structure of $LMNA_{31-476}$ using PredictProtein [211]. The N-terminal ∼350 amino acids of this protein show a high probability of forming an alpha helix, as expected from the known coiled-coil quaternary structure of the lamin rod domain in lamin dimers (**Fig. 4.1a**). The two biggest decreases within the helix probability prediction overlap with known linker regions between coils.[158] The first dip (position 39-53) corresponds to linker L1 between coil 1A and coil 1B. The even bigger dip at amino acid position 200 lines up with the position of linker L12 between coil 1B and coil 2. Additionally, L12 is part of a bigger region (position 176-246) which breaks the typical coiled-coil heptad repeat sequence pattern and leads to an untwisted helical section within the dimer [158]. Further variances in the helix probability prediction might be other irregularities within the sequence, especially the divergence form or composition of the heptad pattern. Since heptad repeats are the basis for coiled-coil formation, these flickers can already indicate regions where inter-chain dimer interactions are compromised like the region around L12. (see **Fig. S4.5** and **Fig. S4.6**). **(b)** Structure prediction of Lamin A by AlphaFold (Uniprot P02545), indicating the alpha-helical rod domain, the C-terminal domain with immunoglobulin-like fold and unstructured segments. Colors indicate model confidence, from dark blue (very high) to orange (very low). The low confidence at the marked position for L12 is reflected in the poor helix probability prediction in (a).

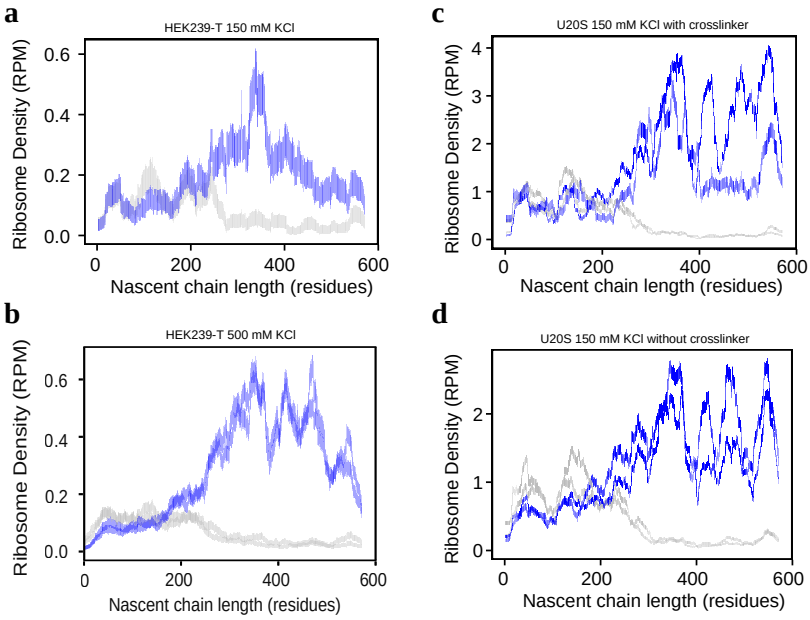

Figure S4.2 | *In-vivo* detection of Lamin nascent chain interactions. Lamin DiSP profiles (codons 1-572) from different cell types, crosslinking, and salt conditions. Blue: density of ribosomes engaged in RNC pairs (coupled by their nascent chains) positioned along the LMNA mRNA (quantified as lamin nascent chain length). Gray: density of single ribosomes (not in pairs). Data are plotted as vertical bars, indicating the position-wise 95% Poisson confidence intervals corrected for library size and smoothed with a 15-codon wide sliding window. The color intensity of the bars represents the amount of reads per position [60]. **(a)** Lamin data from HEK 239-T cells, with 150 mM KCl during lysis (two replicates). **(b)** Lamin data from HEK 239-T cells, with 500 mM KCl during lysis (two replicates). Data reproduced with permission [60]. **(c)** Lamin data from U20S cells with 150 mM KCl during lysis and crosslinked nascent chains (two replicates, crosslinked with 2.5 mM BS3 and 20 mM EDC). **(d)** DiSP data from U20S cells with 150 mM KCl during lysis, without crosslinkers (two replicates). Overall, the curves show that the onset of assembly is similar for all data sets.

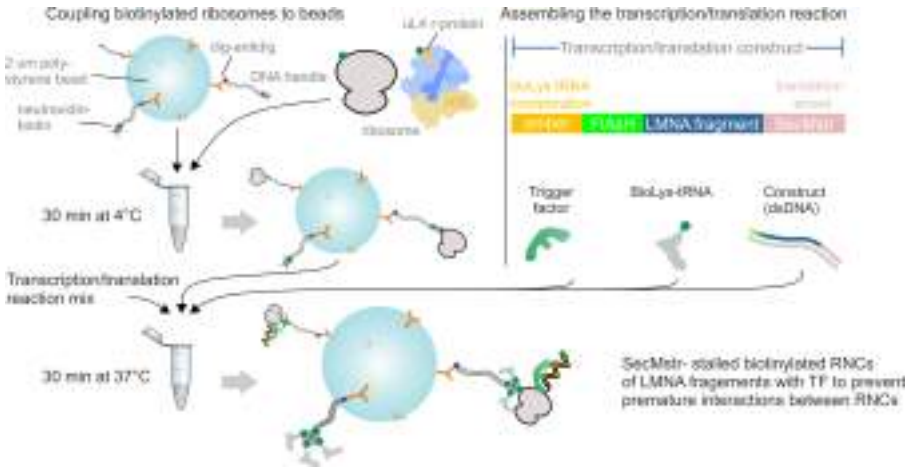

Figure S4.3 | Schematic of the *in vitro* RNC generation protocol. First, biotinylated ribosomes are coupled to Neutravidin-DNA (5 kbp long) coated beads. Next, SecMstr-stalled nascent chains of either $LMNA_{31-123}$, $LMNA_{31-311}$, or $LMNA_{31-476}$ fragments are synthesized using a customized PURE expression system, which included the chaperone trigger factor to mitigate bead clustering via nascent-chain interactions. Forming a pair of two ribosome nascent chain complexes (RNCs) is described in the main text and methods. Briefly, two such beads are brought together such that the RNCs can interact, and then retracted to assess whether a tether of twice the size of a DNA handle is formed (**Fig. S4.4**). When the two corresponding nascent chains form a coiled-coil structure, their N-termini co-localize. These N-termini each contain two adjacent cysteines, such that a bipartite tetracysteine motif forms that binds a FlAsH dye [192]. In order to probe RNC monomers, their nascent chain N-terminus is linked to a DNA handle. For this purpose, biotin is incorporated co-translationally at the N-terminal amber position TAG using a modified tRNA pre-charged with biotinylated lysine, which is linked to the DNA handle using neutravidin. See methods for further details.

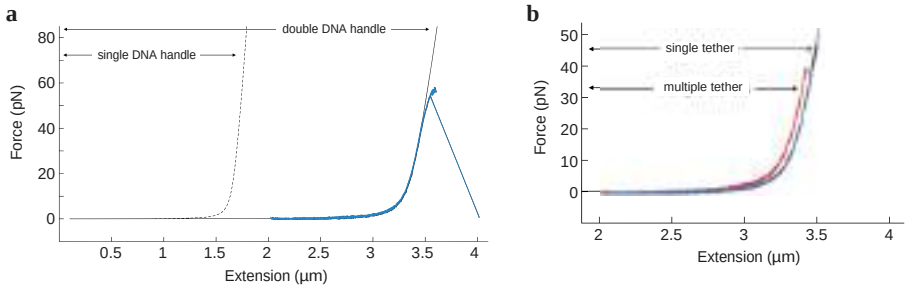

Figure S4.4 | Establishing single tethered RNC pairs. **(a)** The DNA handles used for tethering the RNCs have a length of 5 kbp (dashed black curve, eWLC model for 1.7 µm contour length DNA). To form an RNC pair, two beads coated with DNA-tethered single RNCs are brought together such that the nascent chains can interact. A tether is then formed (blue curve) with a length corresponding to two DNA handles (3.4 µm contour length), which exhibits force-extension characteristics (blue) as predicted by the eWLC model (solid black curve) within a force range of 0-35 pN [212]. Above ∼35 pN individually tethered molecules begin to deviate slightly from the eWLC model due to twisting of the DNA handles. **(b)** More than one such tether can form between the optically trapped beads, which are not aligned in parallel with the bead-bead axis resulting in a shorter bead-bead distance, do not follow the eWLC model, and do not yield a single step break when one tether breaks (red), and can hence be identified.

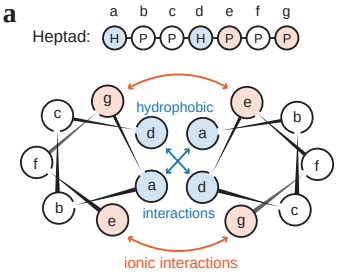

b

Lamin A/C Coil/ Construct:	#heptads	a site L,V or I	d site L,V or I	L,V or I at a & d
1A (res 31-67)	5	2 1	3	2
1B (res 79-222)	17	11 1	6 2	5
2AB (res 241-385)	13	4 1 2	4	1
1 (LMNA 31-123)	11	5 1	5 2	3
2 (LMNA 31-311)	26	15 3 1	11 2	8
3 (LMNA 31-476)	33	18 3 2	13 2	9

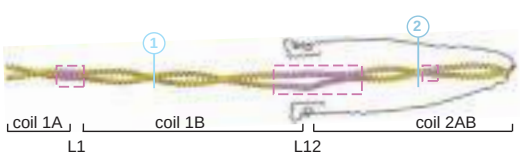

Figure S4.5 | Structural features of lamin coiled-coils. **(a)** Helical wheel representation showing the 7 amino-acid coiled-coil heptad repeat, denoted $(abcdefg)_n$. Residues at positions a and d are predominantly hydrophobic and make up the core of the coiled-coil interface, while e and g positions are filled typically with charged or polar residues and occupy the region between the core and the solvent. [182–184] **(b)** The table shows the number of full heptad repeats for each lamin coil (top) and for each of our constructs (bottom) based on previous sequence analysis [158]. Non-polar hydrophobic amino acids Valine, Leucine and Isoleucine at the a and d position were counted (being the most common in the heptad) [184]. If a heptad had both a and d position filled with either Val, Leu or Ile it was noted in the last column. **(c)** Coiled-coil packing arrangement termed "knobs-into-holes" (KIH) visualized by the side chain arrangement in an N-terminal region of lamin. A 'knob' is the side chain (green) of every first and fourth residue of each heptad (a and d) that projects from one helix and packs into a diamond-shaped 'hole' formed by four side chains of an adjacent helix (blue). Three of the four residues of this diamond are themselves knobs so that a complementary interlocking structure results. [180–182] **(d)** Alpha-fold2 dimer structure prediction for $LMNA_{31-476}$. The lengths of $LMNA_{31-123}$ (1) and $LMNA_{31-311}$ (2) are marked in the structure. Linkers (L1 and L12) and sequence regions where the heptad periodicity is interrupted and is partially substituted by an 11 amino acid repeat, termed the hendecad pattern, are highlighted in pink.

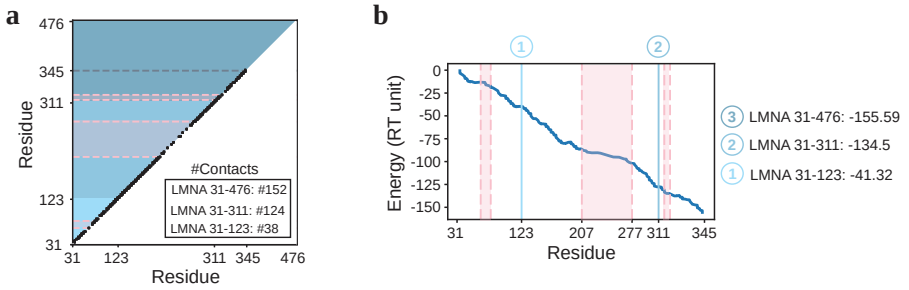

Figure S4.6 | Interaction strength of lamin coiled-coils. **(a)** Inter-chain contact map for lamin dimer structure prediction in **Fig. S4.5d** (see methods). The three constructs are indicated by different shades of blue. Marked pink regions correspond to regions as in panel **Fig. S4.5d**. The grey dotted line at residue 345 marks the end of the coiled-coil structural motif and the start of the C-terminal tail region containing an additional immunoglobin-like domain. For $LMNA_{31-123}$ we found 38 contacts, for $LMNA_{31-311}$ 86 additional contacts compared to $LMNA_{31-123}$ (124 in total) and for $LMNA_{31-347}$ 28 additional contacts compared to $LMNA_{31-311}$ and $LMNA_{31-123}$ (152 in total). **(b)** Environment-dependent inter-residue contact energies for contacts obtained in (a). Stability for individual constructs were estimated by summing energy parameters calculated for an α-helical structure environment (see methods). Marked pink regions correspond to the same regions where the heptad periodicity is interrupted as in **Fig. S4.5d** and (a). Despite the large hendecad region found within the $LMNA_{31-311}$ dimer, we still find the largest decrease in free energy by -93.29 RT units when going from the shortest $LMNA_{31-123}$ to the intermediate $LMNA_{31-311}$, which is consistent with the number of inter-chain contacts as analysed in panel (a).

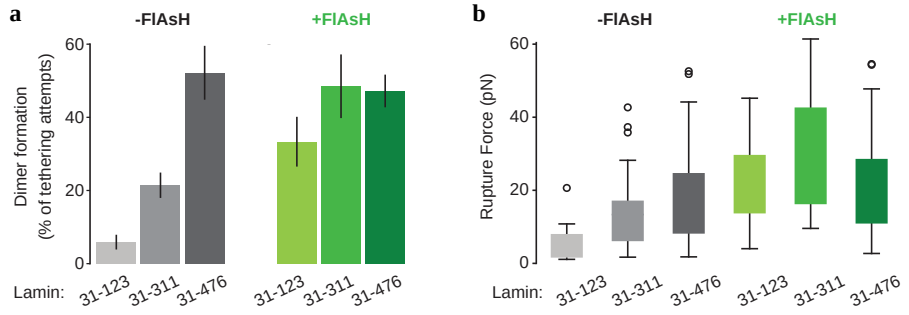

Figure S4.7 | RNC dimer formation frequency and rupture force during stretching. **(a)** Dimer formation as a fraction of dimerization attempts in the presence (n = 91 molecules) or absence (n = 62 molecules) of FlAsH for all lamin C nascent chain fragments. Data in absence of FlAsH (grey), also plotted in **Fig. 4.2b**, is added for comparison. Error bars represent the standard error of proportion. **(b)** Dimer rupture forces in the presence (n = 91 molecules) or absence (n = 62 molecules) of FlAsH for all lamin C nascent chain fragments. Data in absence of FlAsH (grey), also plotted in **Fig. 4.2c**, is added for comparison. Boxes indicate the 25th and 75th percentiles.

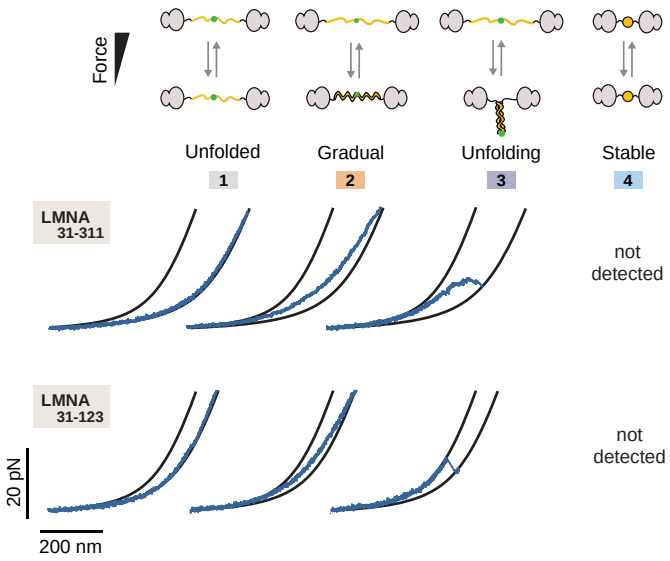

Figure S4.8 | Classes of force-extension behavior of the lamin nascent chain dimers $LMNA_{31-311}$ and $LMNA_{31-123}$. Black lines are theoretical worm-like chain (WLC) curves for both nascent chains being compact (left) or fully unfolded (right). The position of the measured data (blue) in between these two reference curves indicates what fraction of the nascent chain (how many amino acids) is in the compact state, and what fraction is in the extended state. During stretch-relax cycles of these two lamin fragment lengths three classes are observed, with the majority of the chain: (1) remaining unfolded, (2) initially compact and gradually extending and initially extended and gradually compacting under tension, as expected for linear α-helices, and (3) initially compact and unfolding discretely below 45 pN, as expected for coiled-coil dimer structures. The stably compacted class (4), detected during measurements of the longest lamin fragment $LMNA_{31-476}$ (**Fig. 4.5a**), was not observed here, consistent with misfolding being suppressed by nascent chain interactions.

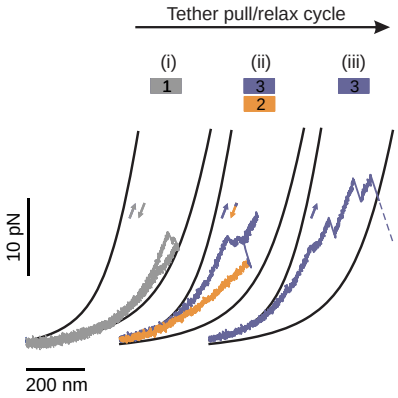

Figure S4.9 | Sequence of conformational transitions. Three consecutive pull-and-relax cycles of a RNC dimer ($LMNA_{31-476}$), showing subsequent conformational transitions, which have a heterogeneous character at the molecular level. Transitions corresponding to three different folding features (1-3) are observed during the three cycles (i-iii). In the first pull the dimer is mostly unfolded (gray), then folds after relaxation to 0 pN, as observed in the second pulling cycle, where it unfolds partially during pulling and relaxation (purple), before gradually compacting during relaxation (orange). In the third cycle the molecule is found to be compact, and then unfolds once more before rupturing during stretching (purple).

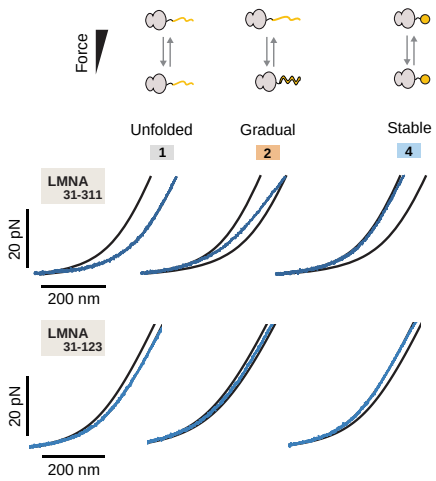

Figure S4.10 | Classes of force-extension behavior of the lamin nascent chain monomers $LMNA_{31-311}$ and $LMNA_{31-123}$. Black lines are WLC reference curves for the single nascent chain being compact (left) or fully unfolded (right). During stretch-relax cycles four classes of conformational states are distinguished, with the majority of the chains: (1) remaining unfolded, (2) initially compact and gradually extending and initially extended and gradually compacting under tension, as expected for linear α-helices, (4) being initially compact and remaining so up to 45 pN, typically for multiple stretch-relax cycles, indicative of entry into a kinetically trapped misfolded state (3). Observations of Class 3 were negligable, which is consistent because the coiled-coil cannot form without the second chain present.

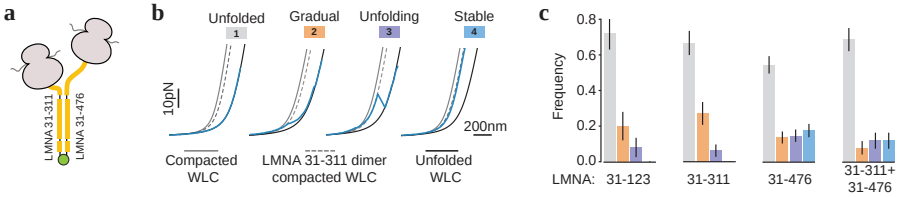

Figure S4.11 | Inter-chain contact formation between different nascent chains of $LMNA_{31-311}$ and $LMNA_{31-476}$. **(a)** Experimental set-up: One ribosome that has translated $LMNA_{31-311}$ is paired with a ribosome having translated the longer nascent chain of $LMNA_{31-476}$, thus mimicking a leading and a trailing ribosome. Nascent chains are linked at their N-termini by the FlAsH dye. **(b)** Corresponding force-extension example traces of the four observed classes of behavior. Solid lines are WLC curves for nascent chains being fully unfolded (right - black) and compact (left - gray). Dotted curve: WLC for the full compaction of a symmetric nascent $LMNA_{31-311}$ dimer. Native inter-chain contacts can be only formed for this segment (see pnael (a)). Class 3 example trace shows corresponding data. **(c)** Frequency of stretch-relax cycles with observed force-extension features (see panel (b)). Left 3 data sets: symmetric lamin nascent chain dimers with equal length pairing as a reference (see **Fig. 4.5b**). Right data set: assymetric nascent chain length pairing between $LMNA_{31-311}$ and $LMNA_{31-476}$ (n = 44 $LMNA_{31-123}$ + $LMNA_{31-476}$ molecules, 51 pulling cycles). Error bars: standard error of proportion. These data show that asymmetric RNC pairs also can generate lamin dimers *in vitro*. As dimers can form only with the segments present in the $LMNA_{31-311}$ nascent chain, we compare the asymmetric dimer with the $LMNA_{31-311}$ symmetric dimer. The fraction of predominantly unfolded tethers (class 1, grey) is around 60% for both. The asymmetric dimer shows more misfolded states (class 4, blue) than the intermediate ($LMNA_{31-311}$) symmetric dimer, which does not show such states. This data is consistent, as the additional segments of the longer chain do not have a partner to dimerize with, and hence provides opportunities for misfolding.

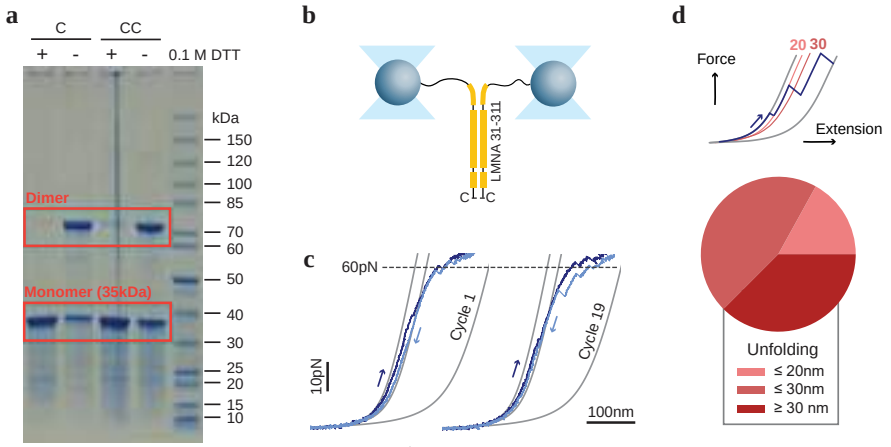

Figure S4.12 | Purified LMNA$_{31-311}$ dimer is stable against forced unfolding. **(a)** SDS Page analysis of purified LMNA$_{31-311}$. One or two N-terminal cysteines were used for covalent intradimer linkage. The linkage was tested and confirmed by adding 0.1 M dithiothreitol (DTT) to reduce the disulfide bond between the cysteines. Samples were further purified with Akta Superdex 200 pg. **(b)** Optical tweezer experimental setup for purified LMNA$_{31-311}$. DNA linkage of purified dimers to 1.3 kbp DNA handles was achieved through the genetically introduced ybbR-tag at each C-terminus, which was then coupled to DNA anchors modified with coenzyme A using Sfp synthase. **(c)** Force-extension curves of LMNA$_{31-311}$. Dark blue indicates the pulling trace, where the extension between the beads is increased, and light blue indicates the relaxation trace, corresponding to decreasing the distance between beads. Light grey lines are WLC models for the fully compact, unfolded and 30 nm unfolded state. Force-extension curves deviate from the WLC model at high forces due to the nonlinear dynamics of the DNA. Despite repeatedly pulling to forces close to our experimental limit of 65 pN, the dimer unfolds only marginally indicating high dimer stability. **(d)** Characterization of the unfolded lengths. Only traces that could be stretched close to the overstretching plateau were considered (n=17 molecules, 122 cycles). We counted if within one cycle the tether would unfold by 20, 30 or more than 30 nm. Over half (62%) of all the cycles only unfolded up to 30 nm or below. This indicates a greater stability as compared to the dimer nascent chain constructs, which suggests a destabilizing effect of the two ribosomes in close proximity.

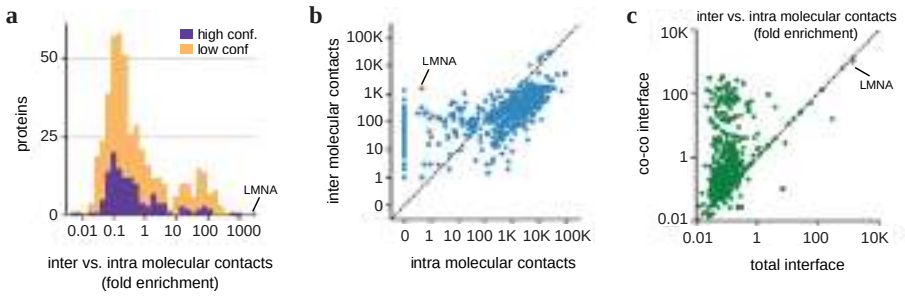

Figure S4.13 | Intermolecular contacts for co-co assembling proteins throughout the proteome. **(a)** Inter- vs. intra-molecular contacts for dimer interfacial residues, of high and low confidence co-co candidates formed during co-co assembly (see methods). Low contact order intramolecular residue pairs (<10 residues apart) were not counted, as they for instance involve alpha-helix formation. Two peaks are observed: A first sub-population of nascent dimers that showed over 10-fold more inter- than intra-chain contacts (15% of dimers, or 95/598), suggesting an important role for the partner chain in stabilization. The second sub-population showed less than 10-fold more inter- than intra-chain contacts at co-co onset (85% of dimers, or 503/598), which could indicate partial domain folding before dimerization. Dimers in this group may also be exploiting self-chaperoning, for instance those with an inter/intra contact ratio of more than 1.**(b)** Satter plot giving the number of contacts at the co-co interface for all high and low confidence co-co candidates (see also panel (a)). **(c)** The ratio of inter- over intra-chain contacts at the co-co assembly onset against that ratio for the total interface of the protein complex after translation. Notably, for most proteins this ratio was larger at the co-co assembly onset than after translation, suggesting a relevance for self-chaperoning and that the initial inter-chain contacts are further stabilized by intra-chain contacts later during translation.

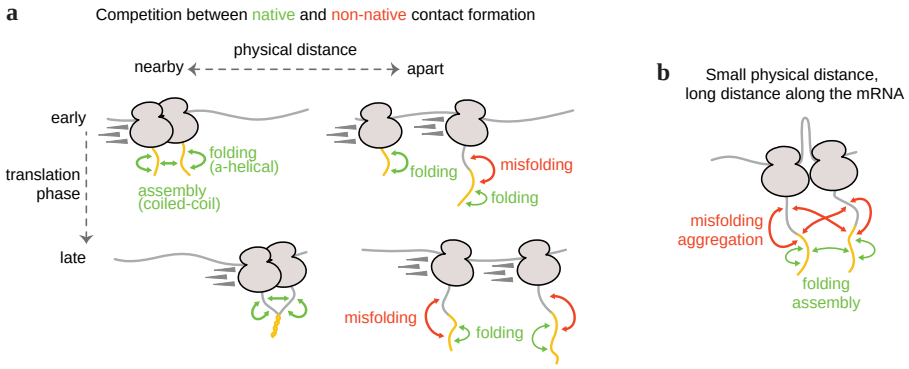

Figure S4.14 | Folding competition in co-translational assembly. Indicated are the possible native and non-native contacts that can form within and between nascent chains during co-co assembly of coiled-coils. **(a)** When both RNCs are in the early stages of translation on the same mRNA strand (top-left), for each residue the native-partner residue is available and nearby, while many possible non-native-partner residues have not yet emerged. This can remain to be the case during translation (bottom-left). RNCs can alternatively be further apart, either because the one ribosome trails the other on the same mRNA (left-right), or because RNCs from different mRNA strand will ultimately interact (not shown). Such distance between RNCs means the nascent chains remain monomeric for a longer time and hence have more opportunities to misfold – both because of increased duration and because the chains become longer and have more options for non-native contact sites. **(b)** RNCs can come into contact because the mRNA loops or because the trailing ribosome catches up with the leading one (not shown).

The trust I lost
I found back by trusting you
To trust in me

Artist impression of co-co assembly of the BTB dimer
Fineliner & Pencil, 2025
Katharina Till

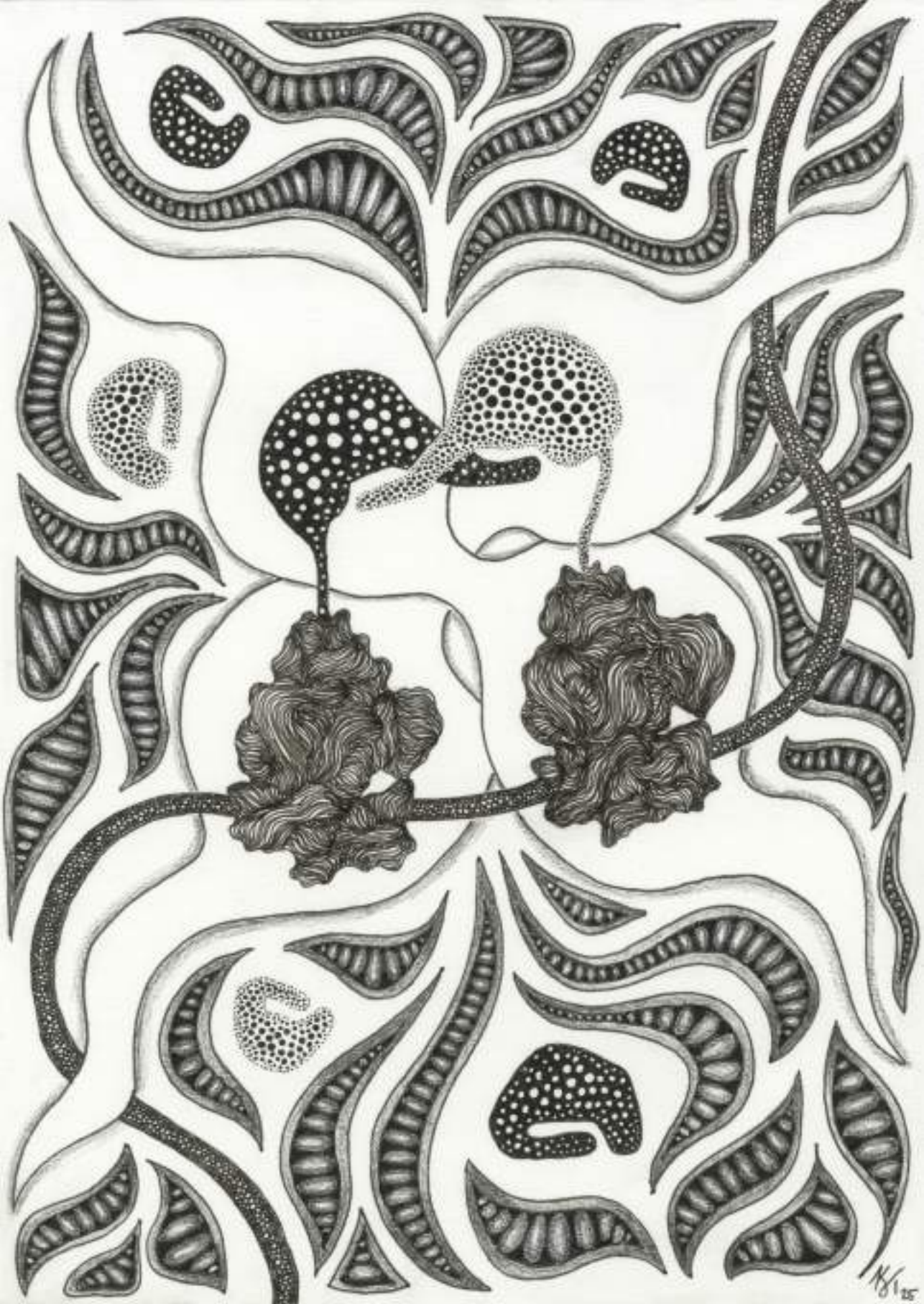

Chapter 5

TRANSLATION-DRIVEN TEMPORAL CONTROL FOR INTERTWINED PROTEIN ASSEMBLY

K. Till, V. Sunderlikova, P. Jevtić, F. Tippmann, M. Bertolini, K. Fenzl, J. Schmitt, A. Katranidis, B. Bukau, G. Kramer, M. Rapé, S. Tans
Manuscript under review

Protein complexes are essential to cells. However, how structurally intertwined protein subunits can assemble faithfully is poorly understood. Here, we reveal a "temporal control" mechanism driven by coupled ribosomes to form intertwined dimers. Using Disome Selective Profiling and optical tweezers, we show that the BTB domains of KEAP1, KLHL12, and PATZ1 form stable closed states as monomers, thus impeding proposed domain-swapping assembly routes. By contrast, the timed emergence of nascent chain segments during translation enables alternative folding-assembly pathways that bypass the closed monomeric state. Analysis indicates that this mechanism works in concert with dimerization quality control by the E3 ligase SCF-FBXL17 and is relevant across the BTB domain family. This study shows that ribosome cooperation expands the range of possible protein architectures.

5.1 | Introduction

Protein complex formation is pivotal to all main cellular functions [26, 213–215]. The assembly of two proteins has long been characterized as a simple binding event [216, 217]. However, many complexes within the proteome exhibit highly intricate protein-protein interfaces and even intertwined polypeptide chains [218]. Examples range from large nuclear pore complexes [219], to E3 ubiquitin ligase Cullin complexes [220], down to interleukin dimers [221]. These features imply major assembly challenges: protein subunits must either be kept partially unfolded until they interact, or initially adopt compact monomeric structures that require remodeling to assemble [222–224]. Moreover, the involved cytosolic exposure of assembly interfaces poses intrinsic risks, with many proteins subunits prone to aggregation [102, 225, 226]. These observations suggest that a vast space of critical folding and assembly mechanisms remains unexplored.

We recently showed that over 800 homodimers assemble co-translationally in human cells [60]. In this process termed co-co assembly, dimerization is driven by interactions between nascent chains emerging from nearby ribosomes translating the same or different RNA messages [152, 227]. BTB proteins were identified as a main co-co assembly class (**Fig. 5.1a**). Human cells contain about 200 different proteins with BTB dimerization domains [228]. They perform functions ranging from gene regulation to actin stabilization, and often contain BTB domains in combination with domains such as Kelch, ion transport, and Zinc finger domains [229]. BTB domains are thought to dimerize by "domain-swapping" [228]. Here, a β-strand that is folded in the monomeric state must dissociate to instead fold onto a dimerization partner, giving rise to an intertwined dimer [228, 230] (**Fig. 5.1b**). However, the involved energetic cost and aggregation risks raise questions about the feasibility of this process [223, 231]. Correct BTB homodimer formation is pivotal to cells, as also highlighted by the dimerization quality control pathway [232–234] that targets BTB heterodimers and monomers for degradation. BTB domain mutations that impair dimerization are linked to erroneous development and diverse medical conditions [235–237].

Here we advance a translation-driven "temporal control" mechanism for the assembly of intertwined protein complexes, and study it at the single-molecule level using BTB dimerization domains as a model system. We hypothesized that translational coupling can offer alternative assembly routes. Specifically, we reasoned that a dimerization domain contains various polypeptide segments that are synthesized in a specific order during translation, and that their ordered emergence could in principle alter the folding-assembly pathway. In our approach, disome selective ribosome profiling (DiSP) is used to detect co-translational assembly of BTB domain proteins *in vivo*, while optical tweezers are employed to study folding and assembly transitions for individual monomers and dimers *in vitro*.

5.2 | Results

5.2.1 In vivo dimerization of BTB domain proteins

We assessed BTB dimer formation *in vivo* using Disome Selective Profiling (DiSP) data [60]. In this method, co-co assembly is detected by the conversion of monosomes into disomes during translation, as quantified by deep sequencing of mRNA ribosome footprints, after mRNA digestion and separation of monosome and disomes on a sucrose gradient. We focused on two Kelch proteins: KEAP1, a key sensor of oxidative and electrophilic stress [238–241] and KLHL12, a substrate-specific adapter of a BCR (BTB-CUL3-RBX1) E3 ubiquitin ligase complex that regulates WNT signaling and ER-Golgi transport [242–244]. We also studied PATZ1, a regulator of embryogenesis, senescence, T-cell development and neurogenesis [245–248]. The DiSP data shows monosome to disome conversion for all these proteins upon translation of their BTB domain (**Fig. 5.1c**, **Fig. S5.1a**), thus indicating that their dimerization *in vivo* involves co-co assembly. Structural analysis showed a high degree of structural similarity between the three proteins, each exhibiting a domain-swapped dimer conformation (**Fig. S5.1b**). PATZ1 contains a 30-amino acid glycine- and alanine-rich central loop between the α-helix A2 and β-strand B3 [249], thus setting it apart from the resolved KEAP1 BTB domain structure [250] and the AlphaFold [251] predicted structure of the KLHL12 BTB domain.

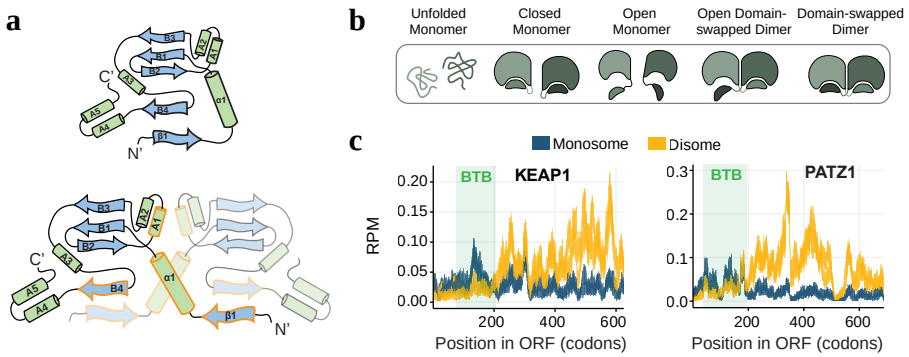

Figure 5.1 | BTB monomer and dimer topology, domain-swapping mechanism and DiSP profiles of BTB domains. **(a)** Topology of closed BTB monomer and BTB dimer. The amino-terminal β-strand β1 folds back onto its own C-terminal β-strand B4 in the closed monomer. In the dimer, β1 folds onto the B4 strand of the other chain. Orange outline: dimerization interface. **(b)** Domain-swapping mechanism cartoon. Closed monomers must open-up to adopt the domain swapped dimer conformation. **(c)** Disome selective profiling (DiSP) for KEAP1 and PATZ1. Monosome (grey) and disome (yellow) footprint density along the position in the ORF (RPM = Reads Per Million). Monosome to disome shift indicates co-co assembly onset. After that disome enrichment levels out and remains high. Data taken for HEK293-T cells [60].

5.2.2 BTB monomers adopt a closed state at the ribosome

It is thought that BTB monomers can alternate between a closed state, in which the β-strand β1 is folded back onto the β-strand B4, and an "open" state, in which β1 dissociates from B4 while the rest of the protein remains folded (**Fig. 5.1b**). The open state is central for BTB dimerization, as it allows β1 to associate with B4 of the dimerization partner. Besides the β1-B4 interaction, the dimerization interface is also composed of the α-helical interactions α1-α1 and A1-A1 (**Fig. 5.1a**, orange outline). However, native BTB domains are almost exclusively observed as dimers, and attempts to purify BTB monomers have been largely unsuccessful [252–254], thus leaving the conformation and stability of BTB monomers unclear. To study monomeric nascent BTB domains we used optical tweezers. We generated stalled ribosome-nascent chain complexes (RNCs) that expose one BTB domain using a modified *in vitro* transcription-translation reaction with biotinylated ribosomes. In a microfluidic chamber, single RNCs were tethered between two laser-trapped polystyrene beads via DNA handles and linked to the ribosome and the N-terminus of the nascent chain (**Fig. 5.2a**). Nascent chains were probed by repeated stretching and relaxation, and the measured Force-Extension curves were fitted to a worm-like chain (WLC) model (**Fig. 5.2b**). Sudden or gradual deviations from the WLC model indicated transitions between folded states. Folded states were identified by their contour length, which is the length of the unfolded part of the nascent chain. Consequently, a contour length of 0 nm corresponds to the fully compacted BTB monomer in the closed state (**Fig. 5.2b**). We probed KEAP1 and PATZ1 nascent chains during multiple stretch-relax cycles, thus obtaining frequencies of contour lengths indicative of specific folding states (**Fig. 5.2c**). Both nascent BTB domains showed broad distributions of folding states, with one peak at the fully compacted closed BTB monomer. The entire BTB domain is outside the ribosomal tunnel due to a 42 residue long Glycine-Serine linker at the C-Terminus (**Fig. 5.2a**). Note that a construct where the BTB domain is pushed outside the tunnel by the natural sequence also showed full compaction (**Fig. S5.2a**), consistent with the closed monomer state. We observed a second frequently populated contour length that is consistent with unfolding from the closed to the open state. For PATZ1 this folded state had a contour length of 16 nm, slightly longer than the 11 nm observed for the BTB domain of KEAP1 (**Fig. 5.2c**). Consistently, the N-terminal segment including α1 and β1 is slightly longer for PATZ1 than for KEAP1 (estimated as 13 nm and 9 nm, respectively). To further test whether this folded state is indeed the open conformation, we translated a truncated version of PATZ1 that lacks β1 and hence cannot fold back to form the closed state (**Fig. 5.2d**). This construct indeed showed reduced frequencies at 0 nm corresponding to the closed state, while the peak for the open state consistently decreased to smaller lengths (from 16 nm to about 11 nm) (**Fig. 5.2d**). In line with reduced stability for this truncated variant, we further noticed decreased unfolding forces ($p = 0.03$, **Fig. S5.2b**) and a wider range of intermediate states (**Fig. 5.2c,d**). The closed state unfolding force for the full-length constructs was 36 pN and 26 pN for KEAP1 and PATZ1 respectively (**Fig. S5.2c**). This stability of the closed state, which must open up to dimerize by domain swapping, underscores the challenge of that assembly route.

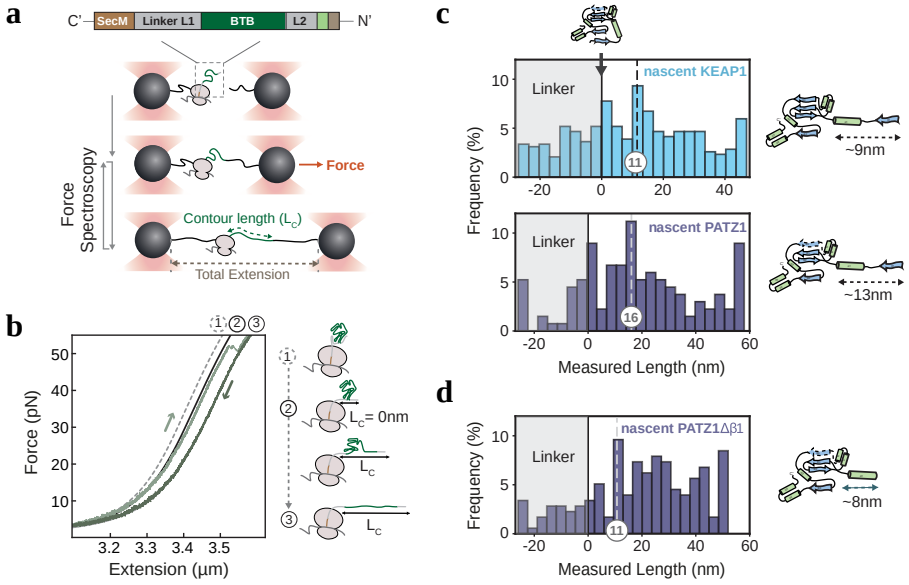

Figure 5.2 | BTB monomers adopt the closed state at the ribosome. **(a)** Cartoon of optical tweezer approach. SecMstr stalls translation. Flexible Gly/Ser linker L1 pushes BTB domains outside the ribosomal tunnel. Flexible linker L2 allows RNC dimer experiments (see **Fig. 5.6a**, **Fig. S5.7d**) (see Methods for amino acid sequences). Stalled RNCs are linked to laser-trapped beads by DNA handles (black). Biotinylated nascent chain N-terminus is linked to a DNA handle attached to the second bead by moving the trap and bringing them in closer vicinity. Nascent chains are exposed to repeated stretch-wait-relax cycles by changing the distance between the beads (extension) while measuring the force. **(b)** Example Force-Extension traces for nascent KEAP1 monomer. WLC fit for (1) fully compacted state including linkers, (2) compacted BTB state, (3) fully unfolded state. Deviations from WLC curves indicate changes in unfolded length of the nascent chain. **(c)** Length histogram for nascent KEAP1 (N = 386 states; see methods for further details) and nascent PATZ1 (N = 134 states). Flexible Gly/Ser linkers unfold at low forces in grey area (**Fig. S5.2b**). Length indicates contour length of the unfolded part of the nascent chain. Fully compacted BTB monomer positions at 0. Dashed line: frequently populated partial fold, consistent with the open monomer state (cartoon right). Cartoons: the N-terminal segment including α1 and β1 is slightly longer for PATZ1 than for KEAP1, estimated as 13 nm and 9 nm, respectively. **(d)** Length histogram for the nascent PATZ1$\Delta\beta$1 variant (N = 177 states), which consistently shows a lower frequency for the fully compacted closed monomer, and a shift for the open conformation to smaller length.

5.2.3 BTB closed states resist unfolding

To assess whether ribosome proximity affected BTB domain folding and stability, we performed a set of experiments with full length BTB domains in the absence of ribosomes. We purified KEAP1 and PATZ1 proteins (termed wtKEAP1 and wt-

PATZ1), as well as the KLHL12 BTB domain (wtKLHL12). To limit measurement noise, short (1.3 kbp) DNA handles were coupled directly to the monomer termini (**Fig. 5.3a**). We developed a protocol to purify the BTB domains as dimers, attach handles, and subsequently tether BTB domain monomers in between beads (see **Fig. S5.3**). This method allowed us to obtain stretch-relax cycles on BTB domain monomers (**Fig. 5.3b**).

Consistent with the nascent BTB domain data (**Fig. 5.2c**), purified wtKEAP1 and wtPATZ1 populated the fully compacted closed state and the partially folded open state (**Fig. 5.3c**), with the open state of wtPATZ1 being slightly more extended than that of wtKEAP1. Surprisingly, the unfolding force of the closed state off the ribosome was lower than on the ribosome for wtKEAP1 (26 vs 36 pN, $p = 5.8 \cdot 10^{-7}$), and wtPATZ1 (12 vs 26 pN, $p = 1.0 \cdot 10^{-6}$) (**Fig. 5.3e**, **Fig. S5.2c**). Likewise, the open state also did not show higher unfolding forces for ribosome-released compared to nascent BTB monomers (29 vs 36 pN for wtKEAP1, $p = 0.3$, and 19 vs 37 pN for wtPATZ1, $p = 0.007$) (**Fig. 5.3e**, **Fig. S5.2c**). We observed fast back-and-forth hopping between open and the fully compacted state during stretching (**Fig. 5.3f**), indicating opening and closing of BTB monomers. Such compaction that can counteract applied forces offers further indication of the stability of the closed state, and the resulting challenges of the domain swapping route.

5.2.4 BTB monomers populate a small core fold

We wondered if the BTB monomers populate additional folding intermediates, as those could be relevant to monomer-monomer interactions during assembly. Hence, we analyzed intra-chain residue-residue contact maps of the BTB monomers (**Fig. S5.4**). For KEAP1 and KLHL12, this analysis showed the most contacts in a sub-fold termed the "core" fold, which comprises three β-strands (B1, B2, B3) and two small α-helices (A1 and A2) (**Fig. 5.3g**, red). Considering that this sub-fold contains roughly 52 residues, it would yield a peak at about 27 nm in the length histograms when it is populated and the rest of the protein is unfolded. Indeed, wtKEAP1 and especially wtKLHL12 showed a pronounced peak at this length within the folded state histogram (**Fig. 5.3c,d**). Consistently, this core BTB structure also showed the highest unfolding forces, reaching 45.4 pN on average for wtKLHL12 (**Fig. 5.3e**).

We found that the (un)folding pathways of wtPATZ1 were overall similar to wtKEAP1 and wtKLHL12, but did show minor differences that are consistent with the known structures. Specifically, the residue-residue contact map for PATZ1 showed fewer contacts for this core state, which can be explained by the distinct flexible loop between A2 and B3 [249], and its two rather than three beta-strands (**Fig. S5.4**). Consistent with these observations, the length histogram showed two instead of one small intermediate (**Fig. 5.3c**, **Fig. S5.5a**), which both also showed a lower mean unfolding force (31 pN and 33 pN) than wtKEAP1and wtKLHL12 ($p = 0.01$) (**Fig. S5.5b**).

These data suggest the core and open states as intermediate folded states, that are positioned in between the unfolded state and the closed monomer state, in a manner that is notably similar for all studied proteins. To further test this, we an-

alyzed the transitions between these states (**Fig. 5.3g**). Consistently, we found that transitions between directly adjacent states along this putative pathway showed the largest frequencies, while transitions that skip one state or go to another state showed lower frequencies (**Fig. 5.3g**, **Fig. S5.6a**). Note that the core state, given its significant stability, did not always unfold during stretching to 65 pN, which is the maximum because of DNA melting. Refolding was studied by quantifying the state populated after the waiting period at 0 pN to allow for folding without a counteracting force (**Fig. S5.6b**). This state after folding is most often the fully

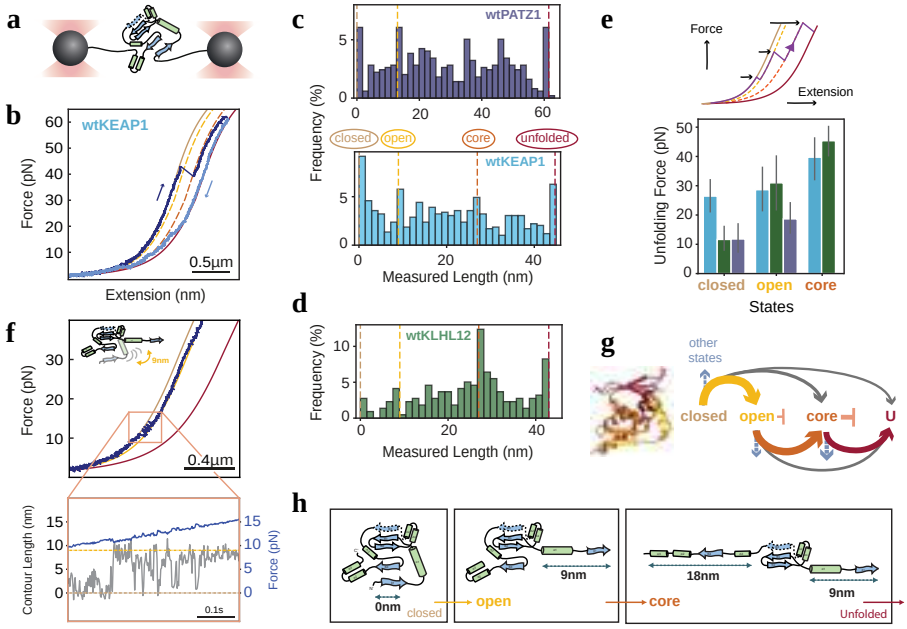

Figure 5.3 | BTB monomers populate a small core fold. **(a)** BTB monomers of KEAP1, PATZ1 and KLHL12 purified and tethered at their C- and N-termini between two optically trapped beads via DNA handles. **(b)** Example force-extension traces for wtKEAP1 monomer, showing unfolding and refolding events indicated by abrupt force changes. **(c)** Contour length histograms showing folded states of wtPATZ1 (N = 495 states; see methods for further details) and wtKEAP1 (N = 589 states). Dotted lines show closed, open, core, and unfolded BTB states. For wtPATZ1 also see **Fig. S5.5a**. **(d)** Contour length histograms showing folded states of wtKLHL12 (N = 218 states). Dotted lines show closed, open, core, and unfolded BTB states. **(e)** Average unfolding forces of the closed, open and core states, using a length window of 5 nm around the dashed lines. Error bars: 95% confidence interval. Colors: see panels (c) and (d). See methods for N-Values. **(f)** Hopping between "closed" and "open" states (yellow dotted WLC). Zoom: time vs. contour length data showing the hopping behavior, indicating repeated unfolding and refolding between open and closed states. **(g)** Right: Observed transitions between BTB folded states, with thickness indicating frequency (see methods). Left: Structural elements involved in these transitions. **(h)** Unfolding sequence for BTB monomers as derived from the experiments.

compacted closed state, while the state before folding is typically the fully unfolded or core state, while the distributions are wide (**Fig. S5.6b**). Thus, the data indicated the following generic folded states ordered from small to large: core (B1, B2, B3, A1 and A2), open (adding B4, A3, A4, A5), and closed (adding β1 and α1) (**Fig. 5.3h**).

5.2.5 Temporal assembly control at the ribosome

Our data suggested the following competing assembly pathways (**Fig. 5.4**): After translation of β1, α1 and the BTB core, the BTB cores fold as monomers in both pathways, which split subsequently in two. In the monomer pathway, continued translation exposes B4 that then contacts β1, thus forming the closed monomer that impedes dimerization by domain-swapping (**Fig. 5.4**, left). In the dimer pathway, two nascent chains can start interacting after core folding, when helices α1 and A1 of the dimerization interface are exposed but B4 is not (**Fig. 5.4**, right). Continued translation exposes the two B4's that then contact the two β1's to form the intertwined dimer. This early dimer pathway thus splits off from the monomer pathway before monomer closure is possible, which promotes the direct formation of intertwined dimers (**Fig. 5.4**, right).

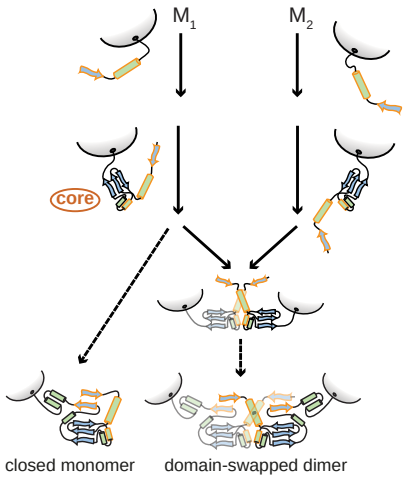

Figure 5.4 | Cartoon model for the formation of intertwined BTB dimers using temporal control driven by translation.

To test whether two nearby BTB polypeptide chains interact, and hence form intertwined dimers when allowed to fold, we purified tandem constructs for wtKEAP1 or wtPATZ1 (**Fig. 5.5a**). In these constructs, two identical BTB monomers were fused head-to-tail, thus exploiting the fact that the N- and C- termini within BTB dimers are close together and hence can be connected by a short linker. The free N- and C- termini of these fused dimers were attached to DNA handles as before. Next, we used optical tweezers to first unfold and then relax them, followed by a 5-10 second time window to refold (**Fig. 5.5a**). When analyzing the refolds, we observed dominant peaks for the fully compacted state (**Fig. 5.5b**). These data indicated direct formation of the intertwined dimer state, rather than an initial formation of closed monomers followed by domain swapping. Note that once formed, closed monomers required force to open up (**Fig. 5.3e,f**), a condition that is not met during the 5-10 s folding time window. To further test dimer formation, we used a dimerization deficient BTB domain of KLHL12 with four mutations in the dimerization interface (L20D/M23D/L26D/L49K) [232] (**Fig. S5.1b**). Consistently, here we did not observe the fully compacted state corresponding to the dimer form (**Fig. 5.5a**). Conversely, a construct based on the wild-type KLHL12 did show the fully compacted dimer state (**Fig. S5.7a**).

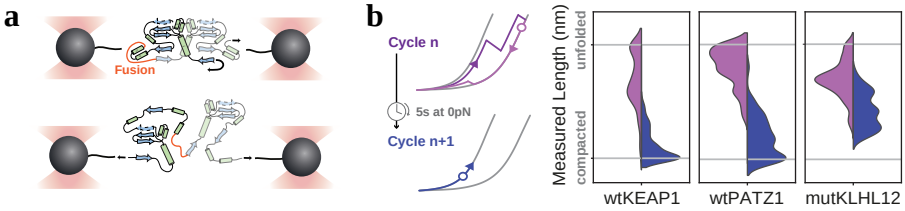

Figure 5.5 | Purified BTB dimer refolding. (a) Optical tweezers cartoon for BTB dimer fusion experiments. Fusion [232] is achieved through a short flexible linker connecting the N-terminus of one subunit chain to the C-terminus of the other subunit chain, which allows for multiple stretch-relax cycles. **(b)** Refolding analysis. Indicated are histograms of the most unfolded state in one stretch-relax cycle (cartoon: purple circle) and the (most compacted) state populated after a waiting period at 0 pN (cartoon: blue circle), for wtPATZ1 (N = 126 events) and wtKEAP1 (N = 236 events), showing a peak at the compacted state indicating dimer formation. In contrast, the dimerization defective mutKLHL12 (N = 136 events) consistently does not show this peak.

As a final test, we wondered if we could directly observe an early assembly intermediate that pre-empts monomer closure (**Fig. 5.4**). This is a challenging aim, as incompletely translated proteins have a strong tendency to aggregate, and hence cannot be purified and interrogated at the single molecule level. In principle, such aggregation can be suppressed in our *in vitro* transcription-translation assay, as the RNCs are attached to beads prior to translation and hence remain spatially separated (**Fig. 5.2a**). However, these assays probe one RNC while assembly requires two. To address these issues, we developed an assay in which two RNC's are coupled by linking the N-termini of their nascent chains using a split FlAsH tag [255] (**Fig. 5.6a**, **Fig. S5.7d**). To focus on the translation timepoint when monomer closure is not yet possible, we arrested translation when B4 (which binds β1) is not yet exposed, while β1, α1 and the BTB core are exposed (**Fig. 5.6a**).
When probing a single RNC as before (**Fig. 5.2a**), the resulting data were consistent with BTB core refolding (**Fig. S5.7b,c**). Next, we coupled two RNCs as described above and performed stretch-relax cycles (**Fig. 5.6a**). We indeed observed full compaction corresponding to an early core-core dimerized state, followed by a length increase consistent with core-core dissociation that produces two tethered monomers in the core state, and finally core unfolding (**Fig. 5.6b**, **Fig. S5.7e**). This early core-core dimer state was disrupted at a mean force of 20 pN (**Fig. 5.6c**). These findings support the suggested model (**Fig. 5.4**) in which early assembly intermediates form before monomer closure, which in turn primes the dimer for proper inter-chain β1-B4 docking once B4 is exposed. This assembly pathway uses the order in which nascent chain segments are translated. Specifically, late B4 emergence yields a time window before this B4 emergence in which monomer closure is not yet possible, and the dimerization pathway can be initiated without monomer pathway competition. In this manner, BTB dimers can be formed co-translationally while avoiding the kinetically trapped closed monomer state.

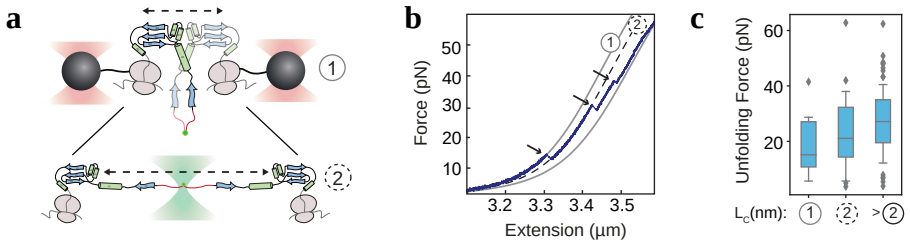

Figure 5.6 | Temporal assembly control at the ribosome. **(a)** Optical tweezers assay for RNC pair. Two beads are brought together to let nascent chains dimerize. Nascent chains are linked using FlAsH dye [255], which binds a bipartite tetracysteine motif formed by two N-termini. Dimer interactions between BTB core states (1), which can form state (2) upon dissociation. **(b)** Example force extension trace of an RNC pair (see panel (a)), showing states sketched in panel (a). Dotted lines: matching WLC curves. **(c)** Corresponding unfolding forces around indicated states in panel (b) within a window of 14 nm around the expected length for (1) and (2). The right-most box shows the forces of unfolding events for unfolded states larger than category (2). (N = 7 unfolding events (1), 16 unfolding events (2), 60 unfolding events (3). Compacted states (1) show lower stability against unfolding consistent with the limited dimerization interface that is disrupted upon unfolding or disassembly. Whiskers: 5th and 95th percentiles, box: interquartile range (IQR).

5.2.6 Assembly control across the BTB proteome

We wondered about the relevance of temporal assembly control for other BTB proteins. Phylogenetic analysis based on BTB domain sequences did not uniformly cluster the entire BTB family, in line with previous work [228]. However, sequences from the BTB-ZF, BTB-BACK-Kelch, and T1 superfamilies did form distinct clusters (**Fig. 5.7a**, blue, yellow, grey). Other clusters (**Fig. 5.7a**, black, red, green) were a mix of different superfamilies (e.g. RhoBTB, Skp1, BTB-BACK-Kelch, T1). Consistently, these clusters had broader domain length distributions (**Fig. 5.7b**). By mapping our DiSP data onto the BTB phylogenetic tree (**Fig. 5.7a**), we found that the BTB-ZF and BTB-BACK-Kelch superfamilies display a higher frequency of co-co assembly candidates (59% and 70% of the proteins, respectively), compared to the other clusters (**Fig. 5.7a,c**). Structural analysis using AlphaFold [251] showed that almost all BTB-ZF and BTB-BACK-Kelch proteins contain the amino-terminal α1, and most also contain β1 (**Fig. S5.8**). Similarly, almost all co-co assembly candidates contain α1, and most also contain β1 (**Fig. 5.7d**). These findings agree with our hypothesis that intertwined BTB proteins, which contain α1 and β1, have a higher need for the temporal control that co-co assembly enables. Consistently, BTB domain proteins from the T1 superfamily proteins all lack α1 and β1 (**Fig. S5.6**) – and none of them is a high-confidence co-co candidate (**Fig. 5.7a,c,d**). The importance of BTB assembly control mechanisms is highlighted by the recently discovered dimerization quality control pathway, in which SCFF-BXL17 ubiquitinates and helps to degrade aberrant BTB heterodimers and monomers during and after translation (**Fig. 5.7e**). FBXL17 is thought to detect aberrant dimers by differences in the stability compared to native dimers [232–234]. The BTB-ZF and

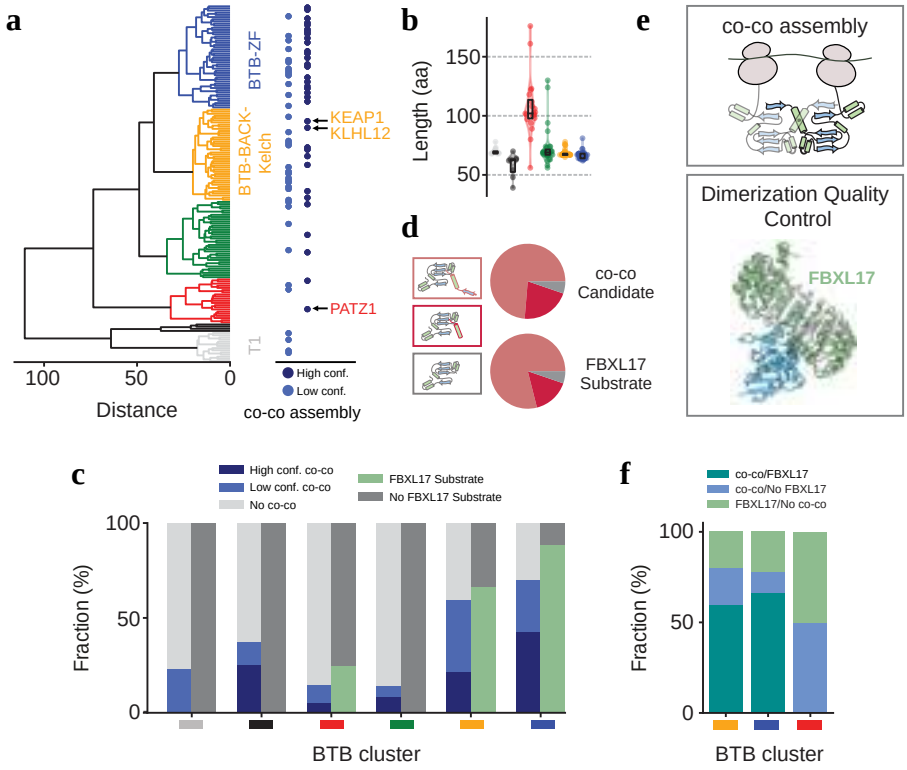

Figure 5.7 | Assembly control across the BTB proteome. **(a)** Phylogeny based on 166 BTB domain sequences (Uniprot [256]). Colors indicate different BTB sequence clusters. High (N = 36) and low (N = 37) confidence coco-assembly proteins [60] are highlighted by light and dark blue dots respectively. **(b)** Length distribution of for BTB domains as annotated in Uniprot for the different clusters. Clusters which could not be assigned to one BTB superfamily had a larger spread of lengths (box: standard deviation) compared to the superfamily clusters of the BTB-ZF, BTB-BACK-Kelch and T1 superfamilies (box: standard deviation). **(c)** Fraction of co-co assembly candidates [60] and FBXL17 substrates [233] for the different sequence clusters. As FBXL17 substrates were not tested genome-wide the fractions were normalized to the total amount of tested substrates per cluster. **(d)** Structural analysis of the BTB amino-terminal extension. AlphaFold [251] structure predictions show that BTB co-co assembly candidates [60] and FBXL17 BTB substrates [233] predominantly either contain the full amino-terminal extension or only α1. **(e)** Two assembly control mechanisms. Top: Translational coupling enables the intertwining of polypeptides for BTB dimer formation. Bottom: Aberrant BTB dimers or monomers (shown here) are recognized by SCF-FBXL17 (pdb: 6w66), a dimerization-quality-control E3 ligase, which ubiquitylates its substrates for degradation. **(f)** Comparison between FBXL17 substrates and co-co assembly candidates shows that most FBXL17 substrates are also co-co assembly candidates.

BTB-BACK-Kelch BTB superfamilies utilize co-co assembly most extensively (**Fig. 5.7c,d**), which could indicate they are the most challenging to assemble and hence are more frequently FBXL17 substrates. A similar mapping showed that this is indeed the case (**Fig. 5.7c**). In addition, almost all FBXL17 substrates [233] contain the α1 and β1 amino-terminal extension (**Fig. 5.7d**). Consistently, within the BTB-ZF and BTB-BACK-Kelch superfamilies, the majority of FBXL17 substrates have also been detected as co-co assembling candidates (**Fig. 5.7f**). Note that the FBXL17 substrate test did not cover the complete genome, hence for many co-co assembly candidates it is unknown if they are also FBXL17 substrates. Thus, the correlation between co-co assembly and FBXL17 interaction may be even stronger. Overall, these analyses are consistent with the idea that intertwined BTB dimers benefit from assembly control mechanisms, as offered by translation-driven temporal assembly control and FBXL dimerization quality control [233].

5.3 | Discussion

While many protein complexes show intertwined subunits, their formation remains poorly understood. The conformational monomer remodeling required for their assembly suggests major activation energies and assembly delays [231, 257–260], which in turn poses aggregation risks [261]. Here, we advanced a temporal control mechanism driven by translation that circumvents this issue (**Fig. 5.4**). It avoids remodeling requirements by preventing unproductive conformations in the first place. Interactions between nascent chains and their progressive emergence during translation are central. Specifically, the mechanism exploits the fact that newly emerged chain segments are transiently safeguarded against unproductive contacts with soon-to-emerge segments encoded upstream, offering an opportunity to form alternative productive contacts with another nascent chain – even if the latter have low probability to form normally, during later phases or after translation. Assembly-folding processes hence can follow pathways that are poorly accessible without temporal control. Hence, by using the energy-driven nature of translation, these assembly-folding pathways break the constraints of equilibrium assembly thermodynamics, to avoid unproductive intermediates directed towards native dimeric states.

As shown for KEAP1, KLHL12 and PATZ1, BTB domain monomers risk forming unproductive stable closed states, in which one β-strand (β1) folds back on another (B4), at the ribosome and away from it (**Fig. 5.4**, left). During translation however, these intra-chain contacts are excluded until B4 emerges, while early inter-chain contacts can already form (**Fig. 5.4**, middle). The β1 segments are then well positioned to fold onto the subsequently emerging B4 of the partner subunit, completing the intertwined dimer structure. The mechanism makes use of the sequential emergence of nascent chain segments to promote certain interactions over others, thus steering folding-assembly pathways away from closed BTB monomers. Temporal assembly control offers an alternative to domain swapping, which has been studied extensively for several proteins including BTB domains [228]. Domain swapping is non-trivial to study, given that domain-swapped dimers interconvert

slowly [257, 258], and closed BTB monomers have been difficult to detect [252–254], possibly due to hinge loop conformations and other stabilizing interactions between subunits [253, 257]. Our approach enabled BTB monomer studies, and revealed a high stability of closed KEAP1, KLHL12 and PATZ1 monomers, as evidenced by substantial unfolding forces (10-35 pN) (**Fig. 5.3e**, **Fig. S5.5b**). Stable closed monomers were also readily formed co-translationally in absence of dimerization partners (**Fig. 5.2c**, **Fig. S5.2a,c**), despite reported destabilizing influence of ribosomes on nascent folds [107]. These stable closed BTB monomers are a barrier for efficient dimerization, and hence underscores the importance of alternative assembly pathways as advanced here.

To explore *in vivio* and cross-proteome relevance we analyzed BTB phylogeny and structural features, and correlated these with our single-molecule and disome selective ribosome profiling data. While the PATZ1 BTB domain we studied at the molecular level has significant phylogenetic distance to KEAP1 and KLHL12, we found that their folding intermediates and assembly mechanisms were notably similar (**Fig. 5.2**-**Fig. 5.6**, **Fig. S5.5**), with small differences in unfolding step sizes consistent with the longer N-terminal extension and the additional flexible loop within the core fold of PATZ1 (**Fig. 5.2c**,**Fig. 5.3c**, **Fig. S5.5**). The analysis showed co-co assembly and FBXL17 interactions are most prevalent in the BTB-BACK-Kelch and BTB-ZF superfamilies (**Fig. 5.7a,e**), with β1 and α1 in the amino-terminal extension being the main structural determinants (**Fig. 5.7d**), which is consistent as they contribute to dimerization. Interestingly however, a certain fraction of BTB domains that lack β1 within the Alpha-Fold predictions do display co-co assembly and FBXL17 interactions (**Fig. 5.7d**). This observation is in line with the notion that dimerization can commence without β1-B4 interactions, before B4 emerges (**Fig. 5.4**). An example is MIZ1, which lacks β1 but does form a homodimer [253]. While the DiSP method could show prevalence [60], it could not address the functional relevance of co-co assembly. Here we show that co-co assembly opens up alternative folding-assembly pathways that avoid kinetically trapped states and slow domain-swapping [257, 258]. The involved temporal control provides a mechanism to assemble intertwined dimers that are challenging to form otherwise, and hence expands the spectrum of protein structures that can be faithfully synthesized, as well as limiting unwanted complexes such as BTB heterodimers [262]. The emergence of polypeptide segments in a specific temporal order is general for all proteins. Temporal assembly control may thus be exploited more generally to enable complex protein structures beyond BTB domains. Our results indicate that assembly-folding pathways can be subjected to regulatory control, which can involve evolutionary tuning of various functions. For instance, assembly pathways may be shaped by processes that affect ribosome-ribosome proximity [263, 264], including translation speed and pausing [27, 36, 265], direct ribosome-ribosome interactions, as well as by protein folding topologies [266–269]. Our findings further suggest that temporal assembly control works in conjunction with dimerization quality control systems such as FBXL17, which act both co- and post-translationally. This interplay may be reciprocal, with its quality control factors regulating the assembly control process or rescuing unsuccessful dimerization.

5.4 | Methods

Disome Selective Profiling (DiSP)

We grew U2OS (ATCC Cat# HTB-96, RRID: CVCL_0042) and HEK293-T cells (DSMZ Cat# ACC 635) in high glucose DMEM media containing GlutaMAX and pyruvate (Gibco) with 10% heat-inactivated FCS (Gibco), 100 100 U/ml penicillin and 100 µg/ml streptomycin (Gibco) and in a humidified incubator with 5% CO2 at 37 °C (HERAcell 150i). For DiSP of HEK293-T and U2OS cells, lysis buffer contained a physiological salt concentration (50 mM HEPES pH 7.0, 10 mM $MgCl_2$, 150 mM KCl, 1% NP40, 10 mM DTT, 100 µg/ml CHX, 25 U/ml recombinant Dnase1 (Roche) and protease inhibitor (cOmplete^{TM} EDTA-free, Roche). For DiSP of HEK293-T cells, we used a high-salt lysis buffer containing 500 mM KCl for possible effects on the onset of disome formation. For DiSP of U2OS cells, lysis was performed with chemical crosslinkers, using 2.5 mM BS3 and 20 mM EDC. For crosslinking to occur with cell lysis, cells were scraped in crosslinker-containing lysis buffer on ice. After lysis, DiSP samples were processed [60]. Briefly, we clarified cell lysates, loaded them on sucrose gradients (5% - 45%), centrifuged them for 3.5 hours at 35.000 rpm, 4 °C (SW40-rotor, Sorvall Discovery 100SE Ultracentrifuge) and collected fractions corresponding to monosomes and disomes. We extracted 30 nt long footprints from both fractions and deep sequenced them. In the DiSP gene density profiles, we show the position-wise 95% Poisson confidence interval corrected for library size, smoothing the read counts with a 15-codon wide sliding window [60].

Cloning

For *in vitro* transcription, the SecMsrt site was added on C-Terminus of pRSET vector (Thermo Fisher). PATZ1 and KEAP1 were cloned using NdeI and SpeI (New England BioLabs) restriction enzymes. The Plasmid DNA of PATZ1 was kindly obtained from the Bukau lab at the Center for Molecular Biology of Heidelberg University (ZMBH) and the DNA plasmids of KEAP1 and KLHL12 from Michael Rapé Lab at the UC Berkley and the Howard Hughes Medical Institute (HHMI). DNA of the gene of interest was amplified by PCR using a gene specific primers and Phire Green Master mix (Thermo Fisher). The fragments were purified from the gel with QIAquick gel purification kit (Qiagen) and digested with restriction enzymes (New England BioLabs), followed by purification with QIAquick PCR purification Kit (Qiagen). 30 ng of digested vector and appropriate amount of insert (1:5 ratio) were ligated using 400U of Hi-T4 ligase (#M2622S, New England BioLabs) in 20 µl set up at room temperature for 1 hour. Ligation mix was used for a heat shock transformation in Dh5-alpha competent cells (New England BioLabs). The cells were allowed to recover at 37 °C for up to 1 hour, followed by plating on the LB plate supplemented with 100 µg/ml ampicillin and grown overnight at 37 °C. Subsequently, positive colonies were grown again in LB medium supplemented with 100 µg/ml ampicillin and used for a plasmid isolation (QIAprep Spin Miniprep Kit, Qiagen). The sequences were verified by sequencing (Eurofins, Germany).

Nascent Chain Constructs: Amino Acid Sequences

Star (*) denotes the UAG (amber) codon that allows introduction of a biotin moiety with a triple aminophenyl spacer.

Coupling of ribosomes to beads with DNA handles

5 kbp long double-stranded DNA (dsDNA) molecules were prepared by PCR amplification using digoxigenin (DIG) and biotin 5'-end-modified primers. Neutravidin (NTV) (ThermoFisher, 31000) was added in a 200 times excess ratio to the PCR fragments (Bio-DNA-DIG) and incubated overnight at 4 °C in a rotary mixer.
Two batches with 0.14 mg/ml anti-digoxigenin coated polystyrene beads (Speherotech, DIGP-20-2) with a diameter of 2.1 µm were incubated in 12 µl TICO buffer (20 mM HEPES-KOH pH 7.6, 10 mM $(Ac)_2Mg$, 30 mM $AcNH_4$, 4 mM β-mercaptoethanol as an additional oxygen scavenger) with 1.4 nM NTV-Bio-DNA-DIG handles at 4 °C in a rotary mixer for around 30 minutes. Afterwards unbound DNA was removed by pelleting and washing NTV-Bio-DNA-DIG coupled beads twice by centrifugation at 4 °C at 3000 rpm for 5 minutes and resuspending in fresh TICO buffer each time. After the last washing step one bead batch was resuspended in 20 µl of TICO buffer and the other in 250 µl. Within the 20 µl, 1.2 U/µl RNase Inhibitor, Murine (New England BioLabs, M0314S) is added together with 390 nM ribosomes that were biotinylated *in vivo* at the uL4 ribosomal protein on the large subunit and subsequently isolated as previously described [165] from

Can20/12E [145]. The mixture was incubated at 4 °C in a rotary mixer for around 45 minutes. Excess unbound ribosomes were removed by two consecutive washing steps with TICO buffer. After the last washing step the mixture was directly resuspended in a modified *in vitro* transcription-translation reaction to generate stalled ribosome-nascent chain complexes (RNCs) as described below.

Cell-free protein synthesis

RNCs of PATZ1 and KEAP1 BTB domains were generated through an *in vitro* transcription-translation reaction using a modified version of the PURE system [146] lacking ribosomes (New England BioLabs, E3313S). The system was supplemented with 10 µM of modified tRNA pre-charged with biotinylated lysine (Bio-Connect, PRX-CLD04) to co-translationally incorporate a biotin-tag at the N-terminus of the nascent chain with an amber stop codon and 0.83 U/µl RNase Inhibitor, Murine (New England BioLabs, M0314S). 5.5 nM linearized plasmid was added to the reaction mixture after mixing it with the biotinylated ribosome bound beads. Synthesis was carried out at 37 °C for 20 min. The bead-tethered RNCs were resuspended in 300 µl TICO buffer and injected in the microfluidic chamber.

Preparation of the FlAsH Dye

FlAsH-EDT_2 (Carbosynth) stock solution was prepared at a concentration of 5 mM by dissolving in DMSO (Thermo Scientific) and storing it at −20 °C under an inert atmosphere [255]. For experiments, the stock solutions were diluted in TICO buffer to a working concentration of 500 nM.

Protein expression and purification

The ybbr tag (DSLEFIASKLA) was added on both termini of KEAP1, KLHL12 and PATZ1 proteins. [92] The proteins were fused to MBP (maltose binding protein). The fused proteins were cloned into pet28(a) plasmid (Novagen) and transformed into Rosetta strain (gift from Matthias Mayer, Germany). The cells were grown in LB medium supplemented with 50 µg/ml kanamycin until an OD of 0.6 was reached. Expression was induced by adding 0.2 µM IPTG (Sigma) at 15 °C overnight with slow agitation. Cells were harvested by centrifugation at 5000 rpm (Beckman) for 20 min. The pellet was resuspended in a pre-chilled lysis buffer (50 mM phosphate buffer, pH 7.5, 200 mM NaCl, 10 mM EDTA, 50 mM Glutamic Acid–Arginine, 1 mM DTT (Sigma) and protease inhibitor (cOmplete^{TM} Mini, EDTA-free (Roche)) and lysed using an Emulsiflex homogenizer. To remove insoluble material, centrifugation at 50.000 g for 1 hour at 4 °C was performed. The clarified lysate was incubated with Amylose resin (NEB) for 1 hour at 4 °C. After washing the resin extensively with buffer A (50 mM Tris-HCl, pH 7.5, 200 mM NaCl, 1 mM DTT), the bound proteins were eluted with buffer A containing 20 mM maltose. Lastly, maltose was removed in a PD10 desalting column (GE Healthcare) and eluted in SFP coupling buffer (50 mM Hepes, 10 mM $MgCl_2$, pH 7.4).

Attachment of DNA handles to purified BTB monomers and dimers and to beads

The purified BTB proteins were conjugated to a 20 nt oligo modified with coenzyme A (Biomers GmbH) in the presence of 50 mM HEPES, 10 mM $MgCl_2$ (both from Merck), and 1 µM SFP synthase (Addgene) at 4 °C overnight. Any remaining oligos were removed through Ni-NTA purification (Protino, MACHEREY-NAGEL). [92] To create the 1.3 kb DNA handles, a PCR amplification was performed using primers with phosphate at one end and either biotin or digoxigenin at the other end (Eurofins, Germany), starting from the pUC19 plasmid (New England Biolabs). The amplified DNA was purified using the Qiagen PCR Purification Kit (Qiagen). The DNA was then digested with Lambda exonuclease (New England Biolabs) at 37 °C for 2 hours, followed by 10 minutes of inactivation at 75 °C.
An equal amount of both ssDNAs (biotin and digoxigenin) were mixed and purified together using an Amicon 30 kDa column (Merck, Darmstadt, Germany). The second strand was completed using Deep Vent (exo-) DNA polymerase (New England Biolabs), dNTP mix (ThermoFisher), and a phosphorylated primer (Eurofins, Germany), starting 20 nt downstream to generate the overhang. The final product was purified using the Monarch PCR Purification Kit.
The 1.3 kb DNA handles with a 20 nt overhang complementary to the oligo attached to the protein, were ligated to the protein-oligo complex using T4 ligase (New England Biolabs) at 16 °C for 4 hours, followed by an overnight incubation on ice. The resulting DNA-BTB-DNA complex were either stored on ice for a few days, if directly measured, or flash-frozen and stored at −80 °C for future analysis. Before measurement the DNA-BTB-DNA construct was mixed with anti-digoxigenin coated polystyrene beads (Spherotech, DIGP-20-2) and incubated together at 4 °C in a rotary mixer for around 30 minutes.

Optical tweezers assay and single-molecule data analysis

Data was recorded using a C-Trap instrument (Lumicks, Amsterdam) equipped with a single high-intensity, polarization-stable 1064 nm laser. The laser is split into two orthogonally polarized beams, one of which can be steered using a piezo mirror relative to the other, enabling dual optical trapping. Additionally, the system includes two fluorescence excitation lasers (532 nm and 638 nm) for multi-color confocal fluorescence detection. This allows to carry out correlated single-molecule force spectroscopy and multi-color confocal laser scanning spectroscopy. Single-photon sensitivity is achieved through the use of photodiodes (APDs). Calibration of the optical traps was performed using the power spectrum method [205], where the power spectra of trapped beads undergoing Brownian motion were fitted with a Lorentzian function, obtaining average stiffness values of $k=0.35\pm0.045$ pN/nm. Measurements were conducted in a monolithic laminar flow cell equipped with a pressure-driven microfluidic system featuring five separate flow channels. This design ensures the separation of beads carrying ribosome-nascent-chain complexes (RNCs) or purified protein from bead-tethered NTV-Bio-DNA-DIG constructs or NTV coated beads (Spherotech, NVP-20-5), respectively.

During experiments, individual molecules were tethered by trapping a bead from each flow channel and transferring them into a separate measurement side channel. This channel was supplemented with a P2O oxygen scavenging system containing 3 U/ml pyranose oxidase, 90 U/ml catalase, and 50 mM glucose (Sigma) to reduce damage by reactive oxygen species induced by the trapping laser and to keep the pH stable. To form a tether of individual molecules, optically trapped beads were brought within close proximity, such that either the biotin tag at the end of the RNC constructs could link up to the NTV-Bio-DNA-DIG constructs attached to the other bead or in the case of the purified BTB proteins bound to the anti-DIG coated beads, the free biotin-DNA handle could bind to a NTV coated bead (**Fig. S5.3**). Measurements were conducted using a cycling force spectroscopy mode, in which the steerable optical trap was moved at a constant velocity of 0.1 µm/s and a maximum force of up to 65 pN. The resulting force-extension curves for individual tethers were analyzed with a custom written python script by fitting two worm-like chain (WLC) models in series: a twistable worm-like chain (tWLC) model to account for the DNA handle contribution [212] and an inextensible WLC model for the protein contribution [127], yielding the following relation between extension (x) and force (F) is given:

$$x = \mathrm{L_C}\left(1 - \frac{1}{2}\sqrt{\frac{k_B T}{F \cdot \mathrm{L_{p\ DNA}}}} + \frac{C}{-g(F)^2 + SC} \cdot F\right) + \mathrm{L_e}\left(1 - \frac{1}{2}\sqrt{\frac{F \cdot \mathrm{L_{p\ Protein}}}{k_B T}}\right)$$

The first term parameterizes the DNA by: the contour length $\mathrm{L_C}$ (884 nm for 1.3 kb and 3400 nm for 5 kb DNA handels), the twist rigidity C (literature [270]: 440±40 pN · nm^2), the stretching modulus S (863 pN/nm (SD 183 pN/nm)) , the persistence length of the DNA $\mathrm{L_{p\ DNA}}$ (average values: 37 nm (SD of 10 nm)) and the twist–stretch coupling g(F). The second term is the inextensible WLC model for protein contribution, where $\mathrm{L_{p\ Protein}}$ (0.75 nm) and $\mathrm{L_e}$ are the persistence and extended length of the protein, respectively. N-values **Fig. 5.2c**: KEAP1 (N = 7 molecules, 53 cycles), PATZ1 (N=8 molecules, 34 cycles). N-values **Fig. 5.2d**: PATZ1 $\Delta\beta 1$ variant (N = 7 molecules, 25 cycles). N-values **Fig. 5.3c**: wtPATZ1 (N = 7 molecules, 72 cycles), wtKEAP1 (N = 10 molecules, 123 cycles). N-values **Fig. 5.3d**: wtKLHL12 (N = 5 molecules, 36 cycles). N-Values **Fig. 5.3e** for bars from left to right, respectively: 53, 7, 23, 37, 15, 39, 26, and 32 unfolding events. N-values **Fig. 5.5b**: wtPATZ1 (N=5 molecules, 68 cycles), wtKEAP1 (N=9 molecules, 127 cycles) and mutKLHL12 (N = 5 molecules, 73 cycles). N-values **Fig. 5.6c**: 7 (states 1),16 (states 2), 60 (states 3) unfolding events. N-values **Fig. S5.2b** for bars from left to right, respectively: 86, 18, 22, 129, 57, 77 unfolding events. N-values **Fig. S5.2c** for bars from left to right, respectively: 22, 8, 27, 11 unfolding events. N-values **Fig. S5.5a**: wtPATZ1 (N = 7 molecules, 72 cycles). N-Values **Fig. S5.5b** for bars from left to right, respectively: 53, 7, 23, 37, 15, 39, 26, 32, 20, and 27 unfolding events. N-Values **Fig. S5.5c**: number of cycles initially in closed state: 22, in open state: 38, in core2 state: 28, in core3 state: 41. N-values **Fig. S5.6a**: number of cycles initially in closed state: 47 (wtKeap1), 8 (wtKLHL12), in open state: 41 (wtKeap1), 14 (wtKLHL12), and in core state: 48 (wtKeap1), 27 (wtKLHL12). N-values **Fig. S5.7a**: wtKLHL12 (N = 2 molecules, 28 cycles). N-values **Fig. S5.7c**: KEAP1 (50-159aa)

(N=15 molecules, 38 cycles). N-values **Fig. S5.7e**: KEAP1 (N = 13 molecules, 31 cycles). The Mann-Whitney U test was used for statistical testing to obtain the p-value.

Calculation of transition probabilities

A molecule was classified as being in the closed, open, core, or unfolded state if its proposed length fell within a ± 3 nm range around the length of the respective state. Based on this classification, the cycles of individual molecules, which transitioned to a state, with a larger length during stretching, or any other state of different length, or remained in the same state without length changes, were counted. Transitions may occur via an intermediate state (e.g., from open to an intermediate state between open and core before reaching core). Transition frequencies were calculated by dividing the number of cycles with a specific transition by the total number of cycles, which included one of the defined states marked as a starting point for each specific transition (see **Fig. S5.6a**).

Hierarchical clustering of BTB domain sequences

BTB domain positions and sequence were obtained from Uniprot using only reviewed SwissProt entries. BTB domains were labeled with high or low confidence assembly if at least 30 residues of the BTB domain were emerged from the ribosomal exit tunnel at the time of coco-onset as determined in *Bertolini et. al.* [60] Table S1. Pair-wise sequence alignment scores of all BTB domains were obtained using the biopython pairwise2.align.globaldx module with blosum62 alignment matrix. Finally, scores were hierarchically clustered using the scipy linkage module and the ward method.

5.5 | Author Contributions

Conceptualization: K.T., V.S., M.B., P.J., F.T., B.B., G.K., M.R and S.J.T. Methodology: K.T., V.S., P.J., M.B., F.T., J.S., M.R., B.B., G.K., S.J.T. Biotinylated ribosomes: A.K. Disome Selective Profiling Experiments: M.B. and K.F. Single-molecule experiments: K.T. Single-molecule data analysis and visualization: K.T., S.J.T. Writing: K.T. and S.J.T. Supervision: S.J.T., M.R., B.B. and G.K.

5.6 | Supplementary Figures

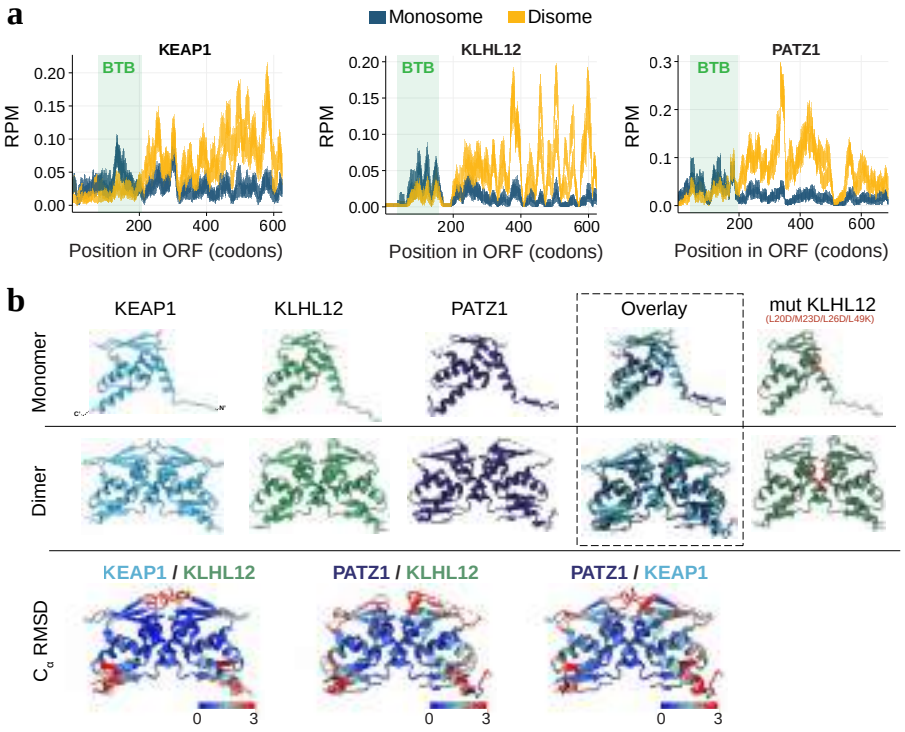

Figure S5.1 | **(a)** Monosome (grey) and disome (yellow) footprint density along the position in the ORF (RPM = Reads Per Million) of KEAP1, KLHL12 and PATZ1. Green bars indicate the position of the BTB domain. A monosome to disome shift of translating ribosomes, the onset of co-co assembly, is observed after the exposure of around 200 amino acids outside of the ribosomal tunnel, shortly after the BTB domain. After that disome enrichment levels out and remains high. DiSP data is from HEK293-T cells [60].**(b)** Structures of KEAP1 (pdb: 7EXI), KLHL12 (AlphaFold [251] prediction: AF-Q53G59-F1-v4), PATZ1 (pdb: 6GUV) monomer and dimer. Point mutations for KLHL12 (L20D/M23D/L26D/L49K) are marked in red within the KLHL12 AlphaFold prediction. Overlay and alpha carbon-root mean square deviation (Cα RMSD) show structural similarity between proteins. The fold is especially conserved for the dimerization interface which has a C_α RMSD of 0 Å (dark blue) between different proteins. Differences larger than 3 Å are observed for N- and C-termini and for the loop region between the beta-strand B3 and α-helix A2. In the case of PATZ1 the B3 β-strand couldn't be structurally resolved due to an additional large flexible linker between the α-helix A2 and β-strand B3, which adds to the poorer C_α RMSD within that region for the comparison between PATZ1 and KLHL12 and between PATZ1 and KEAP1.

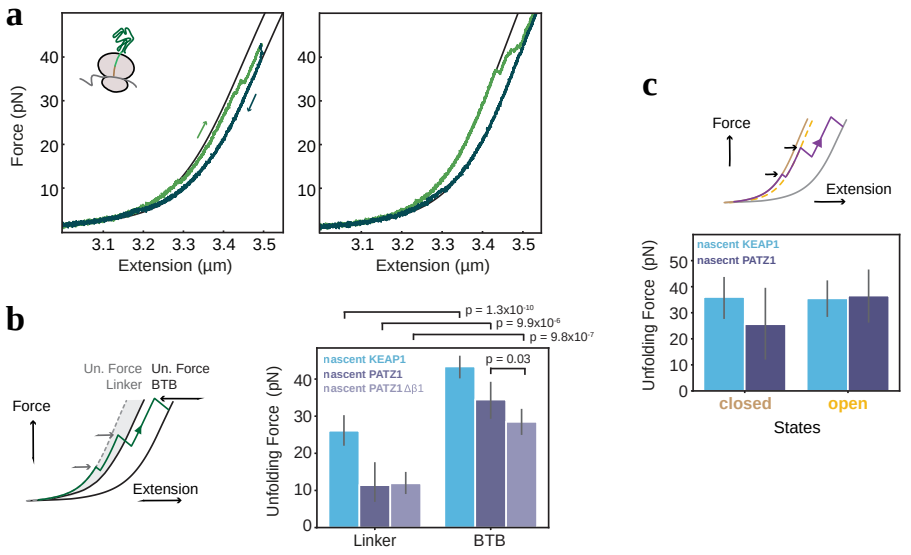

Figure S5.2 | **(a)** Example force-extension traces of a ribosomal nascent chain construct (50-196 aa) of nascent KEAP1 without artificial linkers showing full compaction. Owing to 17 amino acids of the natural sequence at the C-terminus of the BTB domain in addition to the SecM strong sequence, the full BTB domain is exposed outside of the ribosomal tunnel to allow for complete folding. Both traces show how the BTB monomer is initially compacted (left worm-like chain model) during pulling and unfolds stepwise to the calculated length of the fully unfolded length of the monomer (right worm-like chain model). **(b)** Unfolding forces for states at contour lengths corresponding to linkers and BTB domain defined. Since the here artificial linkers may not form stable folds and only weak interactions, those interactions would break and unfold first. Thus, we considered the unfolding forces of the contour lengths corresponding to the linker (grey area in cartoon on the left) and compared them with the unfolding forces of states corresponding to BTB unfolding. Indeed, a significantly lower mean unfolding force ($p < 0.05$) was observed. See methods for N-values. **(c)** Measured unfolding forces to partially unfold the closed and open BTB monomer states. We used a $\pm$ 2.5 nm margin around the lengths of these states and quantified the unfolding forces (black arrows in the cartoon). Mean unfolding forces were quite similar for both states and relatively high (closed nascent PATZ1: 25.6 pN, closed nascent KEAP1: 36 pN, open nascent PATZ1: 36.6 pN, open nascent KEAP1: 35.5 pN), indicating a stability of the fold. See methods for N-values.

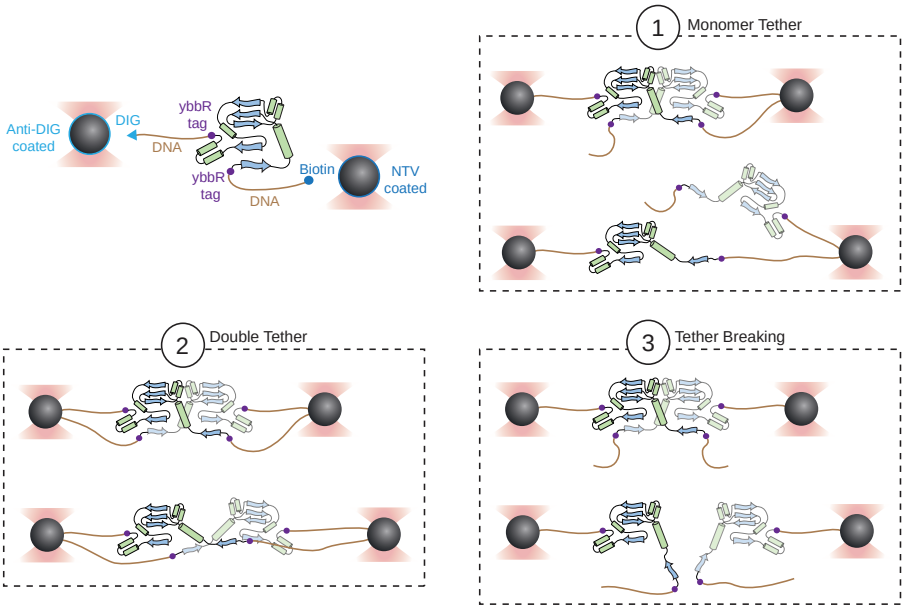

Figure S5.3 | Purified BTB monomer tethering. Visualization of the different tethers that can form and how we obtain tethered monomers (nr. 1, top-right). YbbR tags were genetically introduced at each terminus of the BTB monomer, coupled to 20 nucleotide-long oligos, modified with coenzyme A using Sfp synthase (Sfp 4'-phosphopantetheinyl transferase), and then covalently ligated to DNA tethers. Tethering naturally selects only those constructs where one DNA handle has a biotin and the other has a digoxigenin, as constructs with two of the same handles cannot form a tether between the two beads. This DNA attachment allows one to select for BTB monomers (nr. 1) in our optical tweezer assay, even though up to 4 DNA handles can in principle attach to the 4 termini of purified dimers. Specifically, as visualized in the cartoons, the first stretching curve will either result in: 1) a single BTB monomer tethered at its termini between the beads, 2) two BTB monomers each tethered individually between the two beads, or 3) tether breakage. Case 3 is readily recognized by a sudden complete rupture event in force-extension curves during the first pull that breaks the tether. In case 2 a double tether is formed. It can be identified by the absence of an overstretching plateau at 65pN, owing to the fact that two tethers share the mechanical load and hence can resist a higher load. Only a single monomer tether (case 1) shows an overstretching plateau at 65 pN due to DNA melting.

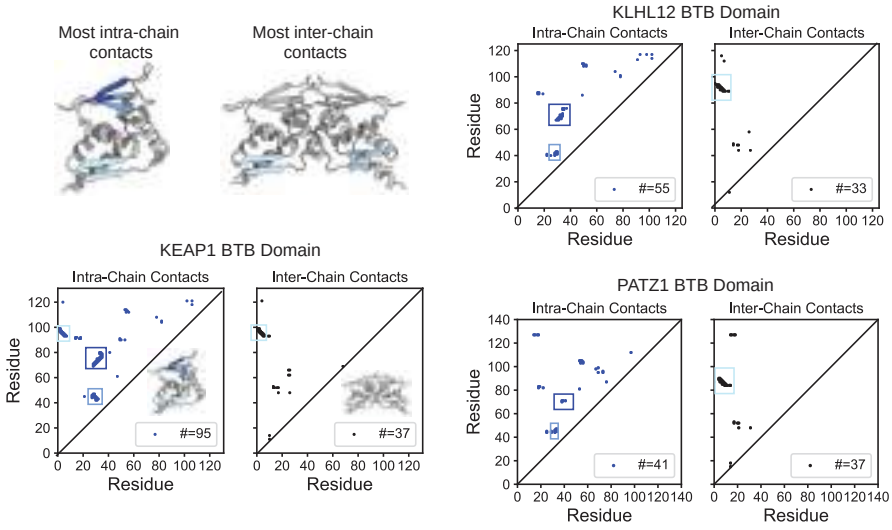

Figure S5.4 | Intra- and inter-chain contacts for BTB domains. Intra- and inter-chain contacts of the studied BTB monomers and dimers. Two residues were considered in contact if their corresponding carbon alpha atoms were in a distance smaller or equal to 7 Å from each other. Atom positions are taken from the same crystal structures as indicated in **Fig. S5.1a**, apart from the closed monomer structure of KEAP1 (pdb: 6w66). Many contacts are found between beta sheets, which are marked and highlighted correspondingly in blue within the structure.

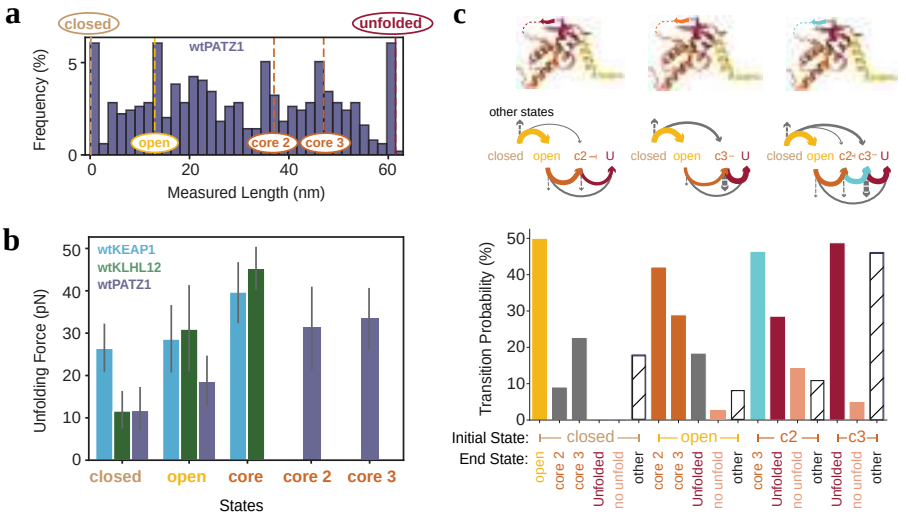

Figure S5.5 | Extended analysis of purified PATZ1 monomer. **(a)** Contour length histogram of purified wtPATZ1 monomer (as in **Fig. 5.3c**) with dotted lines indicating the most pronounced contour length states (partial folds). Due to PATZ1's unique A2/B3 loop, it does not map onto the "core" state as seen for wtKEAP1 and wtKLHL12. Rather, two alternative "core" states match the marked peaks in the histogram: one in which the flexible loop unfolds with the c-terminal region ("core 3") and one where only the c-terminal region unfolds but the loop not ("core 2"). See methods for N-values. **(b)** Mean unfolding forces for wtPATZ1 "core 2" and "core 3" states added to the unfolding forces of wtKEAP1 and wtKLHL12 states as displayed in **Fig. 5.3e**. wtPATZ1 core states show lower unfolding forces in contrast to the unfolding forces of wtKEAP1 and wtKLHL12 core states ($p = 0.01$), which is consistent with decreased stability due to fewer contacts within that region (see **Fig. S5.4**). See methods for N-values. **(c)** Transition probabilities (see methods) between defined states for wtPATZ1 monomer. The colored structures at top indicate the possible unfolding sequences. (1) left: the flexible loop is part of the partial fold which unfolds last (red), giving rise to the intermediate "core 2" (2) middle: the flexible loop unfolds with the rest of the C-Terminus (orange), giving rise to the intermediate "core 3". (3) the unfolding trajectory contains both intermediates, "core 2" and "core 3" with an additionally unfolding step between "core 2" and "core 3" (flexible loop – cyan). See methods for N-values.

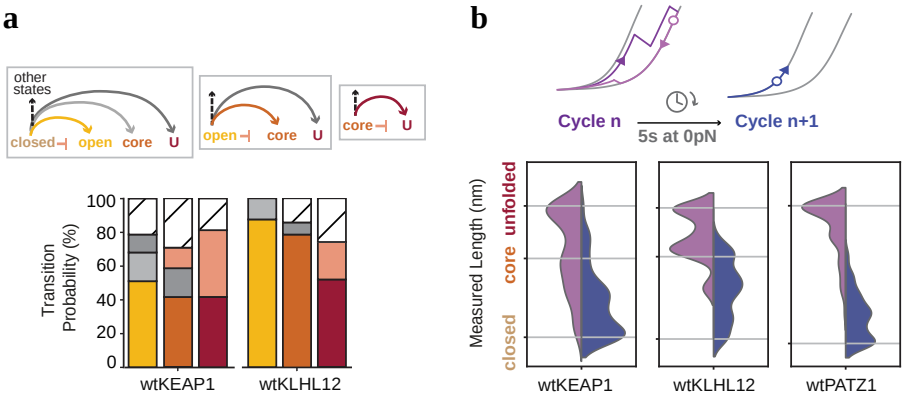

Figure S5.6 | Unfolding and refolding of purified BTB monomers. (a) Transition probabilities between states, as measured using optical tweezer experiments on purified BTB monomers (see main **Fig. 5.3**). For molecules in the closed, open or core states (lengths in a ±3 nm window around their expected lengths, see methods), we scored transitions to one of these states of larger length during stretching, or any other state of different length, or remained in the same state without length changes (see cartoons, top, and **Fig. S5.5c**). Stacked bars indicate transition probability or frequency corresponding to the cartoon arrows. For each protein, first cartoon corresponds to first stacked bar, second cartoon to the stacked bar in the middle and the last cartoon to the third stacked bar. Both proteins showed a similar most prevalent unfolding trajectory, which follows a consecutive sequence of the defined states from closed to open to core and then either remained in the core state or unfolded to the fully unfolded state. See methods for N-values. **(b)** Refolding was studied by quantifying the most unfolded state within one stretch-relax cycle (cartoon: purple circle) and the state populated after a waiting period at 0 pN (cartoon: blue circle) to allow for compaction without a counteracting force. The most unfolded states (purple) and the most compacted states (blue) were plotted on a vertical axis with a kernel density estimation curve. For wtKEAP1 (216 events) and wtKLHL12 (64 events), the most unfolded states within one stretch-relax cycle were often either the fully unfolded state or the "core" state, consistent with our transition probability analysis of panel (a). The most unfolded state for wtPATZ1 (128 events) was most often the fully unfolded state, which is in line with the decreased stability of the core states (see also **Fig. S5.4** and **Fig. S5.5**).

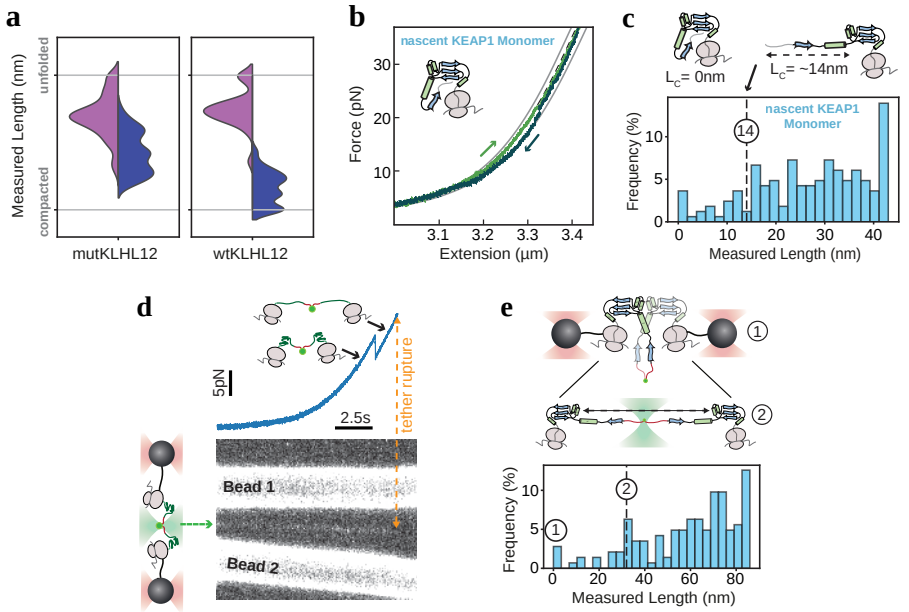

Figure S5.7 | BTB monomer and dimer characterization. **(a)** Refolding analysis as described in **Fig. 5.5b** and **Fig. S5.6b**, here for the wtKLHL12 fusion dimer (52 events) and its dimerization defective mutant. A similar distribution for the most unfolded states per cycle (purple) for both proteins is observed, indicative for similar partial folds for both proteins. Consistently, in contrast to the dimerization defective mutant, the fully compacted state is only observed for the wild-type version of the wtKLHL12 BTB domain, indicating dimer formation. **(b)** Example Force-Extension trace of a stretch-relax cycle for the BTB monomer in an incomplete translation stage (50-159 aa), which misses the C-terminus inclusive the beta-strand B4 that β1 folds back onto. However, all structural elements of the core partial fold are translated. **(c)** Contour length histogram of BTB monomer in incomplete translation stage (50-159 aa) as in (b) (165 states). Compacted states are observed with a low frequency, in line with α1 and β1 and the N-Terminal flexible linker being unfolded (see cartoon). Partial folds bigger than 14 nm, corresponding to the core state being (partially) folded, are more frequently observed. **(d)** To prevent tether loss nascent chains are linked up by a FlAsH dye [255], which binds to a bipartite tetracysteine motif formed by two engineered cysteines at the end of a linker at each nascent chain N-terminus. Cartoon left: Bound FlAsH becomes fluorescent and is detected by scanning a confocal excitation beam (green) along the molecular tether. Corresponding data (right) of detected fluorescence scans in time (bottom) and measured force-time trace (top). The signal between beads corresponds to FlAsH fluorescence. Dashed line indicates tether rupture, which correlates with the loss of fluorescent signal. **(e)** Contour length histogram of the incomplete translation RNC construct pairing (as panels (b) and (c)) (N = 143 states). Dotted lines and numbers indicate contour length states matching the cartoon at top.

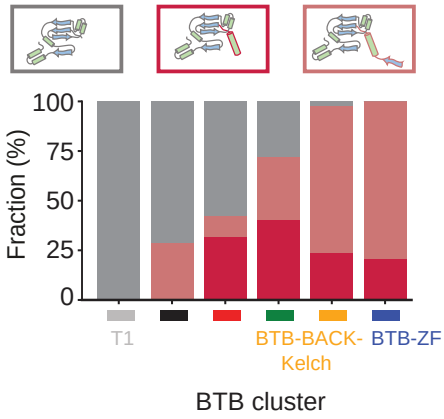

Figure S5.8 | Analysis of structural features across BTB proteome. Structural analysis of the amino-terminal extension for BTB proteins per cluster (see **Fig. 5.7a**). Alpha-fold [251] was used to predict structures and to assess the amino-terminal extension. Only structures with high confidence of the BTB domain region were used. Proteins were categorized in having either no amino-terminal extension (grey), an amino-terminal extension of $\alpha 1$ (dark red) or an amino-terminal extension of both $\alpha 1$ and $\beta 1$ (light red). Superfamily clusters of the BTB-ZF, BTB-BACK-Kelch predominantly consist of BTB proteins containing an amino-terminal extension.

Chapter 6

CONCLUSION AND OUTLOOK

This final chapter briefly summarizes the main discoveries of this thesis, which largely focused on unveiling co-translational molecular folding dynamics. We were able to expand on the intricate mechanisms of chaperone-induced nascent chain folding and protein folding and assembly of interacting nascent chains. I propose themes and experiments for future research, which entail investigating the synergy between translation-driven temporal control and dimerization quality control pathways, chaperone interaction during co-co assembly, and the influence of translation rhythm on complex formation and vice versa. Together, these studies will contribute to a deeper mechanistic understanding of co-translational protein biogenesis.

The role of ribosome-bound chaperones and nascent chain interactions in protein biogenesis holds many open questions. This thesis provides exciting new insights into the intricate mechanisms governing co-translational folding and complex assembly. By combining *in vivo* genome-wide screening results from selective ribosome and disome selective profiling, conducted by our collaborators B. Bukau and G. Kramer at Heidelberg University, with our *in vitro* single-molecule force spectroscopy and correlated confocal imaging results, we not only gained a better understanding of the general prevalence, but also of the mechanistic details of these cellular processes.

We investigated how Trigger Factor (TF), the only ribosome-associated chaperone in bacteria, influences nascent chain folding of a single-domain protein. We show for the first time that TF accelerates folding on the ribosome. This process is regulated by translation, with the emergence of key peptide segments dictating TF's ability to compact nascent chains and stabilize partial folds. Beyond chaperone-modulated folding, we also explored how ribosome cooperation drives protein complex formation. Using the intermediate filament lamin as a model, we demonstrate that ribosome proximity enables nascent chains to 'chaperone each other,' facilitating coiled-coil formation while preventing misfolding. Notably, when early interactions between nascent chains are inhibited or delayed, they become trapped in misfolded states and are no longer assembly-competent. We further examined the role of timing in nascent chain interactions, using the BTB domain as a model to study the challenging formation of intertwined dimers during translation. We identify a translation-driven temporal control mechanism that ensures proper dimerization. This process opens otherwise inaccessible folding-assembly pathways, bypassing unproductive monomeric states.

Taken together, we have managed, through the powerful combination of *in vivo* and *in vitro* approaches, to gain new perspectives on how cells ensure faithful protein biogenesis. Based on these findings, I outline future research directions and experiments that will further unravel the complexities of protein folding and interactions.

Trigger Factor binding during co-co assembly. Chapters 2 and 3 have shown that the bacterial chaperone Trigger Factor (TF) performs a diverse set of functions. Exciting new results from selective ribosome profiling and disome selective profiling reveal that TF also engages with protein subunits during co-co assembly. However, its specific role in this process remains entirely unclear. Given the translation-stage dependence observed in Chapter 3, TF may exert different functions at various stages of co-co assembly. During early translation, it could inhibit premature nascent chain interactions, whereas in later stages, TF might facilitate folding and assembly.

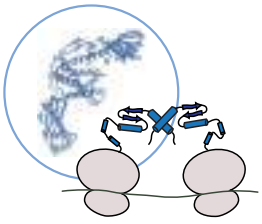

Figure 6.1 | Chaperones, like Trigger Factor (PDB code: 1w26), may affect co-co assembly.

Profiling results provide insights into the time points of TF engagement during translation, while the disome assay developed in Chapters

4 and 5 for optical tweezers could probe the conformational basis of these interactions. Additionally, fluorescently labeled TF could be used to determine binding times, offering insights into the preferred conformational states TF binds to, similar to the findings in Chapter 3. Likewise, integrating fluorescent probes into the nascent chain, as done in Chapter 4, could enable the detection of native contact formation between individual subunits. Beyond TF, it would also be exciting to explore the role of other chaperones in co-co assembly.

Co-co assembly in synergy with dimerization quality control pathways. In Chapter 5, we find that BTB co-co assembly candidates overlap largely with BTB substrates recognized by the E3 ligase SCF^{FBXL17}. Within a dimerization quality control pathway, SCF^{FBXL17} disrupts aberrant BTB dimers and tags BTB monomers for degradation [232]. Given the significant overlap, we proposed that the temporal assembly control mechanism we identified operates in concert with the dimerization quality control pathway. However, how these two mechanisms function together remains to be explored, particularly since SCF^{FBXL17} has also been found to engage with BTB proteins co-translationally. SCF^{FBXL17} may capture BTB proteins that fail to assemble into the native dimer conformation in a timely manner and instead fold into stable monomeric states. Fluorescently labeling FBXL17 and generating ribosomal constructs of the BTB domain at different translational stages could help determine when and to which conformational state FBXL17 binds. By exploring the synergy between these two mechanisms, both dedicated to ensuring faithful BTB dimerization, we could further expand our understanding of the extensive co-translational processes driving accurate complex assembly.

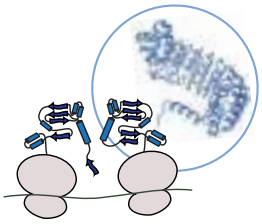

Figure 6.2 | Dimerization quality control (PDB code: 6w66) [232] in synergy with co-co assembly.

Beyond monomer recognition, another aspect that warrants further investigation is the engagement of FBXL17 with BTB dimers. Studies have largely attributed differences in BTB stability to FBXL17's ability to detect aberrant dimers [232, 234, 271]. However, no consensus has been reached regarding the precise factors that lead to FBXL17 recognition of aberrant dimers. It has been proposed that aberrant BTB dimers fail to stabilize the intermolecular β-sheet, allowing FBXL17 to differentiate native from aberrant dimers [232]. However, a recent study suggests that FBXL17 more likely perceives the general strength of protein-protein interactions at the dimeric interface [234]. Investigating the unfolding forces of constructs with mutations at different sites within the dimerization interface would enable quantification of how BTB dimer stability is affected by mutations. Moreover, introducing FBXL17 into these experiments could further illuminate how FBXL17 disrupts aberrant dimers, another aspect that has so far remained insufficiently understood at the molecular level. Combined, those investigations would lead to a better understanding of the molecular mechanisms underlying the dimerization quality control pathway, also in the post-translational context.

Dimerization pathways in co-co assembly In Chapters 4 and 5, we studied dimerization mediated by the interactions between nearby nascent chains. The coiled-coil domain of Lamin A/C and the BTB domain are unique in their structural features. The coiled-coil domain forms extensive intermolecular contacts, requiring its partner subunit for stabilization and to prevent misfolding. In contrast, the BTB domain features a uniquely intertwined dimer interface with a domain-swapped N-terminal β-strand. However, unlike the coiled-coil domain, the BTB domain can also stably adopt a monomeric conformation in the absence of its subunit partner. Consistent with our findings, extensive intermolecular contacts and intertwined dimerization interfaces have recently been proposed as molecular determinants of co-co assembly [61]. However, our observations regarding the different outcomes of delayed assembly at specific translational stages suggest that these structural characteristics not only influence dimer formation but also shape the pathways of dimerization, particularly in the initial subunit interactions and early folding events. Therefore, further investigation into dimerization pathways and their specific assembly requirements, such as preventing misfolding or avoiding stable monomeric structures, could provide additional insights into the molecular determinants of co-co assembly.

An interesting candidate for further study is the SCAN domain, which is among the five major dimerization domain classes implicated in coordinating co-co assembly. SCAN domains consist of five packed α-helices that mediate homo- and hetero-oligomerization in a large family of C2H2 zinc finger proteins [60]. Similar to the BTB domain, the SCAN homodimer adopts a domain-swapped dimer topology [272]. However, it also forms an extensive dimer interface, reminiscent of the coiled-coil domain, though not as extreme. Studying the SCAN domain could help determine the relative contributions of required initial folding and hydrophobic side-chain burial to the assembly process, offering deeper insights into the molecular mechanisms of complex assembly at the ribosome beyond general structural characteristics.

Translation rhythm and co-co assembly. In Chapter 1, the influence of translational rates and rhythm on protein production and folding is briefly discussed. On one hand, ribosome pausing can be beneficial, facilitating co-translational folding and the recruitment of various cellular machineries, such as chaperones, to support subsequent processes. On the other hand, prolonged ribosome stalling can result in the production of aberrant nascent protein products, which may be toxic [27, 273, 274].

Through the pairing of ribosomes via interactions between their concurrently translating nascent chains, it is reasonable to assume that translational rhythm—and, consequently, protein folding and production—is further influenced. However, little is currently understood about the underlying mechanisms driving co-co assembly and how they might be connected to specific coding sequences or secondary structures within the mRNA. One intriguing aspect to investigate is the correlation between pause sites and the onset of co-co assembly. It is well known that pause sites can lead to ribosome collisions, but their role in disome formation remains unclear. These sites could serve a beneficial function by promoting the formation

of disomes, which might additionally help to prevent harmful permanent stalling events. Alternatively, they could lead to premature interactions between nascent chains, potentially resulting in incorrect subunit assembly. In Chapters 4 and 5, we observed how critical the timing of nascent chain interactions is. Therefore, elucidating the regulatory mechanisms governing these interactions would not only shed light on the drivers of co-co assembly but also reveal broader predictors of faithful subunit assembly processes.

Ribosome profiling enables genome-wide detection of ribosome pause and stall sites, which can then be linked to the onset of co-co assembly through disome selective profiling. Optical tweezers could provide insights into the dynamic nature of disome formation, helping to determine, for instance, whether disome formation aids in overcoming stalling.

BIBLIOGRAPHY

[1] Roy Nassar et al. The Protein Folding Problem: The Role of Theory, *Journal of Molecular Biology* **433**, no. 20 (2021).

[2] Ken A. Dill and Justin L. MacCallum. The Protein-Folding Problem, 50 Years On, *Science* **338**, no. 6110 (2012).

[3] Alan R. Fersht. Max Ferdinand Perutz OM FRS, *Nature Structural Biology* **9**, no. 4 (2002).

[4] Christian B. Anfinsen. Principles that Govern the Folding of Protein Chains, *Science* **181**, no. 4096 (1973).

[5] Jiacheng Li et al. Entropy-Enthalpy Compensations Fold Proteins in Precise Ways, *International Journal of Molecular Sciences* **22**, no. 17 (2021).

[6] Ken A Dill et al. The protein folding problem: when will it be solved?, *Current Opinion in Structural Biology* **17**, no. 3 (2007).

[7] Julie S. Valastyan and Susan Lindquist. Mechanisms of protein-folding diseases at a glance, *Disease Models & Mechanisms* **7**, no. 1 (2014).

[8] G Patrick Brady and Kim A Sharp. Entropy in protein folding and in protein—protein interactions, *Current Opinion in Structural Biology* **7**, no. 2 (1997).

[9] Robert W. Newberry and Ronald T. Raines. Secondary Forces in Protein Folding, *ACS Chemical Biology* **14**, no. 8 (2019).

[10] Stewart R. Durell and Arieh Ben-Naim. Hydrophobic-hydrophilic forces in protein folding, *Biopolymers* **107**, no. 8 (2017).

[11] Ken A. Dill. Dominant forces in protein folding, *Biochemistry* **29**, no. 31 (1990).

[12] F. M. Richards. Protein stability: still an unsolved problem, *Cellular and Molecular Life Sciences CMLS* **53**, no. 10 (1997).

[13] Martin Karplus. Behind the folding funnel diagram, *Nature Chemical Biology* **7**, no. 7 (2011).

[14] Ken A. Dill and Hue Sun Chan. From Levinthal to pathways to funnels, *Nature Structural Biology* **4**, no. 1 (1997).

[15] Irena Roterman, Mateusz Slupina, and Leszek Konieczny. Protein folding: Funnel model revised, *Computational and Structural Biotechnology Journal* **23** (2024).

[16] Patricia L. Clark. Protein folding in the cell: reshaping the folding funnel, *Trends in Biochemical Sciences* **29**, no. 10 (2004).

[17] John Jumper et al. Highly accurate protein structure prediction with AlphaFold, *Nature* **596**, no. 7873 (2021).

[18] Carlos Outeiral, Daniel A Nissley, and Charlotte M Deane. Current structure predictors are not learning the physics of protein folding, *Bioinformatics* **38**, no. 7 (2022).

[19] Peter B. Moore et al. The protein-folding problem: Not yet solved, *Science* **375**, no. 6580 (2022).

[20] David A. Agard et al. Solution of the protein structure prediction problem at last: crucial innovations and next frontiers. *Faculty Reviews* (2022).

[21] Zhenyu Yang et al. AlphaFold2 and its applications in the fields of biology and medicine, *Signal Transduction and Targeted Therapy* **8**, no. 1 (2023).

[22] Kiersten M. Ruff and Rohit V. Pappu. AlphaFold and Implications for Intrinsically Disordered Proteins, *Journal of Molecular Biology* **433**, no. 20 (2021).

[23] Eugene Shakhnovich. Protein Folding Thermodynamics and Dynamics: Where Physics, Chemistry, and Biology Meet, *Chemical Reviews* **106**, no. 5 (2006).

[24] Kosuke Hashimoto and Anna R. Panchenko. Mechanisms of protein oligomerization, the critical role of insertions and deletions in maintaining different oligomeric states, *Proceedings of the National Academy of Sciences* **107**, no. 47 (2010).

[25] Carl Frieden. Protein oligomerization as a metabolic control mechanism: Application to apoE, *Protein Science* **28**, no. 4 (2019).

[26] Mayssam H. Ali and Barbara Imperiali. Protein oligomerization: How and why, *Bioorganic & Medicinal Chemistry* **13**, no. 17 (2005).

[27] Anton A. Komar, Ekaterina Samatova, and Marina V. Rodnina. Translation Rates and Protein Folding, *Journal of Molecular Biology* **436**, no. 14 (2024).

[28] Anaïs M E Cassaignau, Lisa D Cabrita, and John Christodoulou. How Does the Ribosome Fold the Proteome?, *Annual Review of Biochemistry* **89** (2020).

[29] Ekaterina Samatova, Anton A. Komar, and Marina V. Rodnina. How the ribosome shapes cotranslational protein folding, *Current Opinion in Structural Biology* **84** (2024).

[30] Michael Thommen, Wolf Holtkamp, and Marina V Rodnina. Co-translational protein folding: progress and methods, **42** (2017).

[31] Philip To et al. Nonrefoldability is Pervasive Across the E. coli Proteome, *Journal of the American Chemical Society* **143**, no. 30 (2021).

[32] Philip To et al. A proteome-wide map of chaperone-assisted protein refolding in a cytosol-like milieu, *Proceedings of the National Academy of Sciences* **119**, no. 48 (2022).

[33] Lisa M. Alexander et al. Non-equilibrium dynamics of a nascent polypeptide during translation suppress its misfolding, *Nature Communications* **10**, no. 1 (2019).

[34] Julian O. Streit et al. The ribosome lowers the entropic penalty of protein folding, *Nature* **633**, no. 8028 (2024).

[35] Chava Kimchi-Sarfaty et al. A "Silent" Polymorphism in the MDR1 Gene Changes Substrate Specificity, *Science* **315**, no. 5811 (2007).

[36] Marina V. Rodnina. The ribosome in action: Tuning of translational efficiency and protein folding, *Protein Science* **25**, no. 8 (2016).

[37] Vijaya L Simhadri et al. Single synonymous mutation in factor IX alters protein properties and underlies haemophilia B, *Journal of Medical Genetics* **54**, no. 5 (2017).

[38] Nathan C. Edwards et al. Characterization of Coding Synonymous and Non-Synonymous Variants in ADAMTS13 Using Ex Vivo and In Silico Approaches, *PLOS ONE* **7**, no. 6 (2012).

[39] Jared J. Gartner et al. Whole-genome sequencing identifies a recurrent functional synonymous mutation in melanoma, *Proceedings of the National Academy of Sciences* **110**, no. 33 (2013).

[40] Jianli Lu and Carol Deutsch. Electrostatics in the Ribosomal Tunnel Modulate Chain Elongation Rates, *Journal of Molecular Biology* **384**, no. 1 (2008).

[41] Yuhei Chadani et al. Intrinsic Ribosome Destabilization Underlies Translation and Provides an Organism with a Strategy of Environmental Sensing, *Molecular Cell* **68**, no. 3 (2017).

[42] Yuhei Chadani et al. Nascent polypeptide within the exit tunnel stabilizes the ribosome to counteract risky translation, *The EMBO Journal* **40**, no. 23 (2021).

[43] Xabier Agirrezabala et al. A switch from α-helical to β-strand conformation during co-translational protein folding, *The EMBO Journal* **41**, no. 4 (2022).

[44] Guy Ziv, Gilad Haran, and D. Thirumalai. Ribosome exit tunnel can entropically stabilize α-helices, *Proceedings of the National Academy of Sciences* **102**, no. 52 (2005).

[45] Edward P. O'Brien et al. Factors Governing Helix Formation in Peptides Confined to Carbon Nanotubes, *Nano Letters* **8**, no. 11 (2008).

[46] Jeetain Mittal and Robert B. Best. Thermodynamics and kinetics of protein folding under confinement, *Proceedings of the National Academy of Sciences* **105**, no. 51 (2008).

[47] Wolf Holtkamp et al. Cotranslational protein folding on the ribosome monitored in real time, *Science* **350**, no. 6264 (2015).

[48] José Arcadio Farías-Rico et al. Effects of protein size, thermodynamic stability, and net charge on cotranslational folding on the ribosome, *Proceedings of the National Academy of Sciences* **115**, no. 40 (2018).

[49] Florian Wruck et al. The ribosome modulates folding inside the ribosomal exit tunnel, *Communications Biology* **4**, no. 1 (2021).

[50] Anaïs M. E. Cassaignau et al. Interactions between nascent proteins and the ribosome surface inhibit co-translational folding, *Nature Chemistry* **13**, no. 12 (2021).

[51] Marija Liutkute, Ekaterina Samatova, and Marina V. Rodnina. Cotranslational Folding of Proteins on the Ribosome, *Biomolecules* **10**, no. 1 (2020).

[52] Günter Kramer, Ayala Shiber, and Bernd Bukau. Mechanisms of Cotranslational Maturation of Newly Synthesized Proteins, *Annual Review of Biochemistry* **88** (2019).

[53] Yu-Wei Shieh et al. Operon structure and cotranslational subunit association direct protein assembly in bacteria, *Science* **350**, no. 6261 (2015).

[54] Ayala Shiber et al. Cotranslational assembly of protein complexes in eukaryotes revealed by ribosome profiling, *Nature* **561**, no. 7722 (2018).

[55] Johannes Venezian et al. Diverging co-translational protein complex assembly pathways are governed by interface energy distribution, *Nature Communications* **15**, no. 1 (2024).

[56] Andre Schwarz and Martin Beck. The Benefits of Cotranslational Assembly: A Structural Perspective, *Trends in Cell Biology* **29**, no. 10 (2019).

[57] Fabián Morales-Polanco et al. Cotranslational Mechanisms of Protein Biogenesis and Complex Assembly in Eukaryotes, *Annual Review of Biomedical Data Science* (2022).

[58] Caia D. S. Duncan and Juan Mata. Widespread Cotranslational Formation of Protein Complexes, *PLOS Genetics* **7**, no. 12 (2011).

[59] Krishnendu Khan and Paul L. Fox. Benefits of co-translational complex assembly for cellular fitness, *BioEssays* **45**, no. 5 (2023).

[60] Matilde Bertolini et al. Interactions between nascent proteins translated by adjacent ribosomes drive homomer assembly, *Science* **371**, no. 6524 (2021).

[61] Saurav Mallik et al. Structural determinants of co-translational protein complex assembly, *Cell* **188**, no. 3 (2025).

[62] Ruth Herbst, Ute Schäfer, and Robert Seckler. Equilibrium Intermediates in the Reversible Unfolding of Firefly (Photinus pyralis) Luciferase*, *Journal of Biological Chemistry* **272**, no. 11 (1997).

[63] Ramon Duran-Romaña et al. Native Fold Delay and its implications for co-translational chaperone binding and protein aggregation, *Nature Communications* **16**, no. 1 (2025).

[64] Sergiy O. Garbuzynskiy et al. How proteins manage to fold and how chaperones manage to assist the folding, *Physics of Life Reviews* **52** (2025).

[65] F. U. Hartl, A. Bracher, and M. Hayer-Hartl. Molecular chaperones in protein folding and proteostasis, *Nature* **475**, no. 7356 (2011).

[66] Stefan Walter and Johannes Buchner. Molecular Chaperones—Cellular Machines for Protein Folding, *Angewandte Chemie International Edition* **41**, no. 7 (2002).

[67] Cindy Voisine, Jesper Søndergaard Pedersen, and Richard I. Morimoto. Chaperone networks: Tipping the balance in protein folding diseases, *Neurobiology of Disease* **40**, no. 1 (2010).

[68] Bob Schiffrin and Antonio N. Calabrese. Chaperones in concert: Orchestrating co-translational protein folding in the cell, *Molecular Cell* **84**, no. 13 (2024).

[69] Junyi Jiao et al. "Single-Molecule Protein Folding Experiments Using High-Precision Optical Tweezers", *Optical Tweezers: Methods and Protocols*. Ed. by Arne Gennerich. New York, NY: Springer New York, 2017.

[70] Carlos J. Bustamante et al. Optical tweezers in single-molecule biophysics, *Nature Reviews Methods Primers* **1**, no. 1 (2021).

[71] Bharat Jagannathan and Susan Marqusee. Protein folding and unfolding under force, *Biopolymers* **99**, no. 11 (2013).

[72] Richard W. Bowman and Miles J. Padgett. Optical trapping and binding, *Reports on Progress in Physics* **76**, no. 2 (2013).

[73] C. Bustamante et al. Single-Molecule Studies of Protein Folding with Optical Tweezers, *Annual Review of Biochemistry* **89** (2020).

[74] Paolo Polimeno et al. Optical tweezers and their applications, *Journal of Quantitative Spectroscopy and Radiative Transfer* **218** (2018).

[75] Annamaria Zaltron et al. Optical tweezers in single-molecule experiments, *The European Physical Journal Plus* **135**, no. 11 (2020).

[76] F. Wruck et al. "Probing Single Chaperone Substrates", ed. by Sebastian Hiller, Maili Liu, and Lichun He. Vol. 29. Biophysics of Molecular Chaperones: Function, Mechanisms and Client Protein Interactions. Royal Society of Chemistry, 2023.

[77] A. Hoffmann, B. Bukau, and G. Kramer. Structure and function of the molecular chaperone Trigger Factor, *Biochimica Et Biophysica Acta-Molecular Cell Research* **1803**, no. 6 (2010).

[78] F. Merz et al. Molecular mechanism and structure of Trigger Factor bound to the translating ribosome, *EMBO J* **27**, no. 11 (2008).

[79] E Crooke and W Wickner. Trigger factor: a soluble protein that folds pro-OmpA into a membrane-assembly-competent form. *Proceedings of the National Academy of Sciences* **84**, no. 15 (1987).

[80] David Baram et al. Structure of trigger factor binding domain in biologically homologous complex with eubacterial ribosome reveals its chaperone action, *Proceedings of the National Academy of Sciences* **102**, no. 34 (2005).

[81] C. M. Kaiser et al. Real-time observation of trigger factor function on translating ribosomes, *Nature* **444**, no. 7118 (2006).

[82] L. Ferbitz et al. Trigger factor in complex with the ribosome forms a molecular cradle for nascent proteins, *Nature* **431**, no. 7008 (2004).

[83] F. Wruck et al. Protein Folding Mediated by Trigger Factor and Hsp70: New Insights from Single-Molecule Approaches, *Journal of Molecular Biology* **430**, no. 4 (2018).

[84] K. X. Liu, K. Maciuba, and C. M. Kaiser. The Ribosome Cooperates with a Chaperone to Guide Multi-domain Protein Folding, *Molecular Cell* **74**, no. 2 (2019).

[85] Tomohide Saio et al. Structural Basis for Protein Antiaggregation Activity of the Trigger Factor Chaperone, *Science* **344**, no. 6184 (2014).

[86] Amanda Raine et al. Trigger Factor Binding to Ribosomes with Nascent Peptide Chains of Varying Lengths and Sequences*, *Journal of Biological Chemistry* **281**, no. 38 (2006).

[87] A. Mashaghi et al. Reshaping of the conformational search of a protein by the chaperone trigger factor, *Nature* **500**, no. 7460 (2013).

[88] S. Haldar et al. Trigger factor chaperone acts as a mechanical foldase, *Nature Communications* **8** (2017).

[89] S. Hiller. Chaperone-Bound Clients: The Importance of Being Dynamic, *Trends in Biochemical Sciences* **44**, no. 6 (2019).

[90] Dongjie Fan et al. Exploring the roles of substrate-binding surface of the chaperone site in the chaperone activity of trigger factor, *The FASEB Journal* **32**, no. 12 (2018).

[91] K. Singhal et al. The Trigger Factor Chaperone Encapsulates and Stabilizes Partial Folds of Substrate Proteins, *Plos Computational Biology* **11**, no. 10 (2015).

[92] Mario J. Avellaneda et al. Simultaneous sensing and imaging of individual biomolecular complexes enabled by modular DNA-protein coupling, *Communications Chemistry* **3**, no. 1 (2020).

[93] Interaction of Trigger Factor with the Ribosome, *Journal of Molecular Biology* **326**, no. 2 (2003).

[94] H. Patzelt et al. Three-State Equilibrium of Escherichia coli Trigger Factor, *Biological Chemistry* **383**, no. 10 (2002).

[95] L. Morgado et al. The dynamic dimer structure of the chaperone Trigger Factor, *Nature Communications* **8** (2017).

[96] Sathish K. Lakshmipathy et al. Identification of Nascent Chain Interaction Sites on Trigger Factor, *Journal of Biological Chemistry* **282**, no. 16 (2007).

[97] Anna Rutkowska et al. Dynamics of Trigger Factor Interaction with Translating Ribosomes, *Journal of Biological Chemistry* **283**, no. 7 (2008).

[98] B. Bukau, J. Weissman, and A. Horwich. Molecular chaperones and protein quality control, *Cell* **125**, no. 3 (2006).

[99] P. Bechtluft et al. Direct observation of chaperone-induced changes in a protein folding pathway, *Science* **318**, no. 5855 (2007).

[100] S. Sharma et al. Monitoring protein conformation along the pathway of chaperonin-assisted folding, *Cell* **133**, no. 1 (2008).

[101] M. M. Naqvi et al. Protein chain collapse modulation and folding stimulation by GroEL-ES, *Science Advances* **8**, no. 9 (2022).

[102] Christopher M. Dobson. Protein folding and misfolding, *Nature* **426**, no. 6968 (2003).

[103] N. Ban et al. The complete atomic structure of the large ribosomal subunit at 2.4 A resolution, *Science* **289**, no. 5481 (2000).

[104] I. Mingarro et al. Different conformations of nascent polypeptides during translocation across the ER membrane, *BMC Cell Biol* **1** (2000).

[105] P. Nissen et al. The structural basis of ribosome activity in peptide bond synthesis, *Science* **289**, no. 5481 (2000).

[106] C. A. Woolhead, P. J. McCormick, and A. E. Johnson. Nascent membrane and secretory proteins differ in FRET-detected folding far inside the ribosome and in their exposure to ribosomal proteins, *Cell* **116**, no. 5 (2004).

[107] C. M. Kaiser et al. The Ribosome Modulates Nascent Protein Folding, *Science* **334**, no. 6063 (2011).

[108] K. C. Stein, A. Kriel, and J. Frydman. Nascent Polypeptide Domain Topology and Elongation Rate Direct the Cotranslational Hierarchy of Hsp70 and TRiC/CCT, *Molecular Cell* **75**, no. 6 (2019).

[109] L. Eismann et al. Selective ribosome profiling reveals a role for SecB in the co-translational inner membrane protein biogenesis, *Cell Reports* **41**, no. 10 (2022).

[110] L. Zhao et al. Bacterial RF3 senses chaperone function in co-translational folding, *Molecular Cell* **81**, no. 14 (2021).

[111] H. Patzelt et al. Binding specificity of Escherichia coli trigger factor, *Proceedings of the National Academy of Sciences* **98**, no. 25 (2001).

[112] G. Kramer et al. L23 protein functions as a chaperone docking site on the ribosome, *Nature* **419**, no. 6903 (2002).

[113] S. K. Lakshmipathy et al. Versatility of trigger factor interactions with ribosome-nascent chain complexes, *J Biol Chem* **285**, no. 36 (2010).

[114] E. Oh et al. Selective ribosome profiling reveals the cotranslational chaperone action of trigger factor in vivo, *Cell* **147**, no. 6 (2011).

[115] A. Hoffmann et al. Trigger factor forms a protective shield for nascent polypeptides at the ribosome, *Journal of Biological Chemistry* **281**, no. 10 (2006).

[116] A. Hoffmann et al. Concerted Action of the Ribosome and the Associated Chaperone Trigger Factor Confines Nascent Polypeptide Folding, *Molecular Cell* **48**, no. 1 (2012).

[117] Björn M. Burmann and Sebastian Hiller. Chaperones and chaperone–substrate complexes: Dynamic playgrounds for NMR spectroscopists, *Progress in Nuclear Magnetic Resonance Spectroscopy* **86-87** (2015).

[118] Timm Maier et al. A cradle for new proteins: trigger factor at the ribosome, *Current Opinion in Structural Biology* **15**, no. 2 (2005).

[119] O. B. Nilsson et al. Trigger Factor Reduces the Force Exerted on the Nascent Chain by a Cotranslationally Folding Protein, *Journal of Molecular Biology* **428**, no. 6 (2016).

[120] Elke Deuerling et al. Trigger Factor and DnaK possess overlapping substrate pools and binding specificities. eng, *Molecular microbiology* **47**, no. 5 (2003).

[121] S. A. Teter et al. Polypeptide flux through bacterial Hsp70: DnaK cooperates with trigger factor in chaperoning nascent chains, *Cell* **97**, no. 6 (1999).

[122] A. H. Becker et al. Selective ribosome profiling as a tool for studying the interaction of chaperones and targeting factors with nascent polypeptide chains and ribosomes, *Nature Protocols* **8**, no. 11 (2013).

[123] A. Katranidis et al. Fast biosynthesis of GFP molecules: a single-molecule fluorescence study, *Angewandte Chemie International Edition* **48**, no. 10 (2009).

[124] F. Cymer et al. Exploration of the arrest peptide sequence space reveals arrest-enhanced variants, *Journal of Biological Chemistry* **290**, no. 16 (2015).

[125] Noémie Kempf et al. A Novel Method to Evaluate Ribosomal Performance in Cell-Free Protein Synthesis Systems, *Scientific Reports* **7**, no. 1 (2017).

[126] Rafayel Petrosyan. Improved approximations for some polymer extension models, *Rheologica Acta* **56** (2016).

[127] T. Odijk. Stiff Chains and Filaments under Tension, *Macromolecules* **28**, no. 20 (1995).

[128] Thomas E. Wales et al. Resolving chaperone-assisted protein folding on the ribosome at the peptide level, *Nature Structural & Molecular Biology* (2024).

[129] Rahmi Imamoglu et al. Bacterial Hsp70 resolves misfolded states and accelerates productive folding of a multi-domain protein, *Nature Communications* **11**, no. 1 (2020).

[130] Thomas Bornemann, Wolf Holtkamp, and Wolfgang Wintermeyer. Interplay between trigger factor and other protein biogenesis factors on the ribosome, *Nature Communications* **5**, no. 1 (2014).

[131] Michael A. Sørensen and Steen Pedersen. Absolute in vivo translation rates of individual codons in Escherichia coli: The two glutamic acid codons GAA and GAG are translated with a threefold difference in rate, *Journal of Molecular Biology* **222**, no. 2 (1991).

[132] A. Prabhakar et al. Dynamic basis of fidelity and speed in translation: Coordinated multistep mechanisms of elongation and termination, *Protein Science* **26**, no. 7 (2017).

[133] Z. Lin and H. S. Rye. Expansion and compression of a protein folding intermediate by GroEL, *Molecular Cell* **16**, no. 2 (2004).

[134] Alex S. Holehouse and Rohit V. Pappu. Collapse Transitions of Proteins and the Interplay Among Backbone, Sidechain, and Solvent Interactions, *Annual Review of Biophysics* **47** (2018).

[135] Jagannath Mondal et al. How osmolytes influence hydrophobic polymer conformations: A unified view from experiment and theory, *Proceedings of the National Academy of Sciences* **112**, no. 30 (2015).

[136] D. S. Libich et al. Confinement and Stabilization of Fyn SH3 Folding Intermediate Mimetics within the Cavity of the Chaperonin GroEL Demonstrated by Relaxation-Based NMR, *Biochemistry* **56**, no. 7 (2017).

[137] J. Martin et al. Chaperonin-Mediated Protein Folding at the Surface of Groel through a Molten Globule-Like Intermediate, *Nature* **352**, no. 6330 (1991).

[138] Alžběta Roeselová et al. Mechanism of chaperone coordination during cotranslational protein folding in bacteria, *Molecular Cell* **84**, no. 13 (2024).

[139] Ruiyue Tan et al. Folding stabilities of ribosome-bound nascent polypeptides probed by mass spectrometry, *Proceedings of the National Academy of Sciences* **120**, no. 33 (2023).

[140] Reto Horst et al. Folding trajectories of human dihydrofolate reductase inside the GroEL–GroES chaperonin cavity and free in solution, *Proceedings of the National Academy of Sciences* **104**, no. 52 (2007).

[141] Daniel H. Goldman et al. Mechanical force releases nascent chain–mediated ribosome arrest in vitro and in vivo, *Science* **348**, no. 6233 (2015).

[142] David Balchin, Manajit Hayer-Hartl, and F. Ulrich Hartl. In vivo aspects of protein folding and quality control, *Science* **353**, no. 6294 (2016).

[143] Günter Kramer et al. The ribosome as a platform for co-translational processing, folding and targeting of newly synthesized proteins, *Nature Structural & Molecular Biology* **16**, no. 6 (2009).

[144] H. J. Rheinberger et al. Parameters for the Preparation of Escherichia-Coli Ribosomes and Ribosomal-Subunits Active in Transfer-Rna Binding, *Methods in Enzymology* **164** (1988).

[145] R. Zaniewski, E. Petkaitis, and M. P. Deutscher. A multiple mutant of Escherichia coli lacking the exoribonucleases RNase II, RNase D, and RNase BN, *J Biol Chem* **259**, no. 19 (1984).

[146] H. Ohashi et al. A Highly Controllable Reconstituted Cell-Free System -a Breakthrough in Protein Synthesis Research, *Current Pharmaceutical Biotechnology* **11**, no. 3 (2010).

[147] T. Cordes, J. Vogelsang, and P. Tinnefeld. On the Mechanism of Trolox as Antiblinking and Antibleaching Reagent, *Journal of the American Chemical Society* **131**, no. 14 (2009).

[148] A. Blazquez-Castro. Optical Tweezers: Phototoxicity and Thermal Stress in Cells and Biomolecules, *Micromachines* **10**, no. 8 (2019).

[149] M. Swoboda et al. Enzymatic Oxygen Scavenging for Photostability without pH Drop in Single-Molecule Experiments, *Acs Nano* **6**, no. 7 (2012).

[150] P D Thomas and K A Dill. An iterative method for extracting energy-like quantities from protein structures. *Proceedings of the National Academy of Sciences* **93**, no. 21 (1996).

[151] Li Lin, George N. DeMartino, and Warner C. Greene. Cotranslational dimerization of the Rel homology domain of NF-κB1 generates p50–p105 heterodimers and is required for effective p50 production, *The EMBO Journal* **19**, no. 17 (2000).

[152] Ivanka Kamenova et al. Co-translational assembly of mammalian nuclear multisubunit complexes, *Nature Communications* **10**, no. 1 (2019).

[153] Chris D. Nicholls et al. Biogenesis of p53 Involves Cotranslational Dimerization of Monomers and Posttranslational Dimerization of Dimers. Implications on the dominant negative effect, *Journal of Biological Chemistry* **277**, no. 15 (2002).

[154] Sambra D. Redick and Jean E. Schwarzbauer. Rapid intracellular assembly of tenascin hexabrachions suggests a novel co-translational process, *Journal of Cell Science* **108**, no. 4 (1995).

[155] Neal K. Williams and Bernhard Dichtl. Co-translational control of protein complex formation: a fundamental pathway of cellular organization?, *Biochemical Society Transactions* **46**, no. 1 (2018).

[156] R. John Ellis. Protein misassembly: macromolecular crowding and molecular chaperones, *Advances in experimental medicine and biology* **594** (2007).

[157] F. Ulrich Hartl and Manajit Hayer-Hartl. Molecular Chaperones in the Cytosol: from Nascent Chain to Folded Protein, *Science* **295**, no. 5561 (2002).

[158] J. Ahn et al. Structural basis for lamin assembly at the molecular level, *Nature Communications* **10**, no. 1 (2019).

[159] Jan Philipp Junker, Fabian Ziegler, and Matthias Rief. Ligand-Dependent Equilibrium Fluctuations of Single Calmodulin Molecules, *Science* **323**, no. 5914 (2009).

[160] Ken A. Dill and Justin L. MacCallum. The Protein-Folding Problem, 50 Years On, *Science* **338**, no. 6110 (2012).

[161] Yael Phillip and Gideon Schreiber. Formation of protein complexes in crowded environments – From in vitro to in vivo, *FEBS Letters* **587**, no. 8 (2013).

[162] Alfonso De Simone et al. Intrinsic disorder modulates protein self-assembly and aggregation, *Proceedings of the National Academy of Sciences* **109**, no. 18 (2012).

[163] André Halbach et al. Cotranslational assembly of the yeast SET1C histone methyltransferase complex, *The EMBO Journal* **28**, no. 19 (2009).

[164] Jonathan N. Wells, L. Therese Bergendahl, and Joseph A. Marsh. Operon Gene Order Is Optimized for Ordered Protein Complex Assembly, *Cell Reports* **14**, no. 4 (2016).

[165] Florian Wruck et al. Translation and folding of single proteins in real time, *Proceedings of the National Academy of Sciences* **114**, no. 22 (2017).

[166] Frank D. McKeon, Marc W. Kirschner, and Daniel Caput. Homologies in both primary and secondary structure between nuclear envelope and intermediate filament proteins, *Nature* **319**, no. 6053 (1986).

[167] Bas van Steensel and Andrew S. Belmont. Lamina-Associated Domains: Links with Chromosome Architecture, Heterochromatin, and Gene Repression, *Cell* **169**, no. 5 (2017).

[168] Howard J. Worman and Gisèle Bonne. "Laminopathies": A wide spectrum of human diseases, *Experimental Cell Research* **313**, no. 10 (2007).

[169] D Z Fisher, N Chaudhary, and G Blobel. cDNA sequencing of nuclear lamins A and C reveals primary and secondary structural homology to intermediate filament proteins. *Proceedings of the National Academy of Sciences* **83**, no. 17 (1986).

[170] Klaus Weber, Uwe Plessmann, and Peter Traub. Maturation of nuclear lamin A involves a specific carboxy-terminal trimming, which removes the polyisoprenylation site from the precursor; implications for the structure of the nuclear lamina, *FEBS Letters* **257**, no. 2 (1989).

[171] M. Sinensky et al. The processing pathway of prelamin a, *Journal of Cell Science* **107**, no. 1 (1994).

[172] Harald Herrmann et al. Intermediate filaments: from cell architecture to nanomechanics, *Nature Reviews Molecular Cell Biology* **8**, no. 7 (2007).

[173] Nico Stuurman, Susanne Heins, and Ueli Aebi. Nuclear Lamins: Their Structure, Assembly, and Interactions, *Journal of Structural Biology* **122**, no. 1 (1998).

[174] Thomas Dechat et al. Nuclear lamins: major factors in the structural organization and function of the nucleus and chromatin, *Genes & development* **22**, no. 7 (2008).

[175] Thorsten Kolb et al. Lamin A and lamin C form homodimers and coexist in higher complex forms both in the nucleoplasmic fraction and in the lamina of cultured human cells, *Nucleus* **2**, no. 5 (2011).

[176] Qian Ye and Howard J. Worman. Protein-Protein Interactions between Human Nuclear Lamins Expressed in Yeast, *Experimental Cell Research* **219**, no. 1 (1995).

[177] O. L. Miller, Barbara A. Hamkalo, and C. A. Thomas. Visualization of Bacterial Genes in Action, *Science* **169**, no. 3943 (1970).

[178] Florian Brandt et al. The Native 3D Organization of Bacterial Polysomes, *Cell* **136**, no. 2 (2009).

[179] Zhiqun Xi et al. Single-molecule observation of helix staggering, sliding, and coiled coil misfolding, *Proceedings of the National Academy of Sciences* **109**, no. 15 (2012).

[180] P. Kumar and D. N. Woolfson. Socket2: a program for locating, visualizing and analyzing coiled-coil interfaces in protein structures, *Bioinformatics* **37**, no. 23 (2021).

[181] J. Walshaw and D. N. Woolfson. Socket: a program for identifying and analysing coiled-coil motifs within protein structures, *Journal of Molecular Biology* **307**, no. 5 (2001).

[182] D. N. Woolfson. Understanding a protein fold: The physics, chemistry, and biology of alpha-helical coiled coils, *Journal of Biological Chemistry* **299**, no. 4 (2023).

[183] B. Y. Zhu et al. Packing and hydrophobicity effects on protein folding and stability: effects of beta-branched amino acids, valine and isoleucine, on the formation and stability of two-stranded alpha-helical coiled coils/leucine zippers, *Protein Science* **2**, no. 3 (1993).

[184] Y. B. Yu. Coiled-coils: stability, specificity, and drug delivery potential, *Advanced Drug Delivery Reviews* **54**, no. 8 (2002).

[185] C. Zhang and S. H. Kim. Environment-dependent residue contact energies for proteins, *Proceedings of the National Academy of Sciences* **97**, no. 6 (2000).

[186] T. Bornschlogl and M. Rief. Single-molecule dynamics of mechanical coiled-coil unzipping, *Langmuir* **24**, no. 4 (2008).

[187] T. Bornschlogl and M. Rief. Single molecule unzipping of coiled coils: sequence resolved stability profiles, *Physical Review Letters* **96**, no. 11 (2006).

[188] M. Goktas et al. Molecular mechanics of coiled coils loaded in the shear geometry, *Chemical Science* **9**, no. 20 (2018).

[189] B. Ramm et al. Sequence-resolved free energy profiles of stress-bearing vimentin intermediate filaments, *Proceedings of the National Academy of Sciences* **111**, no. 31 (2014).

[190] S. Sadeghi and E. Emberly. Length-dependent force characteristics of coiled coils, *Phys Rev E Stat Nonlin Soft Matter Phys* **80**, no. 6 Pt 1 (2009).

[191] P. Lopez-Garcia et al. Structural determinants of coiled coil mechanics, *Physical Chemistry Chemical Physics* **21**, no. 18 (2019).

[192] Nathan W. Luedtke et al. Surveying polypeptide and protein domain conformation and association with FlAsH and ReAsH, *Nature Chemical Biology* **3**, no. 12 (2007).

[193] Marcin Wolny et al. Stable Single α-Helices Are Constant Force Springs in Proteins, *Journal of Biological Chemistry* **289**, no. 40 (2014).

[194] Ingo Schwaiger et al. The myosin coiled-coil is a truly elastic protein structure, *Nature Materials* **1**, no. 4 (2002).

[195] Milo M. Lin, Dmitry Shorokhov, and Ahmed H. Zewail. Dominance of misfolded intermediates in the dynamics of α-helix folding, *Proceedings of the National Academy of Sciences* **111**, no. 40 (2014).

[196] Eviatar Natan et al. Cotranslational protein assembly imposes evolutionary constraints on homomeric proteins, *Nature Structural & Molecular Biology* **25**, no. 3 (2018).

[197] Eman Elzeneini and Sara A. Wickström. Lipodystrophic laminopathy: Lamin A mutation relaxes chromatin architecture to impair adipogenesis, *Journal of Cell Biology* **216**, no. 9 (2017).

[198] A. Buchwalter. Intermediate, but not average: The unusual lives of the nuclear lamin proteins, *Current Opinion in Cell Biology* **84** (2023).

[199] S. A. Adam, K. Sengupta, and R. D. Goldman. Regulation of nuclear lamin polymerization by importin alpha, *Journal of Biological Chemistry* **283**, no. 13 (2008).

[200] Nurzian Ismail et al. A biphasic pulling force acts on transmembrane helices during translocon-mediated membrane integration, *Nature Structural & Molecular Biology* **19**, no. 10 (2012).

[201] Benjamin Fritch et al. Origins of the Mechanochemical Coupling of Peptide Bond Formation to Protein Synthesis, *Journal of the American Chemical Society* **140**, no. 15 (2018).

[202] Federico Cerullo et al. Bacterial ribosome collision sensing by a MutS DNA repair ATPase paralogue, *Nature* **603**, no. 7901 (2022).

[203] Jake F. Watson and Javier García-Nafría. In vivo DNA assembly using common laboratory bacteria: A re-emerging tool to simplify molecular cloning, *Journal of Biological Chemistry* **294**, no. 42 (2019).

[204] Vivek S. Jadhav et al. Single-molecule mechanics of protein-labelled DNA handles, *Beilstein Journal of Nanotechnology* **7** (2016).

[205] Kirstine Berg-Sørensen and Henrik Flyvbjerg. Power spectrum analysis for optical tweezers, *Review of Scientific Instruments* **75**, no. 3 (2004).

[206] Martin Hegner, Steven B. Smith, and Carlos Bustamante. Polymerization and mechanical properties of single RecA–DNA filaments, *Proceedings of the National Academy of Sciences* **96**, no. 18 (1999).

[207] A. E. Keating et al. Side-chain repacking calculations for predicting structures and stabilities of heterodimeric coiled coils, *Proceedings of the National Academy of Sciences* **98**, no. 26 (2001).

[208] J. Moitra et al. Leucine is the most stabilizing aliphatic amino acid in the d position of a dimeric leucine zipper coiled coil, *Biochemistry* **36**, no. 41 (1997).

[209] Y. Bruce Yu et al. The Measure of Interior Disorder in a Folded Protein and Its Contribution to Stability, *Journal of the American Chemical Society* **121**, no. 37 (1999).

[210] M. Bera, S. R. Ainavarapu, and K. Sengupta. Significance of 1B and 2B domains in modulating elastic properties of lamin A, *Scientific Reports* **6** (2016).

[211] M. Bernhofer et al. PredictProtein - Predicting Protein Structure and Function for 29 Years, *Nucleic Acids Research* **49**, no. W1 (2021).

[212] Peter Gross et al. Quantifying how DNA stretches, melts and changes twist under tension, *Nature Physics* **7**, no. 9 (2011).

[213] J. M. Matthews and M. Sunde. Dimers, Oligomers, Everywhere, *Protein Dimerization and Oligomerization in Biology* **747** (2012).

[214] N. J. Marianayagam, M. Sunde, and J. M. Matthews. The power of two: protein dimerization in biology, *Trends in Biochemical Sciences* **29**, no. 11 (2004).

[215] R. E. A. Gwyther, D. D. Jones, and H. L. Worthy. Better together: building protein oligomers naturally and by design, *Biochemical Society Transactions* **47** (2019).

[216] A. De Simone et al. Intrinsic disorder modulates protein self-assembly and aggregation, *Proceedings of the National Academy of Sciences* **109**, no. 18 (2012).

[217] A. P. Minton. Implications of macromolecular crowding for protein assembly, *Current Opinion in Structural Biology* **10**, no. 1 (2000).

[218] S. S. MacKinnon, A. Malevanets, and S. J. Wodak. Intertwined Associations in Structures of Homooligomeric Proteins, *Structure* **21**, no. 4 (2013).

[219] S. Otsuka et al. A quantitative map of nuclear pore assembly reveals two distinct mechanisms, *Nature* **613**, no. 7944 (2023).

[220] L. Buetow and D. T. Huang. Structural insights into the catalysis and regulation of E3 ubiquitin ligases, *Nature Reviews Molecular Cell Biology* **17**, no. 10 (2016).

[221] M. C. Miller and K. H. Mayo. Chemokines from a Structural Perspective, *International Journal of Molecular Sciences* **18**, no. 10 (2017).

[222] Y. Liu and D. Eisenberg. 3D domain swapping: As domains continue to swap, *Protein Science* **11**, no. 6 (2002).

[223] F. Rousseau, J. W. H. Schymkowitz, and L. S. Itzhaki. The unfolding story of three-dimensional domain swapping, *Structure* **11**, no. 3 (2003).

[224] Jessica A.O. Rumfeldt et al. Conformational stability and folding mechanisms of dimeric proteins, *Progress in Biophysics and Molecular Biology* **98**, no. 1 (2008).

[225] E. Braselmann, J. L. Chaney, and P. L. Clark. Folding the proteome, *Trends Biochem Sci* **38**, no. 7 (2013).

[226] Francesco Bemporad and Fabrizio Chiti. Protein Misfolded Oligomers: Experimental Approaches, Mechanism of Formation, and Structure-Toxicity Relationships, *Chemistry & Biology* **19**, no. 3 (2012).

[227] J. N. Wells, L. T. Bergendahl, and J. A. Marsh. Co-translational assembly of protein complexes, *Biochemical Society Transactions* **43**, no. 6 (2015).

[228] P. J. Stogios et al. Sequence and structural analysis of BTB domain proteins, *Genome Biology* **6**, no. R82 (2005).

[229] R. Perez-Torrado, D. Yamada, and P. A. Defossez. Born to bind: the BTB protein-protein interaction domain, *Bioessays* **28**, no. 12 (2006).

[230] A. Bonchuk, K. Balagurov, and P. Georgiev. BTB domains: A structural view of evolution, multimerization, and protein-protein interactions, *Bioessays* **45**, no. 2 (2023).

[231] M. J. Bennett, M. P. Schlunegger, and D. Eisenberg. 3d Domain Swapping - a Mechanism for Oligomer Assembly, *Protein Science* **4**, no. 12 (1995).

[232] Elijah L. Mena et al. Structural basis for dimerization quality control, *Nature* **586**, no. 7829 (2020).

[233] E. L. Mena et al. Dimerization quality control ensures neuronal development and survival, *Science* **362** (2018).

[234] Shiyun Cao et al. Recognition of BACH1 quaternary structure degrons by two F-box proteins under oxidative stress, *Cell* **187**, no. 26 (2024).

[235] L. M. Zipper and R. T. Mulcahy. The Keap1 BTB/POZ dimerization function is required to sequester Nrf2 in cytoplasm, *Journal of Biological Chemistry* **277**, no. 39 (2002).

[236] A. Melnick et al. In-depth mutational analysis of the promyelocytic leukemia zinc finger BTB/POZ domain reveals motifs and residues required for biological and transcriptional functions, *Molecular and Cellular Biology* **20**, no. 17 (2000).

[237] E. Chaharbakhshi and J. C. Jemc. Broad-complex, tramtrack, and bric-a-brac (BTB) proteins: Critical regulators of development, *Genesis* **54**, no. 10 (2016).

[238] K. Taguchi and M. Yamamoto. The KeAP1-NRF2 System in Cancer, *Frontiers in Oncology* **7** (2017).

[239] M. C. Jaramillo and D. D. Zhang. The emerging role of the Nrf2-Keap1 signaling pathway in cancer, *Genes & Development* **27**, no. 20 (2013).

[240] A. T. Dinkova-Kostova, W. D. Holtzclaw, and T. W. Kensler. The role of Keap1 in cellular protective responses, *Chemical Research in Toxicology* **18**, no. 12 (2005).

[241] T. Suzuki and M. Yamamoto. Molecular basis of the Keap1-Nrf2 system, *Free Radical Biology and Medicine* **88** (2015).

[242] G. H. Ye et al. The roles of KLHL family members in human cancers, *American Journal of Cancer Research* **12**, no. 11 (2022).

[243] Z. Y. Chen et al. Identification of a PGXPP degron motif in dishevelled and structural basis for its binding to the E3 ligase KLHL12, *Open Biology* **10**, no. 6 (2020).

[244] S. Angers et al. The KLHL12-Cullin-3 ubiquitin ligase negatively regulates the Wnt-β-catenin pathway by targeting Dishevelled for degradation, *Nature Cell Biology* **8**, no. 4 (2006).

[245] J. H. Cho et al. POZ/BTB and AT-hook-containing zinc finger protein 1 (PATZ1) inhibits endothelial cell senescence through a p53 dependent pathway, *Cell Death and Differentiation* **19**, no. 4 (2012).

[246] L. Andersen et al. The Transcription Factor MAZR/PATZ1 Regulates the Development of FOXP3 Regulatory T Cells, *Cell Reports* **29**, no. 13 (2019).

[247] M. Fedele et al. gene has a critical role in the spermatogenesis and testicular tumours, *Journal of Pathology* **215**, no. 1 (2008).

[248] J. R. Ow et al. Patz1 Regulates Embryonic Stem Cell Identity, *Stem Cells and Development* **23**, no. 10 (2014).

[249] S. Piepoli et al. Structural analysis of the PATZ1 BTB domain homodimer, *Acta Crystallographica Section D-Structural Biology* **76** (2020).

[250] A. Cleasby et al. Structure of the BTB Domain of Keap1 and Its Interaction with the Triterpenoid Antagonist CDDO, *Plos One* **9**, no. 6 (2014).

[251] K. Tunyasuvunakool et al. Highly accurate protein structure prediction for the human proteome, *Nature* **596**, no. 7873 (2021).

[252] N. Ito et al. Crystal structure of the Bach1 BTB domain and its regulation of homodimerization, *Genes to Cells* **14**, no. 2 (2009).

[253] P. J. Stogios et al. Insights into Strand Exchange in BTB Domain Dimers from the Crystal Structures of FAZF and Miz1, *Journal of Molecular Biology* **400**, no. 5 (2010).

[254] P. J. Stogios, L. Chen, and G. G. Privé. Crystal structure of the BTB domain from the LRF/ZBTB7 transcriptional regulator, *Protein Science* **16**, no. 2 (2007).

[255] S. R. Adams et al. New biarsenical Ligands and tetracysteine motifs for protein labeling in vitro and in vivo: Synthesis and biological applications, *Journal of the American Chemical Society* **124**, no. 21 (2002).

[256] A. Bateman et al. UniProt: the Universal Protein Knowledgebase in 2023, *Nucleic Acids Research* **51**, no. D1 (2023).

[257] F. Rousseau et al. Three-dimensional domain swapping in p13suc1 occurs in the unfolded state and is controlled by conserved proline residues, *Proceedings of the National Academy of Sciences* **98**, no. 10 (2001).

[258] M. P. Schlunegger, M. J. Bennett, and D. Eisenberg. Oligomer formation by 3D domain swapping: A model for protein assembly and misassembly, *Advances in Protein Chemistry* **50** (1997).

[259] S. C. Yang et al. Domain swapping is a consequence of minimal frustration, *Proceedings of the National Academy of Sciences* **101**, no. 38 (2004).

[260] M. J. Bennett, S. Choe, and D. Eisenberg. Domain Swapping - Entangling Alliances between Proteins, *Proceedings of the National Academy of Sciences* **91**, no. 8 (1994).

[261] M. J. Bennett, M. R. Sawaya, and D. Eisenberg. Deposition diseases and 3D domain swapping, *Structure* **14**, no. 5 (2006).

[262] S. Barakat et al. Dimerization choice and alternative functions of ZBTB transcription factors, *FEBS Journal* **291**, no. 2 (2024).

[263] S. Meydan and N. R. Guydosh. Disome and Trisome Profiling Reveal Genome-wide Targets of Ribosome Quality Control, *Molecular Cell* **79**, no. 4 (2020).

[264] T. Zhao et al. Disome-seq reveals widespread ribosome collisions that promote cotranslational protein folding, *Genome Biology* **22**, no. 1 (2021).

[265] C. A. Waudby, C. M. Dobson, and J. Christodoulou. Nature and Regulation of Protein Folding on the Ribosome, *Trends in Biochemical Sciences* **44**, no. 11 (2019).

[266] N. V. Dokholyan et al. Topological determinants of protein folding, *Proceedings of the National Academy of Science* **99**, no. 13 (2002).

[267] J. Wang and E. Panagiotou. The protein folding rate and the geometry and topology of the native state, *Scientific Reports* **12**, no. 1 (2022).

[268] N. Rajasekaran and C. M. Kaiser. Navigating the complexities of multi-domain protein folding, *Current Opinion in Structural Biology* **86** (2024).

[269] M. A. Collart and B. Weiss. Ribosome pausing, a dangerous necessity for co-translational events, *Nucleic Acids Research* **48**, no. 3 (2020).

[270] Zev Bryant et al. Structural transitions and elasticity from torque measurements on DNA, *Nature* **424**, no. 6946 (2003).

[271] Benedikt Goretzki et al. Dual BACH1 regulation by complementary SCF-type E3 ligases, *Cell* **187**, no. 26 (2024).

[272] Francis C. Peterson et al. Structure of the SCAN Domain from the Tumor Suppressor protein MZF1, *Journal of Molecular Biology* **363**, no. 1 (2006).

[273] Martine A Collart and Benjamin Weiss. Ribosome pausing, a dangerous necessity for co-translational events, *Nucleic Acids Research* **48**, no. 3 (2019).

[274] Katarzyna Chyżyńska et al. Deep conservation of ribosome stall sites across RNA processing genes, *NAR Genomics and Bioinformatics* **3**, no. 2 (2021).

LIST OF PUBLICATIONS

RELATED TO THIS THESIS

- F. Wruck, M.J. Avellaneda, M.M. Naqvi, E.J. Koers, **K. Till**, L. Gross, F. Moayed, A. Roland, L.W.H.J. Heling, A. Mashaghi, S.J. Tans, *Chapter 11: Probing Single Chaperone Substrates* in Biophysics of Molecular Chaperones: Function, Mechanisms and Client Protein Interactions, ed. S. Hiller, M. Liu, and L. He, Royal Society of Chemistry **29**, (2023). **(Chapter 2)**

- **K. Till**, AB. Seinen, F. Wruck, V. Sunderlikova, C.V. Galmozzi, A. Katranidis, B. Bukau, G. Kramer, S.J. Tans, *Trigger factor accelerates nascent chain compaction and folding*, PNAS **122**, (2025). **(Chapter 3)**

- F. Wruck, J. Schmitt*, **K. Till***, K. Fenzl*, M. Bertolini*, F. Tippmann, A. Katranidis, B. Bukau, G. Kramer, S.J. Tans, *Co-translational ribosome pairing enables native assembly of misfolding-prone subunits*, Nature Communications **16**, (2025). **(Chapter 4)**

- **K. Till**, V. Sunderlikova, P. Jevtić, F. Tippmann, M. Bertolini, K. Fenzl, J. Schmitt, A. Katranidis, B. Bukau, G. Kramer, M. Rapé, S.J. Tans, *Translation-driven temporal control for intertwined protein assembly*, manuscipt under review. **(Chapter 5)**

OTHER PUBLICATIONS

- C.V. Galmozzi, F. Tippmann, F. Wruck, J.J. Auburger, I. Kats, M. Guennigmann, **K. Till**, E.P. O'Brien, S.J. Tans, G. Kramer, B. Bukau, *Proteome-wide determinants of co-translational chaperone binding in bacteria*, Nature Communications **16**, (2025).

- A. Mashaghi, F. Moayed, E.J. Koers, Y. Zheng, **K. Till**, G. Kramer, M.P. Mayer, S.J. Tans, *Direct observation of Hsp90-induced compaction in a protein chain*, Cell Reports **41**, (2022).

- A. Ahmadi, **K. Till**, P.H. Backe, P. Blicher, R. Diekmann, M. Schüttpelz, K. Glette, J. Tørresen, M. Bjørås, A.D. Rowe, B. Dalhus, *Non-flipping DNA glycosylase AlkD scans DNA without formation of a stable interrogation complex*, Communications Biology **4**, (2021).

- A. Ahmadi, **K. Till**, Y. Hafting, M. Schüttpelz, M. Bjørås, K. Glette, J. Tørresen, A.D. Rowe, B. Dalhus, *Additive manufacturing of laminar flow cells for single-molecule experiments*, Scientific Reports **9**, (2019).

- R. Diekmann, **K. Till**, M. Müller, M. Simonis, M. Schüttpelz, T. Huser, *Characterization of an industry-grade CMOS camera well suited for single molecule localization microscopy – high performance super-resolution at low cost*, Scientific Reports **7**, (2017).

* These authors contributed equally

ACKNOWLEDGMENTS

I applied to this PhD position because it aligned closely with my master's research. However, I actually had aimed to escape the tediousness of single-molecule experiments and work on a project related to cancer research. Still, I got the chance for an interview. In the end, it was Amsterdam and the modernity of the AMOLF building, standing in striking contrast to the brutalist concrete "spaceship" of Bielefeld University, often ranked among the ugliest in Germany, that convinced me to give it a try after all. The interview went well, and I received an offer, but I couldn't quite let go of my desire to work in the field of cancer research. I told Sander, as I felt I could be honest with him. We had another chat. We talked about the exciting things I could do in his lab, but in the end, I made my decision not based on the projects but on the people; a decision I could not be happier to have made. Thus, this acknowledgment section is close to my heart and probably, like most of the things I write, far too long.

Having encountered a variety of supervisor types, **Sander** definitely stood out to me. He spoke about his research with a mix of big-picture thinking and realism, which is not always easy to find. He was straightforward and didn't get lost in impossible possibilities. Knowing my challenges, I knew I needed a supervisor with a vision but also with a practical outlook, someone who knew how to guide but also how to trust. Sensing that he could indeed be that person, I felt comfortable being trusting and honest with him from the start. This second chat we had enabled us to build a relationship based on trust and honesty from the beginning, and it became the cornerstone of everything that followed. Being the great, experienced scientist he is, it is no surprise that he always managed to help in difficult phases of research. More importantly for me, he could also lift my mood when I fell into states of despair about my progress. Feeling unafraid to share even the personal side of my struggles and lows, I knew he could always pull me up again. He could calm me with words of perspective and make me laugh by slightly ridiculing the situation and my concerns. Without this, I would have managed far worse. Even though I felt we were a good match from the start, the years of getting to know each other showed me an even deeper layer of like-mindedness, which I think helped us truly understand and see each other despite our necessary differences. Understanding each other and ourselves often made us laugh about our respective obstinacies. Sander coined the term "Kathi Style" to describe my precision-driven, complicated, lengthy ways of going about things, in contrast to his sharp, to-the-point style. In the end, though, we benefited from this and were always able to combine both of our inputs to create something better. Over time, our meetings became more than just an appointment in my calendar. Beyond science, I loved hearing about his opinions and personal life insights, and I always enjoyed bouncing observations about all sorts of matters. Dear Sander, you were able to understand me and helped me overcome many difficulties, both internal and external. You taught me science, but you also taught me to trust in myself as I trusted in you to trust in me, which ultimately enabled me to finish this PhD. For this, and for all the time we shared, I am deeply thankful and appreciative!

It wasn't Sander alone, though, who made me accept this position in the end. During my interview, I also had chats with Florian and Anne-Bart, the post-doc duo in our lab, who, at first glance, could not be more opposite from each other, yet were somehow also best friends. The relaxed, cheerful, reassuring Florian was offset by the unhinged, direct, teasing Anne-Bart. Still, I concluded that both would be great teachers and a support during my PhD journey. So it was, **Anne-Bart** you were the first to show me the lab protocols and experiments, and I ended up taking over the project you had started and shaped, which is now my Chapter 3 in this thesis. Thank you so much for trusting me and handing it over to me! I liked that you were very precise in the lab and analysis, as I like to be precise myself as well. Beyond the jokes and teasing, I could also see your more serious side and sense more similarities beyond being meticulous. I could not have wished for another person to have started my lab days with. It was sad you left two months after I started. Luckily, **Florian** took over guiding me. You became the person who, not only for me but also for many other members in the lab, rescued many situations and was always there to offer advice. Me, being often slightly overconcerned, needed your calmness, which always reassured me. You are tremendously knowledgeable, which allowed me to learn a lot; you are curious, which made me try new experiments; and you are caring, which never let me feel alone. You were reachable every hour of the day and night and always quick to respond and help, perhaps something that shouldn't be for your sake, but I appreciated it greatly. I took on your Lamin project during revision, which is now my Chapter 4 in this thesis, and I am very thankful for it. I consider myself very lucky to have had the chance to work with you, and beyond that, to share exciting steps in your life like your wedding! I value you a lot!

The next person without whom this PhD truly would not have been possible is **Vanda**. There is no exaggeration in saying that Chapter 5 would not have happened without her. Sometimes I feel this project caused you even more sleepless nights than me, which I still feel sorry about. But it just goes to show how deeply caring and supportive you are. I can often get stuck, but your energy always helped me to try more and continue. I don't even want to count the many samples you prepared for me, but all of them kept me going, which is one of the most important steps, a total win in that regard. Despite facing your own personal hardships, you were by my side the whole time and supported me from the start. You cheered for me not only throughout this long run of a PhD, but even when I actually did a long run during the Amsterdam half marathon. I will forever cheer for you as well, because you are not only a gift to the lab but to life in general. One cannot wish for a better partner in crime (or suffering).

A special thanks also to our collaborators from the ZMBH in Heidelberg, as without them and their research, the papers presented in this thesis would not exist in their current form. Thank you, **Bernd, Günter, Jaro, Frank, Mati and Kai**! You were always just a quick e-mail away, ready to help and advice. I greatly appreciated working with you and loved the times we got to meet.

Of course, the rest of my group at AMOLF also helped and supported me tremendously throughout my PhD years. Close in sharing work, and thus also in under-

standing the connected struggles, is another iconic duo: Jack and Dhawal. Again, quite differently nuanced, both of you equally made tweezer lab life so much more doable and fun. **Jack**, you joined us for your master's thesis research project and luckily decided to stay for a PhD. Over the course of an afternoon where we both took joy in having made a fresh batch of nicely labelled buffers, I knew I had found a companion in taking enjoyment from having things in order and in our own system. But you were so much more than my ideal, clean, lab-bench neighbour. Just through the exchange of glances, I could see that we often felt similarly in certain situations. Having this underlying connection, it was always easy to also talk things through with you. I appreciated you checking in on me by coming to my office and saying, "I felt we haven't talked in a while and I wanted to see how you are," which goes to show your kind-hearted nature and genuine care for the people around you. Even though, by age and PhD stage, I should have been checking in with you, I often felt I could also lean on you. Not only in the cases where your empathy and understanding shone, but also in work-related questions. Your thorough way of working made you a person whose opinion I valued and whose insights I trusted. Preserve your drive and inner being and you'll reach every goal you set. **Dhawal**, you might be more different from me, but that made you all the more a support I needed. Your busy life makes one often wonder how you manage to keep up with all of it, but even more, how you still manage to be there for someone when needed most. You saw when I was struggling, always cheered me on, and gave me plenty of pep talks whenever I really needed them. Your proactive nature to take things into your own hands and keep going, not only for your own path but also for the people around you, is a true inspiration! You easily create a home for so many people who have left their original home. You are able to do this because you have been through so many different phases of your life as well and know how it can feel. You once told me the story about the Indian festival that celebrates the bond between brothers and sisters and that I felt like a sister to you. Then it clicked for me: You and Jack are exactly that, my brothers of this period of my life, people to lean on and who are there for you without hesitation or doubt whenever you need them the most. Thanks to you two, I could get a glimpse outside of my only-child worldview and experience a little of what it means to have supportive siblings by your side. You've already achieved so much, and your passion will take you even further. Never stop connecting people, it's one of your greatest gifts. Antoine, Luca, Bibi, Yifei and Marija also have shared the tweezer/single-molecule research experience with me. **Antoine**, even though you were convinced that your jokes are funnier in French, you still made me laugh constantly in English. You are a deeply individualistic thinker, and I loved hearing about your passion for Streamlit, which type of political system would work best for society, how you were close to solving problems in cosmology with your own formula, and of course our mutual love for cats. I missed you when you left, but I admired your courage in making that choice, and I hope it brought you closer to the happiness you seek. Never let your mind stop exploring what few people think about. It is your sparkle, and you will always shine brightly if you keep following the things you are fascinated by. **Luca**, starting just two months before me, we had parallel PhD paths. Your

directness is very different from my own approach, but I often looked to you as a reminder to be bolder. I'm sure the next steps you take will suit you well. To the newcomers: **Bibi, Yifei, Marija and Anna**, it was fun to meet you and spend the time together we had, and I hope you keep enjoying research.
Outside the single-molecule side of our group, there is also the organoid team, less connected research-wise but equally a source of support, joy, and advice in my life. **Max**, I find it almost like a self-fulfilling prophecy that you came up with a research project on pattern recognition, because patterns always felt like something that connected us as well. Our conversations would often circle around exploring and extrapolating our observations into something bigger. I would often ask how you would go about classifying this or that, and you would always deliver, sometimes with a slightly unhinged opinion, which made it all the more fun and insightful. Your curiosity and open-mindedness always made me feel at ease to share the latest edition of my convoluted mind wanderings, as I also felt that we both share a similar liking for oddities and a kind of shared intuition about many things. Thus, I loved getting to know your point of view, whether it was during lunch, coffee, or our late-night cycle rides back home. Even when we weren't talking, simply seeing the light in your office and hearing you hum was comforting, especially during all those late nights we pulled, it never made them feel lonely. I'm sure you'll continue exploring and discovering fascinating new patterns wherever you set your mind, building a great future for your research. And I hope we'll keep doing the same together, unraveling all sorts of patterns and themes in the future! **Kasper**, beyond teaching me about the importance of statistics, you enlightened me in so many other ways. During our long dinners together late at AMOLF, where I faced your judgment and pity for my poor dinner choices, I loved getting to know your perspectives on all sorts of matters. We often had different viewpoints, but precisely that made our conversations great, and we both had fun disassembling each other's thought patterns. Behind your statements, I could always find a reason for why you were thinking that way, often backed up by your tremendous amount of reading. This also always made me believe your uplifting words when I was rummaging through my concerns, as I knew you would not say things without reason. In the end, I think we share the same sort of joy in seeking connections and building up mind palaces of our own unique interests, you just do it, for example, for long-dead presidents of the USA, and I for long-dead Bavarian kings. Thus, it was always a pleasure to step into your inner world and marvel at its detailed interior webbing. All this not only made you a great colleague and friend, but will also make for a great future for you as a father and in the job market. I have no doubt! **Pascal**, lunch table discussions with you were always more fun. I always liked hearing your opinions on all sorts of subjects and found your viewpoint always something I could relate to. You are not afraid to speak your own mind, but more so, I like that you are able to do this with a gentle attitude and humour. Thanks also for letting me experience a bit more of Swiss culture with home-brought cheese fondue. We now share the same situation of pondering the next career steps, but I am sure you will find something nice!
Thanks also to all the other members of my lab, former and present. **Kim**, I felt

we only really started to connect when your master's thesis research was almost over, something I do regret a bit. Thus, I am all the happier we still got to connect in the end, as it is rare to encounter someone as supportive as you are. All your encouragements come from pure honesty, which is why they felt so great. Your positivity is a bright light in many people's lives, and I am sure it will also show you your path. Keep being eager to explore! **Rutger, Jasper, Nebojsa and Susi**, I value you, your insights, and your life experience stories a lot. You all completed our group in your own unique way, and I am happy to have shared some time together with all of you.
Beside the people in my workgroup, I was more than blessed to be surrounded by other truly amazing and inspirational people, who made my time in Amsterdam one of the best phases of my life. Through being with them, I could experience myself fully and freely, something you cannot do with just anyone and which is the true key to finding happiness. Thus, while not directly work-related, those connections allowed me to be in a healthy state of mind, which is also one of the most important things to have while doing a PhD.
Evan, you came into my life as a mystery. For quite a while, I only knew your name as it was put onto our office name tag long before you arrived at AMOLF, so I pondered who that person with this cool name could be. When you then finally arrived and we started to share an office, I quickly realized that not only your name was cool, but that in fact I had won the main prize of the mystery box! You stepped into my life when I was going through a bit of a rougher patch in my PhD trajectory, but you were able to brighten it so much. With your presence in my life, a new chapter unveiled, the beginning of a friendship excelling in mutual comfort and support. I learned so much from you through our conversations. You introduced me to so many new things, from communist cinema groups to alternative ways of living (and the vocabulary that comes with them). You always ask the right questions, which make me think deeper and reconsider, something I love. When I am with you, I feel grounded, a testament to how safe I feel in our relationship, which also allows me to show my weirdest parts, including sharing my obsessions, something I deeply cherish, as I find it is very rare to receive such unconditional acceptance. Who would have thought that a person almost ten years younger than me could be such a guiding star? You'll always shine brightly in my firmament. Let us forever be a place to feel at home. Thus, for all of it, I am more than glad to have you also be my paranymph. Thank you! You are so aware of our world and its people; I am sure your future path will guide you somewhere amazing, just as you are!
Next in my mental backup system are the members of the *Tiefenpsychologischer Kreis*, Chris and Manuel. This group of the three of us quickly became much more impactful than its initial intent to escape the bland Dutch lunch repetitiveness. We created a space where we could share, and it needed both of you and your perspectives to open a new world for me, one where I learned that being not okay is okay, but also how to cherish and celebrate the little moments in life. **Chris**, when I'm with you, my inner world stops spinning at full speed. You radiate a calmness that goes far deeper than a first impression might suggest. I think it's your broad

perspective, your ability to see the many facets of what drives people, combined with your understanding and tolerance, that gives you a special inner peace one can sense immediately from the outside. You have a gift for asking the right questions at the right moments, opening new viewpoints for others without ever forcing them. I've benefited from this many times myself, and I truly admire that skill. It reveals both your inner radar for emotions and your deeply empathetic side. You meet life's experiences and emotions with curiosity and openness, something I find both inspiring and reassuring, encouraging me to express myself. You've shown me that it's not always about control, as I like to have it; sometimes, you simply need to let go a little. That's why you're able to slow me down so well. I also cherish your humour, which can skilfully highlight the absurdity of certain mental spirals, turning them into something to laugh about rather than stress over. For all of this, I'm deeply grateful to have you at my side, also as a paranymph. Thank you! Your adventurous spirit, in exploring both the inner and outer worlds, will carry you to many more extraordinary experiences and places, I'm sure. The other third of our special trio is **Manuel**. With you, I feel I can achieve anything, not only because of your open-mindedness and curiosity to embrace life in all its opportunities, but also because you are one of the most dependable people I know. This is deeply special to me, as I'm usually not someone who likes to hand things over. Yet with you, I have complete trust that whatever I entrust to you will be handled with care and competence. Perhaps this trust comes from your rare ability to improvise and find quick solutions. I have watched you navigate tricky situations with efficiency and calm, staying cool where I would have become a nervous wreck. You're there finishing movies when my eyes can no longer stay open, and you're equally there for everything else I might need. With you, I always knew I had someone close by who would truly listen to my concerns and look out for me, texting me with thoughts about situations we had discussed long before. A testament to how deeply you care for the people in your life. I've always valued your inputs. Your drive to keep growing and exploring, while staying deeply connected to those around you, will surely lead you to many more incredible experiences. Manuel and Chris, you have brought a different kind of light into my life, I have learnt so much from both of you, and I am endlessly thankful for all our shared time. I hope we will always hold on to our special connection, one built on so much mutual support.

Then there are the women in my life, all of whom I couldn't be prouder of, and I am so happy to have them close to me with all their amazing energy. One of the first connections I made at AMOLF was with **Xuan**, who was also in Sander's group but became so much more than a colleague to me. As the only other female PhD student in Sander's group, I sought to connect with her from the start, and luckily for me, that worked out even better than anticipated. From dumpling-making, flat renovations, cinema visits, yearly Muiden trips, and you coming to my hometown to explore German Christmas markets, to our shared love for cute cafés and matcha, we have experienced so many things together. Even though we are a great team to explore the real world together, I found even more of a companion in you to also explore the inner world of our minds, thoughts, and worries. Your observational skills, empathy, and emotional intelligence always made it super easy to share any-

thing with you, as you would understand so easily. Beyond understanding, your calm encouragements always gave me trust and a positive outlook again. Next to your gentle, kind-hearted nature, there is also a deep drive for equality within you. You are very sensitive to detecting unfairness and speaking up about it, which is maybe also why you are so skilled at giving perspective. You are not someone who simply follows; instead, you analyse situations, reflect, and then carve your own path, often also by immersing yourself in little adventures sparked by your newest interests. This shows not only your determination but also your open-mindedness. This is why I have a deep trust that wherever your path will lead you, it will be a great one! I hope I can keep your energy forever in my life, as it feels like an endless blanket of comfort, and that we will keep learning about the world and its people together. Up next in my timeline of connecting to awesome power women in my life is **Mareike**. From inviting newly-arrived-in-Amsterdam me to Christmas cookie baking during COVID, to guiding me through the final phase of my PhD, you have been a constant source of positivity, energy, and support. Through your drive to experience life to the fullest, I discovered a way of living I never imagined possible, one built on sharing, growing stronger together, and truly embracing each moment. You are a true genius when it comes to connecting people (and staying connected!), something which made Amsterdam a home away from home. You were the cornerstone of the amazing friendship group we built, and I cannot even describe how hugely grateful I am to be a part of it and how much it has given me. I admire how much you intuitively know what you want and how you don't stop fighting for it, even if it's hard, until it feels right. You also have a huge drive for fairness and justice, which inspires me not to settle for less. But you don't just fight for your own rights; you care deeply for the people around you, often advocating for them even more strongly than for yourself. For you, there is no "alone," only "together". It's a rare and pure kind of support, one I will never take for granted. I hope to always keep your passionate fire in my life, as it can brighten even the darkest places and remind me of the true essentials of happiness, filling life with meaning and purpose. Then my partner in crime, **Lori**. I don't remember how we went from barely greeting each other to having hour-long conversations in the dark tweezer room, turning any lengthy experiment into something enjoyable. As I got to know you, I realized how often we see and feel things in a similar way. That made sharing anything with you feel special, I often felt deeply understood. We navigated tough moments side by side, yet your wit could just as easily make us laugh a ton. You were an incredible source of support, especially during the final phase of my PhD. Your cheers made moving forward so much easier. I am deeply grateful for that. Your energy and passion have also been a constant inspiration, they're truly contagious. I loved when you came to me with your latest ideas or showed me the things you'd created with your inventive mind and skilled hands. I often found myself marvelling at your design choices. Some of my most memorable moments also happened with you, if in Amsterdam (nightlife) or even on Texel. You always find the coolest events and things to do. Thank you for letting me be part of your rich world, which you shape so purposefully, where everything carries meaning. That same intentionality makes you a driven person. I've always

admired your ability to push through challenges, and it has inspired me to do the same. I'm sure you'll achieve any dream you set your mind to, even if it takes time for things to take shape in just the right way. I hope we continue to inspire and support each other through whatever life brings next. Then there are Lucie and Laura. We connected a little later, but both of you left an equally big impact on me. **Lucie**, you are like the sun, a guiding star. Your bright smile radiates positivity, instantly lifting the spirits of everyone around you. But you also see beneath the surface, recognizing the complexity behind things, and you have a natural compass for right and wrong. Your ability to notice every nuance means you never simply agree or disagree, which makes hearing your opinions such a joy. This wisdom stems from your many life-shaping experiences, which have also given you a deep understanding of yourself. I have rarely met anyone who knows themselves as well as you do, and I have always admired how this makes you so self-assured, aware of your boundaries, and therefore incredibly strong. All of this together allows you to offer perspective while also instilling a quiet trust that things will be all right, something that has always done me so much good. And this is exactly how you live your life: you fight for the things you hold dear, yet you have also learned to trust the process. That is why I am convinced all your dreams will come true, as many already have. You will always remain a true inspiration to me, and I hope to keep your nourishing, bright energy in my life. I will anyway follow you wherever you may siren me. **Laura**, you are like the moon, shining bright in a calm night. I have always liked the night for its comfort and tranquillity, and this is somehow also how I feel around you. Your heart is as big as the night sky. You are incredibly strong, as I see you carry a lot and still always have others' well-being in mind first. Drinking tea and eating chocolate with you was always a powerful fix for a lot of things. I truly appreciate having you there as a pole I know I can always return to comfortably.

My experience at AMOLF and during my PhD would not have been the same without a few other remarkable people as well. The first person I truly connected to, as we also started our PhD journey only two weeks apart, was **Timo**. Amid the cycle of going in and out of lockdowns during COVID, a time when connecting with people felt especially difficult, you were the one who made that challenging phase so much easier as I felt I had gained a connection I cherished right from the start. You are a naturally cheerful person who always looks out for those you care about, sometimes so much that I think you forget yourself. Your positivity never failed to make me smile, and you were such a steady source of support, always noticing when I needed to be cheered up. Your heart feels as vast as the meadows and forests you love to explore, another quality of yours that inspires me. I can easily get stuck in my own head, but your love for cooking and for exploring nature often brought me back to the present, reminding me how important it is to truly experience each moment and to enjoy the world with all our senses. Of course, getting to eat your cooking will always remain one of my favourite ways to indulge in life. Beyond telling me about your weekend excursions, our conversations would also often drift into more philosophical topics. During lunch, we would discuss books you had read (by the way, you gave me some of the best books I have read in recent years) or

something you had picked up on a podcast. I loved that you always had your own opinion, making for some interesting discussions. Anyone would be lucky to have you in their life, and I hope you will always remain part of mine. **Yorick**, we shared the same office corridor, and that was such a joy, especially during late hours when you and I would do long experimental shifts. We would visit each other's offices and chat, making empty AMOLF feel not empty at all. We explored the Netherlands through Google Maps and your bike routes, which easily span the whole country and beyond. Your laugh was always something that made me feel positive again. **Imme**, I remember meeting you first online during a PhD start-up course. I was impressed by how reassured you seemed. Over the years, I got to know you much more in person. When you are fascinated by something, you radiate a contagious energy, always prompting me to explore and ponder with you the themes you were curious about. There was always something about how open and honest you were in expressing your feelings and opinions, which I appreciated a lot. Every encounter we had was a happy moment for me, even when topics were not as cheerful, which made me feel even more connected to you though. **Bernat**, our office became more complete with you. Even though it took a little time, I was so glad we finally managed to connect in such a way that it always cheered me to see you and talk to you. In a way, you are the most chill person I know. You always keep a positive outlook and trust that things will turn out all right, an energy which helped me a lot in the end phase of my PhD. Your honest concern for me was also something I appreciated greatly, especially when I was scheduled to be kicked out of the office. Now every time I see you, I love catching up with you, and I love that we keep sharing and caring, which I hope will stay like this. **Wessel**, I knew our brains were set up in a very similar way when we became philosophical about the question "How are you?", a question we had exchanged on a random weekend when we both happened to be at AMOLF during the corona time. You listen in a very special way, a way which reminds me of myself, and so we unveiled over time so many similarities in thinking and feeling that, even despite sensing our like-mindedness, I was still always a bit surprised by how much we could relate. I am proud of both of us for facing some of our inner demons and pushing for a happier and freer state of being. We both got this, I know it! **Bob**, simply running into you in the AMOLF corridors or having a blast at all the AMOLF events together will be something I miss. From first meeting randomly while I was overfilling my water bottle in the canteen, to me and Imme peeling off the wallpaper in your flat, or to us designing your glass throne on top of AMOLF for your reign, we would always laugh together. Our contact was always light-hearted and would often lift my moods. Your mindset on how you imagine your life is quite determined, which was also somehow calming to me, having always too many options in my mind. **Alex**, you became a source of true reliability to me. During the shooting of Mareike's defence movie, where you had bought special microphone equipment to improve the quality, I became aware of how much thought you put into almost anything. Thus, I loved discussing with you all sorts of matters, as you never fail to surprise me with your own opinions, formed from thoroughly thinking things through and researching. You are also eager to experience and explore, which always made you a great companion in many

of our adventures, adventures I hope we will share more of in the future together! **Chi**, you were always such a positive spirit ever since you joined for your master's thesis research. You always showed a deep care not only for your research projects, but even more for the people around you. When I was talking to you, I always felt you genuinely wanted to know how one was doing, which made our encounters a joy. Your gentle nature is accompanied by strong stamina. You overcame many hurdles in tricky projects already, and I know you will manage everything in the end, as you are a person who will keep fighting. **Fotis**, we shared so many late lab hours together that I knew without turning who was entering the lab late at night behind me. It would probably have been better for both of us to pull fewer long nights and weekend shifts, but it was also always a source of comfort for me knowing you were there as well. Even though you now live across the Atlantic, I still get reminded of you quite often through architecture reels we both seem to like. Who would have thought brutalism could connect in such a way? Maxime and Lucas, I met you both through your incredible partners, thus it is no surprise that you also became people I always looked forward to meeting again. **Maxime**, you have a very special way of going about things, shaped by your unique viewpoints. I love getting to know your perspectives, as there is always something interesting to uncover behind how and why you go about things in a certain way. You have also been an incredible support, encouraging me and listening to how I was doing. You always conveyed a deep trust that things would turn out alright for me, leaving no space for doubt, which I deeply appreciate. **Lucas**, you equally have a unique drive within you, which also comes through in your humour. You can untangle the oddities in life and present them in a way that never failed to make me laugh. Whether singing Hare Krishna mantras or trying your homemade beer and kimchi, I always enjoyed hanging out with you. Of course, there are many other people I was very fortunate to meet, but I cannot keep writing at such lengths. Thus, **Anne-Sophie, Tamara, Burak, Colin, Age, Daan, Nick, Falco, Ananya, Parisa, Antony, Lukas, Nassim** and the many others I might have missed to name here: feel equally valued for all the moments I was able to spend with you and the nice chats we had.

I also want to acknowledge some people from my past science life at Bielefeld University, as without them I would likely not be writing this acknowledgment section to begin with. **Mark Schüttpelz**, you were my bachelor and master's thesis supervisor and the first to support my scientific journey. And you allowed it to be a true journey; in the best way possible. Thanks to you, I was able to experience what interdisciplinary research meant by enabling me to travel throughout Europe and meet so many amazing scientists from different disciplines. I went to Madrid, to Oslo (even three times), and attended conferences just because of you, who fought to finance all those experiences for me. This showed me a different side to science, which I very much enjoyed, next to the sometimes quite challenging lab days. You truly shaped my view of the research world, and I will be forever grateful and will never forget your part in my journey! Then, of course, there are Robin Diekmann and Arash Ahmadi, the best daily supervisors one could hope for. **Robin**, I most vividly remember your smile and your "why not try" approach, both crucial for

my scientific development. Research is about trying, failing, and trying again; not losing hope; and still having fun along the way. This I learned through you. You were a safe haven for my anxiety and could calm the inner storm of all my doubts just with your positivity and vast knowledge. Your support even extended to my PhD applications. If I ever were to call somebody a mentor in my life, it would be you. **Arash**, my master's thesis exists thanks to you. We shared lab days longer than 12 hours, which never felt that long with you. You showed me true persistence and the attitude to keep trying until things finally worked out, despite being in the dark or in background noise most of the time. Going through one of the toughest PhDs I know of, you managed to pull through equally tough. You were so inspiring to me. And I still have fun thinking about all the things we discussed beyond science. I deeply value our shared time together, and you will forever be a bright light in my memories. Of course, **Anders, Tung-Cheng, Alice, and Stephan** were all essential parts of my early science and D3 experience, experiences I would not want to miss! Thank you for being there for me, encouraging and supporting me.

Next to that are, of course, the people I have shared my studies with, who made studying physics not only tough but also a fun experience. The many hours in the Diskoflur, lunches, and parties are something I like to look back on. Without you, I would not have managed, especially when it came to all those exercise sheets and tutorials. Thus, thank you **Alex, Bernhard, Christoph, Luise, Luis, Fabian, Timo, Björn, Nadine, Tobi, and Tillmann**. Many of you kept in contact, and it was always nice to meet up again. You are the kind of friends one can return to after months or even years and still feel as if no time has passed, despite all the changes we've gone through. The ones I've remained closest to, and whom I especially want to thank for their continued support long after our studies ended, are Steffen, Marius, and Dominik. **Steffen**, your Amsterdam visits will stay among the moments I'll keep cherishing, but even more I'll cherish your continued understanding of all my worries and concerns connected to the tough parts of science and life in general, as you could often connect to them through your own experiences. Having a friend like you, someone who matches my obsession with drinking tea and exploring Japanese culture, while also being someone I can lean on is deeply precious. I hope we will keep sharing life, whether through meetups, hour-long phone calls, or sending parcels. Dominik and Marius, soon after I left for Amsterdam we started celebrating New Year's Eve together, a tradition we have not broken since 2020. **Dominik**, you literally helped me set foot in Amsterdam by joining the moving van drive and unloading all my life stored in boxes into my new flat. I learned how much you are a person one can rely on. I am sure you would be there for me whenever I need you, something I truly appreciate about you. **Marius**, we both shared the experience of doing a PhD abroad, and I saw how it impacted us both equally. Thus, I would often feel understood by you. You also never fail to make me laugh with your unique sense of humour, which relies on being able to see beneath the surface, whether of people or politics. Non-study-related but equally profound in his support and meaning in my life is **Tim**. We started connecting over having a blast together while going out and drinking tea in our little pre-Christmas

get-together tradition. Over the years, I learned to appreciate that we not only always have a great and fun time together, but that we're also able to have deep conversations about all sorts of life decisions. Your insights have always guided me on. You can effortlessly make me laugh but also make me feel loved and cared for, something so natural to you, which I have always admired and appreciated. Thus, I look more than forward to all our future adventures and conversations.
Finally, there are the few people who have been at my side the longest and are secured deeply in my heart and soul, and I will never let them go. **Helen**, my love, our relationship is the longest non-blood-related one I have. From nodding at me with a cheerful smile during physics class presentations to consoling me whilst I cried on your floor over the again failed university exam, you were always there for me and one of the best supporters throughout my life. You match my inner freak like no one else, which allows you to see straight through me, to recognize all of me, including the weirdest corners. Thus, you always gave me the best advice for all my life decisions, which is also a testament to your deep insightfulness in general. You inspire me to dream big and to actually make those dreams a reality, just as you did when you moved to New York for your studies or started your own perfume business. I'm endlessly grateful to have you in my life; you've taught me to trust in true friendship again. Being each other's constant and weathering so many changes together, I'm certain we're set to never leave each other's sides. **Julia** is next in line. From classmates to PhDs, our lives have been deeply intertwined. There are few people with whom I can experience life as fully as I do with you, proof of how true to myself I feel in your presence. With you, I am in the here and now, not lost somewhere in the "there and nowhere". Thus, all our little travels, which I cherish deeply, always brought me back into the right frame of mind. You never lose your smile, and you are a true inspiration to me, overcoming so many challenges in your life. And what a life you have lived so far, one of the most adventurous ones I know of. Your inner motor to keep exploring and learning motivates me to keep going as well. Your calm positivity would often lighten up my days and your insights always put everything into perspective. Tied by our deep connection, I am sure we will keep learning and exploring together for the rest of our lives. Talking to either of you has always made everything instantly better. How lucky am I to share life with you both! Und natürlich, **Mirko**! Wir haben nun schon fast ein Drittel unseres Lebens so eng miteinander verbracht, dass ich mir keinen zukünftigen Moment mehr ohne dich vorstellen kann. Du bist wahrlich das i-Tüpfelchen auf all den süßen Erfahrungen, die das Leben zu bieten hat, und das Licht in meinen dunkelsten Momenten. Auch nach all den Jahren des Zusammenseins sind es immer noch deine Meinungen und Ansichten, die ich als erstes suche. Du schenkst mir neue Perspektiven und bringst mich zum Lachen wie kein anderer. Du bist das Schiff, das mich durch so viele Stürme getragen hat. Du kannst mich lesen ohne Worte zu benötigen und allein deine Präsenz schenkt mir den Raum völlig frei zu sein. Neben deiner Hilfe bei meinen unzähligen „for"- und „while"-Loops bedeutet mir deine Unterstützung in allem die Welt. Oft mag ich es kaum begreifen, welch großes Glück ich genieße, durch dich so viel Stabilität zu finden, besonders in einer Welt voller flüchtiger Augenblicke, eines der kostbarsten Geschenke meines Lebens. An

deiner Seite fühle ich mich gewappnet für den unvorhersehbaren Strom des Lebens. Danke, dass ich durch dich auch deine tolle Familie in meinem Leben wissen kann, besonders **Simone**. Du bist ein Ruhepol der Geborgenheit für mich. Über deine Fürsorge und Anteilnahme kann ich mich nicht genug freuen, sowie über jeden Moment mit dir!
Zum Schluss möchte ich meinen Eltern danken, den Unterstützern von meiner ersten Stunde an. Ohne euch wäre ich nicht an dem Punkt, an welchem ich jetzt bin, denn ihr beide habt mir die Neugierde an der Welt beigebracht. **Papa**, durch dich habe ich die Welt der Bücher entdeckt und die Begeisterung an der Erkundung von Zusammenhängen. Du siehst vieles in seiner Vielschichtigkeit und inspirierst mich, weiter zu lernen, so wie du es auch tust. Wir können ernste Gespräche haben, aber auch total oft zusammen lachen, ob nun dir oder mir das Ei vom Löffel fällt. Deine Worte des Stolzes haben mich immer aufgebaut. Danke, dass du mir, gemeinsam mit Mama, so vieles ermöglicht hast, von den tollen Reisen, um dem Karneval zu entfliehen, über meine Sprachreise nach England bis hin zur Finanzierung meines Studiums! **Mama**, durch dich habe ich die Welt der schönen Dinge entdeckt. Ob Kunst, Mode, Design oder Schlösser, viele von deinen Interessen haben sich auch in mir manifestiert, wenn auch auf ihre eigene Art. Ich bin so froh, dass du mir immer so viel gezeigt hast und dass nun von dir so viel auch in mir ist. Du hast immer an mich geglaubt, mit unerschütterlicher Ausdauer, etwas, was mir immer unendlich viel Rückhalt gegeben hat und mich hat weiterkämpfen lassen. Denn auch du bist eine wahre Kämpferin, lässt dich nicht unterkriegen und hast mich somit daran glauben lassen, dass man jede Hürde überwinden kann. Ihr beide seid ein großer Anker in meinem Leben. Neben eurer unermüdlichen Unterstützung und eurem Zuspruch werde ich euch auch immer dankbar sein, dafür, dass ihr mir erlaubt habt, ganz frei ich selbst zu sein und meine eigenen Entscheidungen zu treffen, um die Welt auf meine Weise zu erfahren, auch wenn das bestimmt nicht immer einfach war. Ich bin so froh, euch als meine Eltern zu haben!

ABOUT THE AUTHOR

Katharina Till was born in 1993 in Düsseldorf, Germany, the most beautiful city on the river Rhine. Driven by a desire to better understand the rules that govern the world around us, she began studying Physics in 2012 at Bielefeld University. Already during her Bachelor's degree, she discovered a deep fascination with the intersection of physics and biology. This led her to join the Biomolecular Photonics group of Prof. Thomas Huser for both her Bachelor's and Master's theses.
Under the supervision of Dr. Mark Schüttpelz and Dr. Gerd Wiebusch, she built a compact super-resolution microscope for her Bachelor's thesis, which indeed was so compact that it could be shipped to Madrid, where she presented it during a workshop at a scientific meeting.
For her Master's thesis, she wanted to shift her focus to how microscopes, like the one she had built, could be utilized to uncover the hidden dynamics of biology at its smallest scale. To do so, she joined a collaboration with the structural biology and DNA repair group of Dr. Bjørn Dalhus at the Oslo University Hospital. During three separate research stays in Oslo, she learned about protein purification techniques, data analysis, and protein–DNA interaction experiments, which she then conducted in Bielefeld under the supervision of Dr. Mark Schüttpelz and Dr. Arash Ahmadi from the group of Dr. Bjørn Dalhus. Seeing DNA repair proteins scanning along DNA strands left a lasting impression and strengthened her desire to further explore the molecular mechanisms at the heart of biology and to contribute to a better understanding of the processes constantly *un*folding within our bodies. Thus, in 2020, she joined the Biophysics group of Prof. Sander Tans at AMOLF in Amsterdam for her PhD. This not only brought her back to a beautiful city full of water, but more importantly, was a perfect match to further pursue untangling the complicated but beautiful dynamics of protein–protein interactions, which silently and diligently keep the intricate system of life running.